ACTIVE SPACE DEBRIS REMOVAL USING CAPTURE AND EJECTION

A Dissertation

by

JONATHAN WILLIAM MISSEL

Submitted to the Office of Graduate Studies of
Texas A&M University
in partial fulfillment of the requirements for the degree of

DOCTOR OF PHILOSOPHY

Approved by:

Chair of Committee,	Daniele Mortari
Committee Members,	John Junkins
	John Valasek
	J. Maurice Rojas
Department Head,	Rodney Bowersox

May 2013

Major Subject: Aerospace Engineering

ABSTRACT

Low Earth Orbit is over-cluttered with rogue objects that threaten existing technological assets and interfere with allocating new ones. Traditional satellite missions are not efficient enough to collect an appreciable amount of debris due to the high cost of orbit transfers. Many alternate proposals are politically controversial, costly, or dependent on undeveloped technology. This dissertation attempts to solve the problem by introducing a new mission architecture, *Space Sweeper*, and bespoke hardware, *Sling-Sat*, that sequentially captures and ejects debris plastically. Resulting momentum exchanges are exploited to aid in subsequent orbit transfers, thus saving fuel. *Sling-Sat* is a spinning satellite that captures debris at the ends of adjustable-length arms. Arm length controls the angular rate to achieve a desired tangential ejection speed. Timing the release exacts the ejection angle. This process redirects debris to burn up in the atmosphere, or reduce its lifetime, by lowering its perigee.

This dissertation establishes feasibility of principles fundamental to the proposed concept. Hardware is conceptualized to accommodate *Space Sweeper*'s specialized needs. Mathematical models are built for the purpose of analysis and simulation. A kinematic analysis investigates system demands and long-term behavior resulting from repeated debris interaction. A successful approach to enforce debris capture is established through optimal control techniques. A study of orbital parameters and their response to debris interactions builds an intuition for missions of this nature. Finally, a J_2-compliant technique for path optimization is demonstrated. The results strongly support feasibility of the proposed mission.

DEDICATION

To my wife, Hannah

ACKNOWLEDGMENTS

I wish to thank my advisor, Dr. Daniele Mortari, for always encouraging me to dream, and my committee members, Dr. John Junkins, Dr. John Valasek, and Dr. J. Maurice Rojas, for their investments in my research. Thanks to the Aerospace Engineering Department at Texas A&M University, and the National Defense Science and Engineering Graduate Fellowship, for their financial support throughout my doctoral studies. To my friends and family: thank you for your inspiration, humor, and unwavering love. Special thanks to my parents, Daniel and Linda Missel, for being shining examples of life, even in their old age. Finally, I would like to express my sincere appreciation for my devoted wife, Hannah, for her strength and sacrifice, as the spouse of a graduate student. My achievements are those of God and others. "But you, O Lord, are a compassionate and gracious God, slow to anger, abounding in love and faithfulness." - Psalm 86:15

NOMENCLATURE

a	semi-major axis [km]
α	ejection angle [rad]
D	active arm length [m]
e	eccentricity
$\mathcal{E}$	energy [J]
E	eccentric anomaly [rad]
J_h	hub moment of inertia [kg·m^2]
L	passive arm length [m]
L_{cm}	center of mass location [m]
m	debris mass [kg]
M_A	arm mass [kg]
M_C	collector mass [kg]
M_h	hub mass [kg]
M	total satellite mass [kg]
R_{atm}	radius of atmosphere [km]
$\mathbf{r}$	debris position [km]
$\dot{\mathbf{r}}$, $\mathbf{v}$	debris velocity [km/s]
$\mathbf{R}$	satellite position [km]
$\dot{\mathbf{R}}$, $\mathbf{V}$	satellite velocity [km/s]
u	control input
μ	standard gravitational parameter [m^3/s^2]
$\boldsymbol{\omega}$	angular velocity [rad/s]

TABLE OF CONTENTS

LIST OF FIGURES

FIGURE Page

LIST OF TABLES

TABLE Page

1. INTRODUCTION*

Article I(d) of the Convention on International Liability for Damage Caused by Space Objects states that *"The term 'space object' includes component parts of a space object as well as its launch vehicle and parts thereof."* Based on this definition, space debris are uncontrolled space objects serving no function, such as expired satellites, jettisoned components, and collision shrapnel. Traveling at speeds around 27,000 km/hr in Low Earth Orbit (LEO), space debris poses a growing threat to manned and unmanned missions alike. In 2009, Cosmos-2251 and Iridium-33 collided, marking the first significant satellite "accident" in history [14]. Combined with the successful anti-satellite test conducted by China in 2007, the skies have become littered with debris [30]. Functioning orbiters are often burdened with avoidance maneuvers, delays, and impact damages as a result of the estimated 500,000 pieces of man-made clutter larger than 0.04 inches in LEO [17]. To avoid future uncontrolled conjunction cascading (the "*Kessler Syndrome*" [15]), active debris removal is necessary; unfortunately, this is a nontrivial task.

Though traditional satellites and mission structures are well practiced and easily deployed, they are not efficient enough to offer lasting improvements; successively transferring orbits to collect debris consumes excessive fuel. Also, acquiring mass increases fuel consumption on subsequent maneuvers. Many alternative proposals to remove space debris have been made: laser impingement [5], ground-based laser design "Project Orion" [3], ion guns [4], remote vehicles that capture debris and return to a central station [6], passively intercepting debris with a foamy ball of

*Portions reprinted with permission from "Sling Satellite for Debris Removal with Aggie Sweeper" by Jonathan Missel and Daniele Mortari, 2011. Advances in Astronautical Sciences, volume 140, pages 70–74, Copywrite 2011, Advances in Astronautical Sciences.

aerogel to decay its orbit [19], and inflating balloons around objects to increase atmospheric drag. In the past three years, the Defense Advanced Research Projects Agency, the National Academy of Engineering, and NASA have all released studies which state, among other things, that no proposal has ever been deemed feasible for space debris removal [8]. The reasons for these conclusions vary, but often include high cost, political sensitivity (from weaponizing aggressive plans), potential to create more debris, and accidental interception of active spacecraft (passive plans) [17]. This is a clear indication that a new way of approaching the problem is needed.

This work introduces the two parts of a conceptually new method, called "*Sling-Sat Space Sweeper*" (*4S*). *4S* reclaims the fuel losses of a traditional mission by capturing and ejecting debris through plastic collisions. Welcoming collisions strongly reduce (or even eliminate) the need to burn fuel for rendezvous, and ejecting the debris mass keeps the craft light. In addition, the momentum exchanged in the capture and ejection of each object can be intelligently used as two *free impulses* for the satellite to transfer to the next object, in place of fuel. *Space Sweeper* is the mission architecture that optimally exploits these free ΔVs by finding paths of maximum efficiency and effectiveness. *Sling-Sat* is the bespoke hardware designed to carry out the mission [20]. It is a spinning satellite with collectors at the ends of adjustable arms. Rotation rate is controlled by adjusting the arm lengths. At capture, the tangential velocity of the collector is used to reduce, *or even eliminate*, the relative impact of the debris. To achieve a specified ejection velocity, the tangential speed is again controlled by arm length, and the ejection angle is exacted by timing the release. Ejected debris is sent into a lower perigee orbit to eventually re-enter and burn up in the atmosphere. The principles of *4S* are scalable for a wide range of debris sizes and orbits.

This dissertation looks at the most pressing matters concerning *4S* by focusing

on its two parts. First, *Sling-Sat*'s basic design, dynamics, and control are addressed, followed by orbital analysis and path optimization pertaining to *Space Sweeper*. The goal is to support feasibility of *4S*'s key principles through analysis, simulation, and proof of concept.

2. LITERATURE REVIEW

Near unanimous agreement identifies space debris, also known as space waste or orbital debris, as an increasingly serious problem. Within the subject of space debris exists a wide range of topics, including, but not limited to, population density modeling, risk assessment, legal regulation and tracking. This section gives a brief history of space debris, the threat it poses, methods to overcome it, and research surrounding it.

2.1 A Brief History of Space Debris

Space debris usually refers to inactive man-made objects orbiting Earth. Accordingly, it has a brief, yet rich, history that began on October 4th, 1957 when the Soviet Union launched Sputnik 1–the first artificial satellite to successfully orbit Earth. Upwards of 30,000 satellites have since been deployed by countries, organizations and companies around the globe. Of these, only 1,047 (exact number changes frequently [24]) are still in operation, providing the communication, security, and scientific discovery that has come to define civilization. Figure 2.1 shows the classification of orbital altitudes and their primary functions.

Shortly after Sputnik 1, the United States began flying satellites of their own. In 1958, Vanguard 1 (ID: 1958-Beta 2) was launched into a Medium Earth Orbit (MEO) and operated by the United States Navy. Communications were lost in 1964, making it the oldest piece of space debris to date–a title it plans to defend for some time. According to the National Space Science Data Center (NASA's mission data archive), Vanguard 1 has an orbital life expectancy of 240 years [11].

With access to space increasing, the private sector and emerging nations are certain to add to future traffic. Every successful launch consequently places rocket

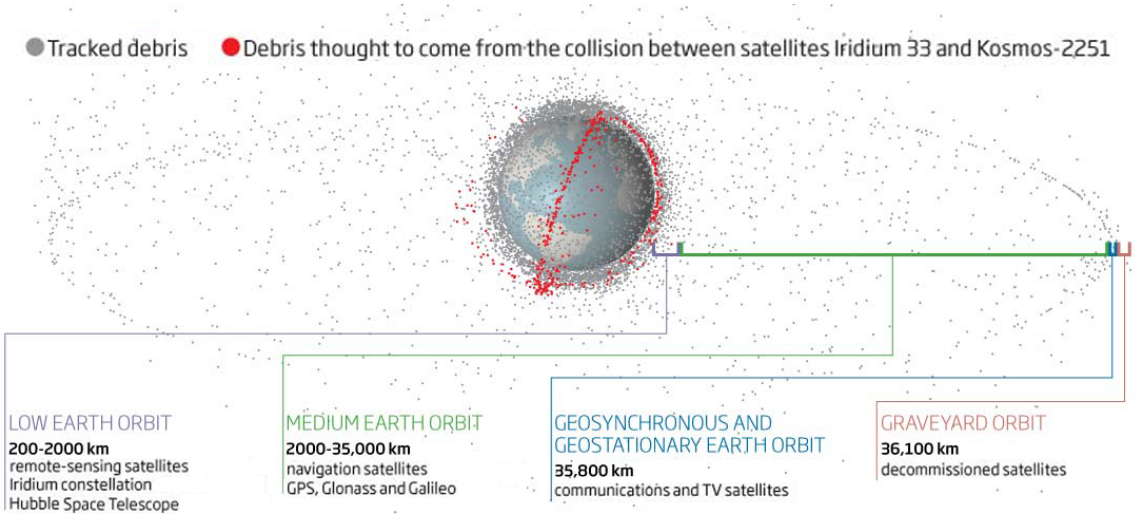

Figure 2.1: Orbit classifications and functionality (Image: NASA)

stages, hardware, and other mission byproducts in orbit. As satellites lose functionality, due to failure or planned expiration, they become debris themselves. Dead satellites that breakup, or fragment due to collision, produce fields of constituent parts that are exponentially more threatening than the original objects. Fragmentation ejecta accounts for over 40% of all space debris [13].

Source	Year	Pieces	Cause
OV2-1 Rocket Body	1965	473	Explosion
Nimbus 4 Rocket Body	1970	374	Explosion
SPOT 1 Rocket Body	1986	492	Explosion
STEP 2 Rocket Body	1996	713	Explosion
CBERS 1 Rocket Body	2000	343	Explosion
TES Rocket Body	2001	370	Explosion
Fengyun-1C	2007	2,841	Anti-Sat
Cosmos 2421	2008	509	Disintegrated
Cosmos 2251	2009	1,267	Collision
Iridium 33	2009	521	Collision

Table 2.1: History of major debris events

Table 2.1 gives a historical account of the most significant sources of debris [26]. Most orbital debris have similar origins and composition (satellites and rocket bod-

ies); however, there are unique examples. Extra-Vehicular Activities (EVAs), also know as space walks, have provided the most amusing forms of space debris. In 1965, astronaut Ed White started the trend when he accidentally let go of a glove, which remained in orbit for about a month. In 2006, astronaut Piers Sellers lost a spatula he was using to apply experimental heat shielding. In 2007, a pair of pliers and a camera were lost in separate events. In 2008, astronaut Heide Stefanyshyn-Piper lost grip of an entire tool bag, and it drifted away.

Another intriguing brand of space debris originated in the early 1960's when the U.S. Military commissioned Project West Ford. The intent was to deploy 480,000,000 copper needles into MEO to create an artificial ionosphere for communication purposes. The project ultimately failed twice, as the needles did not disperse as expected. Clumps of these needles are still in orbit today [33].

2.2 Risk Analysis and Tracking

Since 1978, the year Donald Kessler brought to light the potential for space debris collisions to cascade out of control, analysis and observation of space debris has been the focus of a large body of research [15]. Figure 2.2 shows the Kessler Syndrome (bounded by only 1-σ) as a predictive tool for the future space environment. Satellites in high-risk orbits are currently subject to constant wear and erosion from collisions with small debris. Threat and damages increase with debris size, so shielding and avoidance maneuvers are necessary to increase the odds of successful missions. An object only a few centimeters in size may be enough to catastrophically fragment an entire craft–these are the pawns driving the Kessler Syndrome.

A great deal of effort has been dedicated to constructing models that map debris population density as a function of altitude. Population is measured using optical and radar instruments from the ground and orbit. Modeling is used to both interpolate

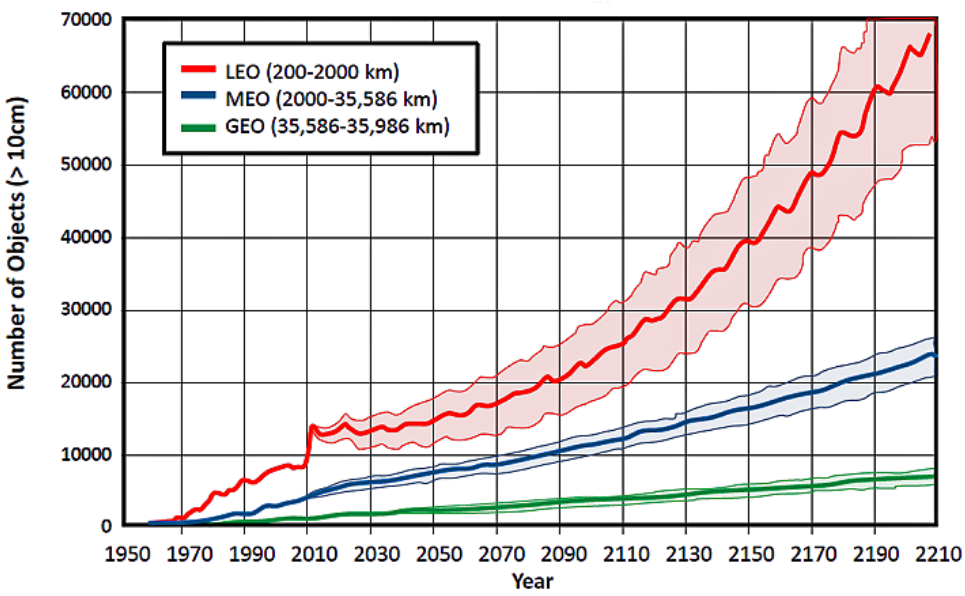

Figure 2.2: Kessler Syndrome projected debris growth, including 1-σ bounds (Image: NASA)

data in regions blind to sensors, and propagate debris populations forward in time. Improvements on these models work to include lesser effects that cause disparity between current models and measurements. One such study looks at the effect of rotational motion on the ballistic coefficients of debris [35]. Like spin on a tennis ball, rotating debris interacts with the upper atmosphere to bend its trajectory. Similarly, eddy currents and eddy-current damping have gradual influences that accumulate over time. In addition, eddy-current damping and drag slow down debris rotation, making it a compounded, time-varying effect that is challenging to model.

The largest source of information on orbital debris is the Space Surveillance Network of the United States, which tracks, correlates, and catalogs tens of thousands of objects in Earth orbits. The measurements themselves come from various sources before being combined with models to generate estimates. These sources include the European Space Agency (ESA) Space Debris Telescope, TIRA system, Goldstone radar, Haystack radar, EISCAT radar, and the Cobra Dane phased array radar [16],

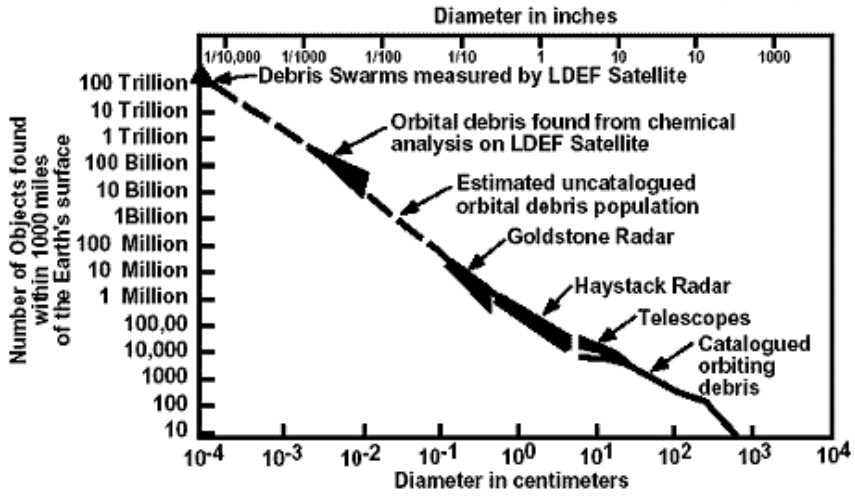

Figure 2.3: Debris size and measurement decomposition (Image: NASA)

[27]. Ultra High Frequency (UHF) radar is commonly used for continuous monitoring of the debris environment, and Super High Frequency (SHF) radar pinpoints more precise measurements. Figure 2.3 shows a debris size distribution model, and corresponding measurement methods. Physical impact sampling is also used to estimate the flux of debris classes in given orbits. Purpose built panels leave traceable impact signatures that are recovered and analyzed. In addition, hardware recovered from unrelated missions is used to gather data. In 1993, ESA was charged with counting and categorizing impact craters from solar arrays retrieved from the Hubble Space Telescope. Similar analyses were carried out on components of the Mir Space Station and other large pieces of hardware. This information helps build and confirm statistical models for small debris impacts.

Breakup modeling is equally important to confidently predict results of collision events. ESA and NASA have done extensive materials testing and simulation to better understand hypervelocity impacts on spacecraft. In the past, results from the Satellite Orbital debris Characterization Impact Tests (SOCIT), a NASA and DoD project, provided detailed collision models. However, these results are becoming

outdated due to modern advances in material and construction technology. Slated for impact testing in early 2014, DebrisSat is a hypervelocity experiment, co-sponsored by NASA and the U.S. Air Force, that is designed to update these models. DebrisSat is a dummy satellite that is representative of modern equipment. It will serve as a target to study fragmentation and ejecta patterns during controlled impact. Results from this test will improve prediction accuracy of post-collision debris clouds for modern satellites [9].

2.3 Mitigation

The orbital debris problem can be attacked from five different angles: prevention, protection, avoidance, passive removal, and active removal. Without putting all current space operations on hold, finding a solution will require collaboration between several–likely all–of these approaches. The magnitude, threat, and cost mandates careful planning for both long and short term solutions.

2.3.1 Prevention

Most prevention methods involve mission regulations to reduce the chance of fragmentation in the immediate or distant future. This includes passivation: the act of removing any internal energy from a satellite at the end of its life to avoid accidental explosions. As residual propellant is spent, or compressed gasses are expelled, the resulting impulse is often directed, combining passivation with a final maneuver. In LEO, this means a re-entry or perigee reduction (to reduce orbit life). In GEO, the craft is placed in a "graveyard orbit," about 300 km above GEO (see Figure 2.1). However, this is a temporary solution–*a carpet can only hide so much dust.*

All spacefaring nations have contributed to orbital debris, and all spacefaring nations are at risk because of it. Individual entities have made significant steps

in understanding and addressing the problem, but the most successful long-term impacts originate in the regulations, treaties, and recommendations put forth by collaborative unions. These include the International Astronomical Congress (IAC), the Committee on Space Research (COSPAR), the United Nations (UN), the European Space Agency (ESA), the International Organization for Standardization (ISO), the Union of Concerned Scientists (USC), the Inter-Agency Debris Coordination Committee (IADC), and many others. Their efforts unite and educate the world's nations to arrive at peaceful preventative solutions. As a result, actions like passivation, end-of-life disposal, and weapon bans are becoming standard procedure [10].

2.3.2 Protection

Regardless of the presence of man-made space debris, shielding satellites is necessary to protect against natural objects like micrometeoroids and radiation. Early shielding often used layered monolithic aluminum plates to protect from damages. These are still in use for GEO orbits, but they are outdated for the high-speed, high-traffic LEO environment [12]. Most modern spacecraft are protected by Whipple shields. A sacrificial aluminum bumper mounted on a standoff breaks up the debris. An inner pressure wall, composed of Nextel^{TM}ceramic fabric and Kevlar^{TM}high-strength fabric, serves as a final barrier [36]. A "stuffed" version also exists, which incorporates a blanket between the two barriers. In some respect, shielding is also a form of prevention, because it reduces debris growth by keeping spacecrafts intact. Shielding protects space assets from small impacts, but offers little protection against debris that is large enough to be tracked.

2.3.3 Avoidance

Collision avoidance is a necessary part of safely navigating LEO. Launch delays and evasive maneuvers are a standard part of mission operations. In 2012, the

International Space Station performed four avoidance maneuvers due to man-made debris, and two near misses would have warranted maneuvers had they been detected in time [25]. This rate is growing, and with over 1,000 missions currently in operation, avoidance has become a massive task. Constant monitoring, prediction, and planning are critical for successful avoidance; however, mishaps like the 2009 Iridium/Cosmos collision are getting harder to avoid, especially for uncontrolled objects.

2.3.4 Passive Removal

Passive removal methods use *uncontrolled* interactions to mitigate space debris. This eliminates the need for uncooperative rendezvous (or other controlled interactions), and permits removal of a wide range of debris sizes, including those too small to track. Most passive missions have a similar format: let the debris run into something that slows it down for re-entry or reduced orbital life. This requires no trajectory or attitude control, which is inexpensive to operate. The most passive mechanism of all is self-removal. This is simply the act of drag from the upper atmosphere decaying the orbit and causing it to re-enter. Space debris has reached a point where self-removal is not enough to prevent collision cascading from taking place. Misting is a passive removal concept that, in a way, brings the atmosphere to the debris. A well placed spray of mist creates a drag-inducing cloud that slows down passing objects, causing their orbits to decay [17]. In another concept, a slab of polyimide foam is placed in a targeted orbit. Debris passing through the foam are slowed, and orbit decay is accelerated [37]. Several variations of this type of mission exist, each proposing a different medium or structure for the debris to interact with. The primary disadvantage to passive missions is that they make no distinction between operational satellites and debris–all are at risk for removal [19].

2.3.5 Active Removal

Active debris removal methods involve some form of *controlled* interaction with a targeted object; therefore, they are limited to objects that are large enough to track. The "one-up/one-down" launch license is a policy currently under consideration by several unions and committees. It requires any launch vehicle operator flying a new mission to pay for (or conduct) the removal of a dead satellite of similar size, in a similar orbit. This requires active removal. If each mission operator were to develop and conduct their own removal mission, the total cost and risk would devastate the industry. However, the cost of removal would be reasonable if efforts focused on a few promising methods, and financing were the shared responsibility of launch operators. If left open to a free market, this would likely result in removal services for hire. The "one-up/one-down" launch license may be the economic solution to active debris removal, but it does not establish how a removal mission might work.

Several laser impingement methods have been proposed to actively remove debris. Ground or space-based lasers are focused on the leading edge of the debris, and the pressure gradually slows and decays their orbit [5], [3]. Ion beams have been proposed for use in the same way [4]. These methods greatly reduce, or eliminate, the need for costly orbit transfers by interacting with debris at a distance, *but they are easily weaponized and stifled by political sensitivity.* Also, more work is needed to study feasibility. With impingement lasting several months for large objects, it is unclear if material degradation will lead to fragmentation, thus compounding the problem [17]. In addition, modeling often assumes perfect surface interactions, but some of the effectiveness will be lost in favor of attitude dynamics.

Navigating the political grounds of active debris removal will likely require some form of grappling mission. The traditional process of transferring orbits to dock with

an uncooperative object requires too much fuel to remove large numbers of debris. Therefore, it (and its close variants) is only practical for removing high-risk debris that are large or in particularly threatening orbits. Another challenge for grappling missions is that debris properties (such as size, shape, mass, composition, and spin) are frequently unknown. Eddy-currents damp the rotation of small, conductive debris, but large objects often tumble, making capture or docking difficult.

The standard approach to capturing space debris is broken up into four phases: pre-capture, contact (impact), post-capture, and stabilization. Research on capture often spans one or two of these phases, and a goal of each phase is to minimize the reaction moment on the collecting satellite [32]. Recent developments include image-based docking, and reactionless capture for large tumbling objects [7], [34]. In 2012 the Swiss Space Center announced their plans for Clean Space One, a nanosat demonstration of rendezvous and conjoined re-entry with a similarly sized defunct nanosat. This is a noteworthy step for working out the details of a grappling mission, but it is still a traditional mission, and does not address the issue of fuel consumption.

For some time, researches have been rethinking mission architectures to extend beyond the limitations of on-board fuel capacity. Some involve a refueling station. In terms of active debris removal, this means a team of debris-capturing satellites that periodically return to a central docking station to unload debris and refuel [6]. The ElectroDynamic Debris Eliminator (EDDE) vehicle is a proposal that focuses on spacecraft efficiency. An EDDE is a propellantless craft that uses the Earth's magnetic field to climb and torque its orbit. It climbs to rendezvous with an object, grabs it, and then descends to deorbiting altitudes. It then releases the debris and climbs back up for another, removing objects one at a time. The process is highly fuel efficient, but glacially slow. To help overcome this, the mission calls for a fleet of EDDEs to simultaneously pick apart the debris field. Still, simulations estimate

that a team of 12 EDDEs would take decades of constant operation to making an appreciable difference [29].

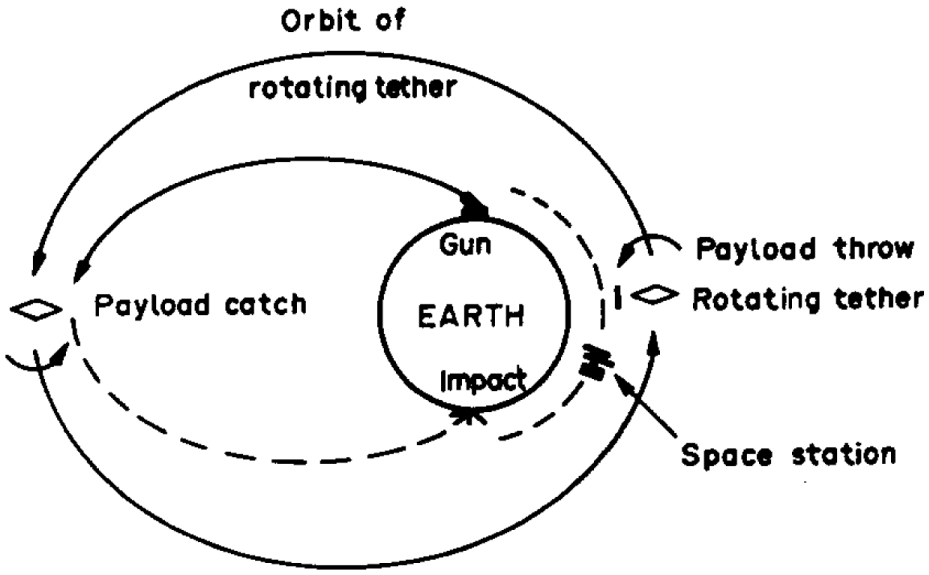

Figure 2.4: Gun/tether refueling concept (Image: NASA)

In the late 1980's, NASA proposed an interesting low-cost launch system and orbital fuel depot to service the NASA space station. Though unrelated to debris removal, its operations are relevant to the proposed *4S* mission. Seen in Figure 2.4, the system consists of an electromagnetic gun that launches fuel tanks into MEO, where they are captured by a long, rotating tether satellite. The tether satellite is in an elliptical orbit that ranges from MEO down to LEO, where it drops the fuel tanks into an orbit near the Space Station. The tangential velocity of the rotating tether is used to both "throw" and softly capture the payload [28].

In 1990, a method was proposed for removing expired GEO satellites using techniques related to *4S*. A satellite docks with its target, attaches a tether, and then uses thrusters to put the system into a spin. Upon release, the satellite and object are placed into new orbits. This tethered ejection is estimated to be six times more fuel efficient than rocket propulsion [31]. Though the ejection process is similar to that

of *4S*, the broader mission differs. It requires full rendezvous capture, and thrusters to initiate and terminate spin. In addition, it focuses on GEO, where as *4S* is likely to focus on LEO debris for reasons explained in Section 7.

3. HARDWARE

Space Sweeper's specialized objectives impose many requirements on accompanying hardware. It needs a craft that is light enough to be launched, robust enough to withstand repeated plastic collisions, dexterous enough to capture, aim, and expel debris, and stable enough to handle capture/ejection without uncontrolled tumbling. Efficiency is also critical, as it is an underlying argument for *Space Sweeper*. As a first step toward ensuring these tasks are attainable, a purpose built craft is conceptualized here, starting with the basic design and expanding into sensor options.

3.1 Design Overview

Settling on a proposed satellite design to partner with *Space Sweeper* required several iterations. Early designs used separate mechanisms to capture, reposition, and eject debris. Aerogel or netting provides an essentially plastic collision to collect debris, a robotic arm extracts and loads the debris for expulsion, and a railgun or catapult then aims and ejects it. Designs like this have recurring faults, they are highly dependent on the size, shape, and composition of the debris, and impacting debris velocities that do not pass through the satellite's center of mass disrupt its attitude. Additionally, using three separate mechanisms to handle the debris is complicated, time consuming, heavy, and inefficient.

The next logical step is to combine the capturing and ejecting mechanisms, eliminating the need to relocate debris. Energy from the impacting debris is stored (e.g., by compressing a spring) and then used for ejection. This design lacks precision and does not address the disturbances from misaligned impacts.

After several iterations, a design called "*Sling-Sat*" emerged as a likely partner for *Space Sweeper*. In short, it is a spinning satellite with collectors on the ends

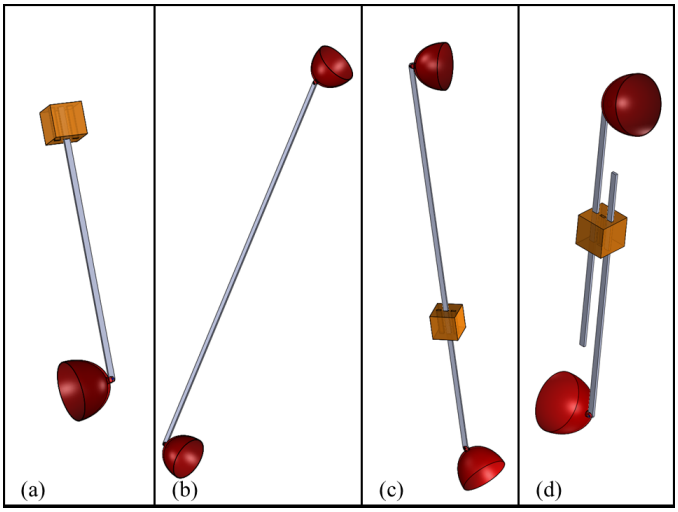

Figure 3.1: Design configurations

of variable-length arms. Adjusting the length of these arms controls rotation rate, effectively controlling the debris' ejection speed. The ejection angle is exacted by simply timing the release. This design provides a straightforward solution to the challenge of coordinating mechanisms to capture, handle, and eject debris. It also efficiently makes use of the dynamics of the interaction. Existing momentum of the two bodies may be all that is needed to favorably redirect both trajectories. Natural spin stabilization assuages the chance of tumbling from miscalculated collisions; off-axis impacts induce harmonic perturbations that are addressed by nutation dampers or similar devices. In addition, *Sling-Sat* provides an effective means of estimating the unknown debris mass (see Section 4). It does so in two ways: 1) monitoring the angular velocity change, and 2) adjusting the opposing arm length to reset rotation about *Sling-Sat*'s geometric center. Figure 3.1 shows some configurations used to develop simplified mathematical models for design analysis, and Figure 3.2 shows a conceptual rendering of what an advanced design may look like.

Specific designs for the end collectors are under consideration. One possibility is the Universal Jamming Gripper currently being developed at Cornell University

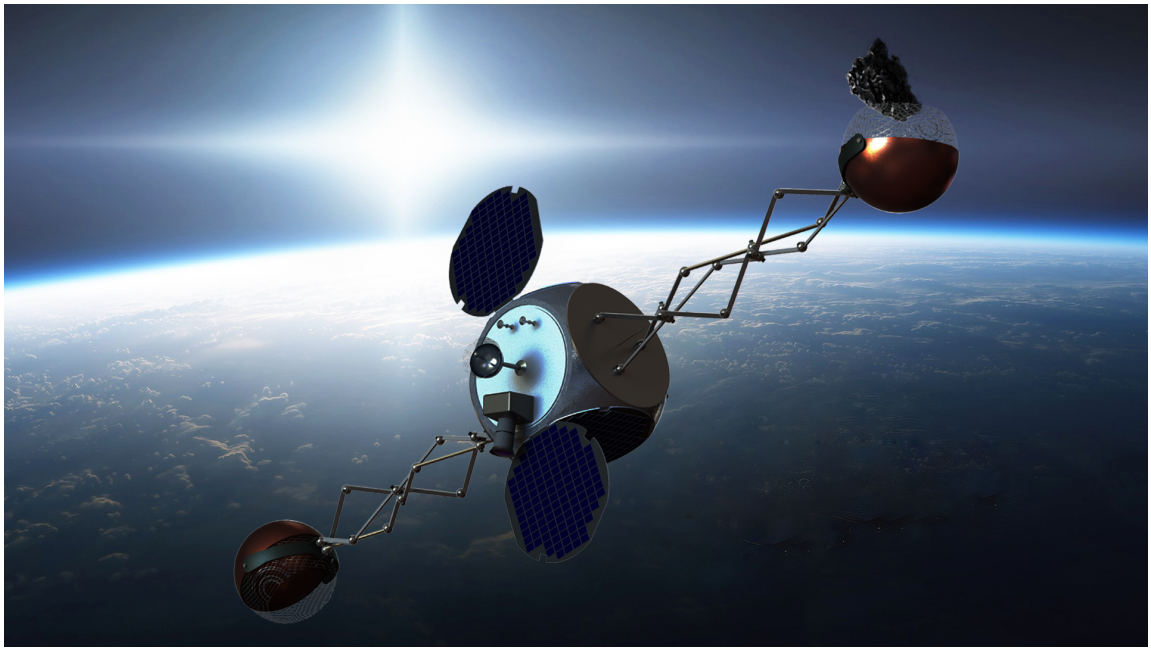

Figure 3.2: Conceptual rendering

[1]. It is an elegantly simple end-effector that conforms to an impressive range of objects. Currently, it relies on atmospheric pressure to operate, but future versions may be compatible with the vacuum of space. Another option is to have inwardly barbed fingers of ceramic Kevlar (similar to that protecting the International Space Station). This material is proven to withstand impacts in orbit. Regardless of their final design, the collectors are represented here by simple cup-shaped mechanisms.

3.2 Arm Design

When considering arm design, it is important to remember that *Sling-Sat* functions by changing its moment of inertia to control tangential velocity at the collectors. A straight, retractable bar-type arm is limiting for this. Retracting past its midpoint will begin to increase the moment of inertia again. Tethers provide the desired adjustability, but lack the rigidity needed to properly transfer the momentum exchanges to the rest of the craft. For these reasons, folding arms are an attractive option.

Figure 3.3 illustrates the mechanization of the suggested tri-scissor design. These arms work much like a standard scissor lift, but use sets of three linkages, rather than two, for structural integrity. The symmetry and compactness of the structural configuration is favorable for adjustment. Fully retracted, the collectors sit close to the body for high spin rates; this is also advantageous when packing for initial launch. A rod extends from the hub and threads into the first joint of the arm. This secures the arm, and centrifugal forces act to push the remaining points of contact against the hub. Rotating the threaded rod is a sufficient means of actuating arm length control. With linkages that collapse evenly, low-fidelity models represent the arm with uniform linear density that is a function of length. Therefore, they have a constant mass, and the center of mass of an arm corresponds to its geometrical center.

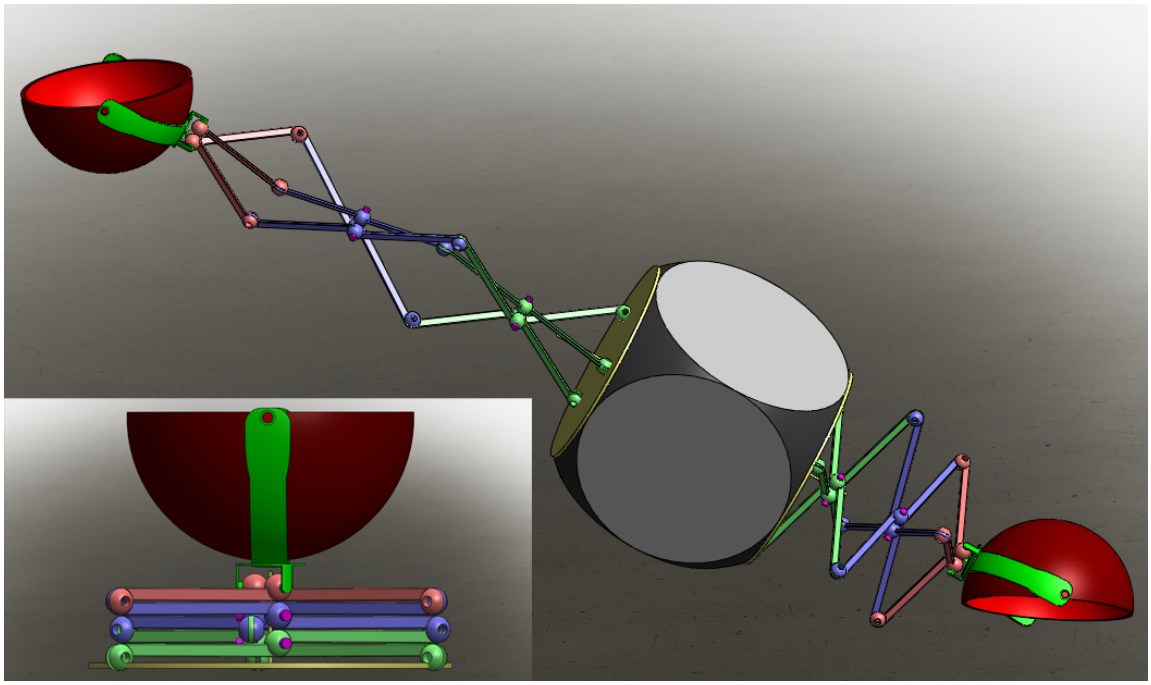

Figure 3.3: Tri-scissor arm concept

Arm design is an important feature of *Sling-Sat* that warrants further research.

Several alternative concepts have potential for success. For example, jointed segments (elbows) provide an addition degree of freedom (per arm) to assist in capture and ejection. This adds dexterity, but is more complex and prone to failure. A highly simplified concept is a rigid straight arm of fixed length. Ballast masses[1] traveling along the arm vary its moment of inertia. Fixing the arms enables a higher range of tangential velocities when compared to the tri-scissor design undergoing the same change in moment of inertia. The level of simplicity also improves simulation accuracy, even for low-fidelity models.

As a general statement on future development, analysis and simulation will govern sizing and properties of all component. Masses, moments of inertia, and arm dimensions are vital to *Sling-Sat*'s performance. These need to be optimally designed to maximize effectiveness, and verified through simulation.

3.3 Sensing and Communication

To provide a more consistent platform for sensing and communication, *Sling-Sat* has a dual-spin design, where a portion of the central hub rotates independently from the arms. *4S* requires a nearly continuous signal with the ground, because path optimization is too tasking for on-board processors (see Section 8). Measurements are sent to a dedicated computer on the ground, and trajectory plan updates are transmitted up to the satellite. This likely requires intermediate Tracking and Data Relay Satellites (TDRS) for regions in the orbit that are unable to directly contact the ground.

Identifying an adequate suite of sensors relies on more detailed studies of control feedback and path optimization needs. General needs include attitude and rate measurement, and proximity tracking of targeted debris before capture. Star trackers

[1]Ballast masses composed of functional hardware components add no unnecessary net mass the satellite.

provide a reliable means of attitude and angular rate estimation throughout the orbit. Their accuracy and speed are particularly desirable for backing out debris mass estimates after capture. Executing the final moments of capture control requires precise debris state feedback. In addition to the external measurement techniques cited in Section 2.2, a combination of on-board binocular imaging and SHF radar gives accurate measurements of the relative position and velocity of the debris, even from a distance [29], [16]. Detailed sourcing and testing of these sensors are necessary to determine their limitation for tracking debris of various sizes, compositions, and velocities.

Standard robotics and satellite sensors are also required to enforce and confirm *Sling-Sat*'s detailed functions. For example, encoders, membrane potentiometer, EMF feedback, and accelerometers may be used to measure the relative states of actuated components. Inertial measurement units and gyros build detail and redundancy into the measurement of the satellite's collective motion.

4. MATHEMATICAL MODELING

With the exception of capture control (see Section 6) and orbit propagation, the analyses and simulations conducted in this study do not require a set of differential equations of motion to model behavior. The states of *4S* are determined sequentially using basic conservation principles and geometry. This section walks through these steps for the two most commonly used physical models.

4.1 Five-Mass Model

Here, a five-mass planar model is used to represent *Sling-Sat*. Figure 4.1 illustrates the three distinct actions of *4S*–capture, spin-up, and ejection–along with their notation. A set of equations is derived to relate these actions and determine critical unknowns. At stages two and three, the center of mass calculations include the debris mass because it is contained by the satellite.

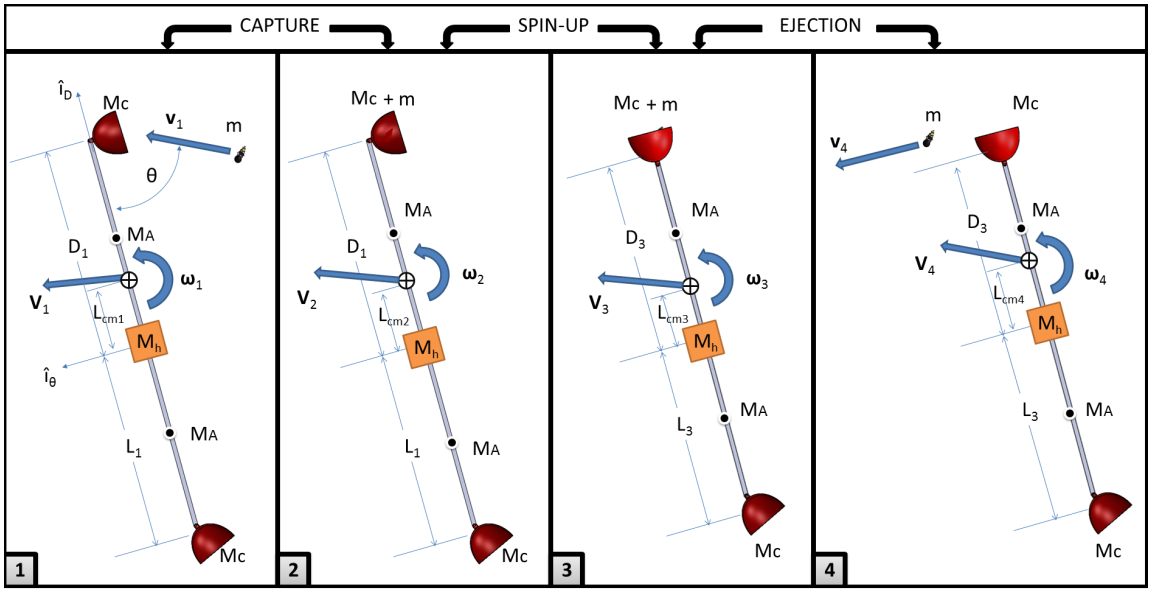

Figure 4.1: Phases of removal for five-mass system

4.1.1 Capture

Capture control enforces the intersection of the debris with the collector which restrains it. Mechanically, this is a plastic collision. Managing the arm length prior to capture controls the relative impact velocity between the collector and debris, *possibly reducing it to zero.* The debris mass m, new satellite velocity $\mathbf{V}_2$, new center of mass $\mathbf{L}_{cm2}$, and the new angular rate $\boldsymbol{\omega}_2$, are all unknown. Kinetic energy is not conserved for plastic collisions; therefore, geometry, translational momentum, and angular momentum are used to solve for them. The arm design is modeled with a linear density that is uniform over the length of the arm, but varies as a function of arm length. Therefore, the center of mass of each arm is always half the arm length.

In reference to Figure 4.1, the combined center of mass $\mathbf{L}_{cm2}$ after capture is located by,

$$\mathbf{L}_{cm2} = \frac{(M_C + M_A/2)(D_1 - L_1) + mD_1}{M + m}\,\hat{\mathbf{i}}_D \tag{4.1}$$

where, M_C is the collector mass, M_A is the arm mass, M_h is the satellite hub mass, m is the debris mass, $M = M_h + 2(M_A + M_C)$ is the total satellite mass, D is the capturing arm's length, and L is the opposite arm's length. A straight forward application of the conservation of translational momentum yields the resulting velocity after capture.

$$\mathbf{V}_2 = \frac{M\,\mathbf{V}_1 + m\,\mathbf{v}_1}{M + m} \tag{4.2}$$

To be consistent in this and the remaining stages, angular momentum is observed about the satellite hub M_h. For the capture process, this looks like,

$$\begin{aligned}\boldsymbol{\omega}_1 \left(M_C D_1^2 + \tfrac{1}{3}M_A D_1^2 + J_h + M_C L_1^2 + \tfrac{1}{3}M_A L_1^2\right) + m\left[\mathbf{D}_1 \times (\Delta\mathbf{v}_1 + \boldsymbol{\omega}_1 \times \mathbf{L}_{cm1})\right] \\ = \boldsymbol{\omega}_2 \left[(M_C + m)D_1^2 + \tfrac{1}{3}M_A D_1^2 + J_h + M_C L_1^2 + \tfrac{1}{3}M_A L_1^2\right]\end{aligned}$$

where, $\Delta\mathbf{v}_1 = \mathbf{v}_1 - \mathbf{V}_1$ is the debris velocity with respect to the satellite's center of mass, $\Delta\mathbf{v}_1 + \boldsymbol{\omega}_1 \times \mathbf{L}_{cm1}$ is the debris velocity with respect to the satellite hub, J_h is the moment of inertia of the satellite hub, and the arm moments of inertia follow a thin rod assumption. Asserting that all angular rates are in the same direction $\hat{\mathbf{i}}_\omega$ for the planar case, θ is the debris' angle of impingement with respect to the arm, and $\Delta\mathbf{v}_1 + \boldsymbol{\omega}_1 \times \mathbf{L}_{cm1} = D_1(\Delta v_1 \sin\theta + L_{cm1}\omega_1)\hat{\mathbf{i}}_\omega$, the angular momentum can be reduced to a scalar equation. Finally, this is arranged to give an expression for debris mass as a function of angular rate.

$$m = \frac{(\omega_2 - \omega_1)\left[J_h + \left(M_C + \dfrac{M_A}{3}\right)(D_1^2 + L_1^2)\right]}{D_1(\Delta v_1 \sin\theta + L_{cm1}\omega_1 - D_1\omega_2)} \tag{4.3}$$

Equation (4.3) is extremely useful as it provides a means of estimating the unknown debris mass using angular rate measurements before and after capture. Knowledge of the debris mass gives $\mathbf{V}_2$ and $\mathbf{L}_{cm2}$ from Equations (4.2) and (4.1), respectively. Though not of great concern, uncertainty in θ is expected to be the dominant source of error in estimating debris mass. Also, for the special case of zero impact–where the incoming debris velocity matches the tangential velocity of the collector–angular momentum gives:

$$m[\mathbf{D}_1 \times (\boldsymbol{\omega}_1 \times \mathbf{D}_1)] = mD_1^2\boldsymbol{\omega}_1$$

Therefore, $\boldsymbol{\omega}_1 = \boldsymbol{\omega}_2$, and Equation (4.3) becomes indeterminate, $m = 0/0$. Near the zero-impact case, estimates will be unreliably sensitive.

There are (at least) two ways of addressing the sensitivity to mass estimation. An accelerometer at the hub center measures $-\ddot{r}_{(L_{cm2})}$, the centripetal acceleration. The center of mass is then known by $L_{cm2} = -\ddot{r}_{(L_{cm2})}/\omega_2^2$, and Equation (4.1) is solved

for debris mass.

$$m = \frac{\left(M_C + \frac{M_A}{2}\right)(D_1 - L_1) - L_{cm2}M}{L_{cm2} - D_1} \tag{4.4}$$

The second method determines debris mass by extending the opposing arm to a length $L_{2'}$, such that the center of mass returns to the center of the hub. The equation for the new center of mass is:

$$L_{cm2'} = 0 = \frac{(M_C + M_A/2)(D_1 - L_{2'}) + mD_1}{M + m}$$

This is solved to determine the debris mass.

$$m = \frac{(M_C + M_A/2)(L_{2'} - D_1)}{D_1} \tag{4.5}$$

Both of these methods rely on determining the center of mass and then backing out the debris mass. Equations (4.4) and (4.5) can be used to improve or replace the estimates provided by Equation (4.3) at any impact velocity.

4.1.2 Spin-Up

The mission plan determined by *Space Sweeper* specifies an optimal ejection velocity $\mathbf{v}_4$ to mutually assist the debris in deorbiting and *Sling-Sat* in transferring to the next targeted object. The goal of spin-up is to match this prescribed tangential ejection velocity by varying the arm lengths.[1] Determining the length of the independent arms is therefore a priority. This starts with the center of mass equation.

$$\mathbf{L}_{cm3} = \frac{(M_C + M_A/2)(D_3 - L_3) + mD_3}{M + m}\,\hat{\mathbf{i}}_D$$

[1]Ejection nearly always requires increased angular rates, so this action is referred to as spin-up, rather than spin-down.

Conservation of angular momentum relates the angular velocities,

$$\boldsymbol{\omega}_3 = \boldsymbol{\omega}_2 \frac{\Phi_2}{\Phi_3} \tag{4.6}$$

where,

$$\begin{cases} \Phi_2 &= (M_C + M_A/3)(D_1^2 + L_1^2) + J_h + mD_1^2 \\ \Phi_3 &= (M_C + M_A/3)(D_3^2 + L_3^2) + J_h + mD_3^2 \end{cases}$$

are the combined moments of inertia, respectively.

In terms of $\boldsymbol{\omega}_3$, the desired debris velocity $\mathbf{v}_4$ is expressed as:

$$\mathbf{v}_4 = (D_3 - L_{cm3})\, \boldsymbol{\omega}_3 \times \hat{\mathbf{i}}_D + \mathbf{V}_3$$

Let $\Delta\mathbf{v}_4 \equiv \mathbf{v}_4 - \mathbf{V}_3$ define the relative ejection velocity of the debris with respect to the combined center of mass before ejection. Recognizing that the cross product is orthogonal gives the relative tangential ejection velocity.

$$\Delta\mathbf{v}_4 = \mathbf{v}_4 - \mathbf{V}_3 = (D_3 - L_{cm3})\, \boldsymbol{\omega}_3 \times \hat{\mathbf{i}}_D = \omega_3 (D_3 - L_{cm3})\, \hat{\mathbf{i}}_\theta$$

In the interest of determining the unknown arm lengths D_3 and L_3, this is expanded in terms of otherwise known quantities.

$$\begin{aligned} \Delta\mathbf{v}_4 = \omega_2 \; & \left[\frac{(M_C + M_A/3)\,(D_1^2 + L_1^2) + J_h + mD_1^2}{(M_C + M_A/3)\,(D_3^2 + L_3^2) + J_h + mD_3^2}\right] \cdot \\ & \left[D_3 - \frac{(M_C + M_A/2)\,(D_3 - L_3) + mD_3}{M + m}\right] \hat{\mathbf{i}}_\theta \end{aligned} \tag{4.7}$$

Equation (4.7) has two unknown arm lengths. Therefore, the prescribed ejection condition can be achieved with multiple combinations of the two arm lengths. The energy equation for the spin-up process is used to develop a cost function that,

when minimized, will provide the most energy efficient combination. Assuming the changes in potential and translational kinetic energy are negligible,[2] the rotational kinetic energy gives:

$$\frac{1}{2}\omega_2^2\Phi_2 = \frac{1}{2}\omega_3^2\Phi_3 - \text{Work}_2$$

Substituting in the relation from Equation (4.6) and solving for the work, this is rewritten as:

$$\text{Work}_2 = \frac{1}{2}\omega_2^2\Phi_2\left(\frac{\Phi_2}{\Phi_3} - 1\right) \tag{4.8}$$

Everything in Equation (4.8) is known, except elements of Φ_3; therefore, minimizing work is effectively maximizing Φ_3. Removing constant terms, the problem of choosing D_3 and L_3 to minimize work is further reduced to minimizing the cost function:

$$J = -D_3^2\left(M_C + M_A/3 + m\right) - L_3^2\left(M_C + M_A/3\right)$$

Taking the partials with respect to D_3 and L_3, setting them equal to zero, and equating them provides the relation describing the line of critical points.

$$L_3 = D_3\left(1 + \frac{m}{M_C + M_A/3}\right) \tag{4.9}$$

Equations (4.7) and (4.9) are used to solve for the optimal arm lengths. Combining and simplifying these equations yields:

$$\begin{aligned} D_3 =& \frac{\omega_2\Phi_2}{6\Delta v_4}\left(\frac{1 + mM_A}{M_C + m(3+m)M_A/3 + J_h}\right) \\ L_3 =& \frac{\omega_2\Phi_2}{6\Delta v_4}\left(\frac{1 + mM_A}{M_C + m(3+m)M_A/3 + J_h}\right)\left(1 + \frac{m}{M_C + M_A/3}\right) \end{aligned} \tag{4.10}$$

[2]Potential and translational kinetic energy are constantly changing in orbit, but there are no appreciable differences for this short time interval.

These are the energy optimal ejection arm lengths, entirely in terms of known, determined, and measured quantities. Conveniently, these arm lengths minimize the angular rate at ejection as well.

4.1.3 Ejection

Given a prescribed debris ejection velocity, the resulting motion of the satellite is the only remaining variable to be solved for. After ejection, the center of mass of the satellite is:

$$\mathbf{L}_{cm4} = \frac{M_C + M_A/2}{M} (\mathbf{D}_3 - \mathbf{L}_3)$$

Translational momentum is directly solved for the final satellite velocity.

$$\mathbf{V}_4 = \mathbf{V}_3 + \frac{m}{M}(\mathbf{V}_3 - \mathbf{v}_4)$$

Using the relation $\mathbf{V}_3 = \mathbf{v}_4 - \boldsymbol{\omega}_3 \times (\mathbf{D}_3 - \mathbf{L}_{cm3})$, The final satellite velocity is expressed in terms of known variables.

$$\mathbf{V}_4 = \mathbf{v}_4 - \left(1 + \frac{m}{M}\right) [\boldsymbol{\omega}_3 \times (\mathbf{D}_3 - \mathbf{L}_{cm3})] \tag{4.11}$$

Applying conservation of angular momentum gives:

$$\boldsymbol{\omega}_3 \Phi_3 = \boldsymbol{\omega}_4 (\Phi_3 - m D_3^2) + m \left[\mathbf{D}_3 \times (\mathbf{v}_4 - \mathbf{V}_4 + \boldsymbol{\omega}_4 \times \mathbf{L}_{cm4})\right]$$

All cross products are orthogonal and result in the $\hat{\mathbf{i}}_\omega$ direction; therefore, all terms have the same unit vector. Substituting in $\mathbf{V}_4$ from Equation (4.11) gives the final angular velocity.

$$\boldsymbol{\omega}_4 = \boldsymbol{\omega}_3 \frac{\Phi_3 - m D_3 (D_3 - L_{cm3})(1 + m/M)}{\Phi_3 - m D_3 (D_3 - L_{cm4})}$$

The above equations represent the most generic ridged-body configuration of *Sling-Sat* considered in this preliminary work. Often, an analysis permits assumptions that simplify the model, such cases are clearly noted.

4.2 Two-Mass Model

This evaluation looks at the planar, symmetrical-arm, two-mass model, where the total mass M is concentrated in the end collectors. This model provides a simple means of describing *Sling-Sat*'s most fundamental principles. There are four distinct actions (capture, spin-up, ejection, and return) that cyclically transfer between four configurations. Figure 4.2 illustrates this cycle. A set of equations is derived to relate these states and determine unknowns sequentially.

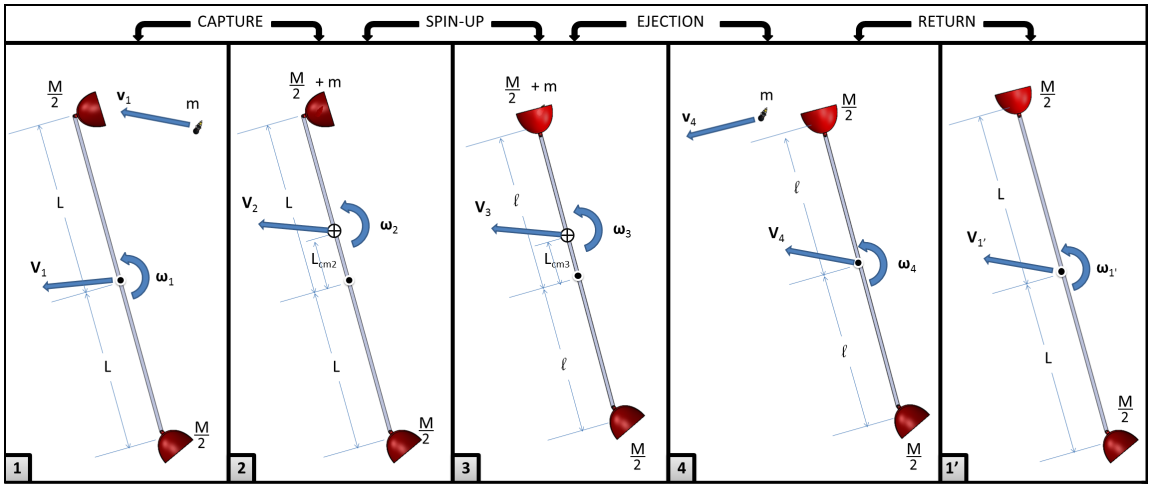

Figure 4.2: Phases of removal for two-mass system

4.2.1 Capture

As the two orbits intersect, collectors at the ends of massless arms plastically capture the debris. At this point, the debris mass m, new satellite velocity $\mathbf{V}_2$, new center of mass $\mathbf{L}_{cm2}$, and new angular velocity $\boldsymbol{\omega}_2$ are all unknown. Kinetic energy is not conserved for plastic collisions; therefore, geometry, translational momentum,

and angular momentum are used to determine them.

The combined center of mass after capture is:

$$\mathbf{L}_{cm2} = \frac{m\,L}{m+M}\,\hat{\mathbf{i}}_L \tag{4.12}$$

where, $\hat{\mathbf{i}}_L$ is the unit vector along the arm on the debris side. Applying the conservation of translational momentum gives:

$$M\,\mathbf{V}_1 + m\,\mathbf{v}_1 = (M+m)\,\mathbf{V}_2$$

This is rearranged to solve for $\mathbf{V}_2$ as a function of unknown debris mass m.

$$\mathbf{V}_2 = \frac{M\,\mathbf{V}_1 + m\,\mathbf{v}_1}{M+m} \tag{4.13}$$

Applying conservation of angular momentum about the center of the satellite addresses this dependence on m. The angular momentum from debris rotation is negligible, under the assumption that eddy current damping from the Earth's magnetic field has stopped its rotation.

$$\boldsymbol{\omega}_1 ML^2 + m(\mathbf{L} \times \Delta\mathbf{v}_1) = \boldsymbol{\omega}_2\,(M+m)\,L^2 \tag{4.14}$$

$\Delta\mathbf{v}_1 = \mathbf{v}_1 - \mathbf{V}_1$ is the relative debris impact velocity with respect to the satellite. This gives an expression for the angular velocity after capture as a function of m.

$$\boldsymbol{\omega}_2 = \frac{\boldsymbol{\omega}_1 ML + m(\hat{\mathbf{i}}_L \times \Delta\mathbf{v}_1)}{(M+m)\,L} \tag{4.15}$$

As specified by the mission, angular velocity measurements are provided by on-

board instrumentation before and after capture. Therefore, Equation (4.15) is used as a measurement model for simulations. Measuring $\boldsymbol{\omega}_2$ directly after capture provides a means of estimating the debris mass. Dividing Equation (4.14) by L, and then subtracting the right-hand side gives:

$$\boldsymbol{\omega}_1 ML + m\left[(\hat{\mathbf{i}}_L \times \Delta\mathbf{v}_1) - L\boldsymbol{\omega}_2\right] - \boldsymbol{\omega}_2 ML = 0 \tag{4.16}$$

Under the planar assumption, the cross product $\hat{\mathbf{i}}_L \times \Delta\mathbf{v}_1$ and angular velocity $\boldsymbol{\omega}_2$ are in the same direction. Therefore, Equation (4.16) can be written as a scalar expression to solve for the unknown debris mass.

$$m = \frac{ML(\omega_2 - \omega_1)}{\|\hat{\mathbf{i}}_L \times \Delta\mathbf{v}_1\| - L\omega_2}$$

Estimating this debris mass is a pivotal advantage of *Sling-Sat*. The location of the center of mass, and the velocity after capture are readily calculated by Equations (4.12) and (4.13), respectively.

4.2.2 Spin-Up

Spin-up is the action of pulling the arms in to achieve a desired ejection velocity. This process deals only with geometry and angular momentum–any velocity changes result from orbit propagation, and are determined as such. The ejection arm length l, new center of mass $\mathbf{L}_{cm3}$, and new angular rate $\boldsymbol{\omega}_3$ are unknown. The center of mass is found by:

$$\mathbf{L}_{cm3} = \frac{ml}{m+M}\,\hat{\mathbf{i}}_L \tag{4.17}$$

Observing the conservation of angular momentum about the center of the satellite (*not the combined center of mass*) gives:

$$\boldsymbol{\omega}_2(M+m)L^2 = \boldsymbol{\omega}_3(M+m)\,l^2$$

This is solved to determine the angular velocity prior to ejection.

$$\boldsymbol{\omega}_3 = \boldsymbol{\omega}_2 \left(\frac{L}{l}\right)^2 \tag{4.18}$$

At this point, the desired debris ejection velocity $\mathbf{v}_4$ (as specified by *Space Sweeper*'s path optimization) is introduced as the directive for spin-up; therefore, it is known. Kinematics defines this as the summation of the satellite's velocity and the relative velocity.

$$\mathbf{v}_4 = \boldsymbol{\omega}_3 \times (\mathbf{l} - \mathbf{L}_{cm3}) + \mathbf{V}_3$$

Substituting in $\boldsymbol{\omega}_3$ from Equation (4.18), and letting $\Delta\mathbf{v}_4 \equiv \mathbf{v}_4 - \mathbf{V}_3$ be the relative debris ejection velocity with respect to the satellite center, gives:

$$\Delta\mathbf{v}_4 = \left(\frac{L}{l}\right)^2 [\boldsymbol{\omega}_2 \times (\mathbf{l} - \mathbf{L}_{cm3})] \tag{4.19}$$

The factors $\boldsymbol{\omega}_2$ and $(\mathbf{l} - \mathbf{L}_{cm3})$ are orthogonal for the rigid planar case, with a cross product in the tangential direction $\hat{\mathbf{i}}_\theta$. The relative ejection velocity direction $\frac{\Delta\mathbf{v}_4}{\|\Delta\mathbf{v}_4\|} = \hat{\mathbf{i}}_\theta$ is also tangential, allowing Equation (4.19) to be written as a scalar expression to solve for l.

$$\Delta v_4 = \left(\frac{L}{l}\right)^2 \omega_2\,(l - L_{cm3})$$

Substituting in for L_{cm3} from Equation (4.17) gives:

$$\Delta v_4 = \frac{ML^2\omega_2}{l(m+M)}$$

This is rearranged to solve for the required ejection arm length.

$$l = \frac{ML^2\omega_2}{\Delta v_4(m+M)}$$

Equation (4.18) is now solved for ejection angular velocity in terms of known variables.

$$\boldsymbol{\omega}_3 = \frac{1}{\omega_2}\left(\frac{\Delta v_4(m+M)}{ML}\right)^2 \hat{\mathbf{i}}_\omega$$

In scalar form, this can be expressed as:

$$\omega_3 = \frac{\Delta v_4^2(m+M)^3}{LM^2\left(\omega_1 ML + m\Delta v_1 \sin\theta\right)}$$

The energy equation determines how much work is required of the satellite to fight against centripetal force when pulling in the arms.

$$\begin{gathered}\tfrac{1}{2}\omega_2^2\left[\left(m+\tfrac{M}{2}\right)(L-L_{cm2})^2 + \tfrac{M}{2}(L+L_{cm2})^2\right] = \\ \tfrac{1}{2}\omega_3^2\left[\left(m+\tfrac{M}{2}\right)(l-L_{cm3})^2 + \tfrac{M}{2}(l+L_{cm3})^2\right] - \text{Work}_2\end{gathered}$$

Substituting for the center of mass definitions, this rearranges to:

$$\text{Work}_2 = \frac{\omega_2^2 L^2}{2}\left(\frac{1}{l^2}-1\right)\left(m+M-\frac{2m^2}{(m+M)}+\frac{Mm^2}{(m+M)^2}+\frac{m^3}{(m+M)^3}\right)$$

4.2.3 Ejection

Prior to ejection, the final velocity $\mathbf{V}_4$, and angular velocity $\boldsymbol{\omega}_4$ of the satellite are unknown. In determining these, the assumption is made that angular momentum due to rotation of the ejected debris is negligible. Its angular rate $\boldsymbol{\omega}_3$ is known, but it is relatively small in size and has unknown mass distribution; therefore, it is considered a point mass. Conservation of translational momentum gives the satellite's final velocity.

$$\mathbf{V}_4 = \frac{(m+M)\,\mathbf{V}_3 - m\,\mathbf{v}_4}{M}$$

Applying the conservation of angular momentum about the satellite's geometric center gives:

$$\boldsymbol{\omega}_3(m+M)l^2 = \boldsymbol{\omega}_4 M l^2 + m(\Delta\mathbf{v}_4 \times \mathbf{l})$$

The cross product $\Delta\mathbf{v}_4 \times \mathbf{l}$ is in the $\hat{\mathbf{i}}_\omega$ direction and orthogonal; therefore, scalar and vector forms of the final angular rate are respectively defined as:

$$\omega_4 = \omega_3 \left(1 + \frac{m}{M}\right) - \Delta v_4 \frac{m}{Ml}$$

$$\boldsymbol{\omega}_4 = \boldsymbol{\omega}_3 + \frac{m}{M}\left(\omega_3 - \frac{\Delta v_4}{l}\right)\hat{\mathbf{i}}_\omega$$

4.2.4 Return

After ejection, the process is ready to be repeated for the next encounter, but some insight is gained by adding another step. By returning the arms to their original lengths L, the total amount of work required to remove a piece of debris can be determined. This is the *cost* of the *free* ΔVs that are exploited in path optimization, though they are still considered free because arm length changes are ultimately driven by renewable solar energy. Applying the work-energy equation for

the return process gives:

$$\frac{1}{2}\omega_4^2 M l^2 = \frac{1}{2}\omega_{1'}^2 M L^2 - \text{Work}_4 \tag{4.20}$$

Conservation of angular momentum gives the new angular velocity.

$$\boldsymbol{\omega}_{1'} = \boldsymbol{\omega}_4 \left(\frac{l}{L}\right)^2$$

This is used in Equation (4.20) to solve for the return work.

$$\text{Work}_4 = \frac{M}{2}\,\omega_4^2\, l^2 \left[\left(\frac{l}{L}\right)^2 - 1\right]$$

The total work to spin-up for ejection and then return to the original capture configuration is:

$$\text{Work} = \text{Work}_2 + \text{Work}_4 \tag{4.21}$$

5. KINEMATIC ANALYSIS

This section analyzes the spin-up phase to gain a fundamental understanding of the mechanics associated with reconfiguring the arms. Both the two-mass model and the five-mass model of *Sling-Sat* are evaluated, and comparisons are made to determine when each model is valid. Where possible, similar properties are assigned to both models. These models closely follow the derivations of Section 4, with the added assumption that the arm lengths in the five-mass model adjust symmetrically, rather than independently.

5.1 Two-Mass Analysis

The simplified two-mass model of Section 4.2 assumes only the collectors have mass, and both arms move in unison, such that $2L$ is the total length at capture, and $2l$ is the total length at ejection. The collectors are point masses, each responsible for half of the satellite's total mass. The change in debris tangential velocity, satellite angular velocity, and the work done are observed over a swept range of capture and ejection arm lengths. Results are obtained for an $M = 100$ kg satellite, $m = 5$ kg debris, and an initial angular momentum $H_2 = 50$ J·s. Angular momentum is used to determine the initial angular velocity.

$$\omega_2 = \frac{H_2}{L^2(m+M)} \tag{5.1}$$

Figure 5.1 shows the initial angular rate according to Equation (5.1) for the range of L values. In this scenario, the satellite never rotates with a frequency greater than 0.5 Hz.

As the arms are adjusted, conservation of angular momentum dictates the new

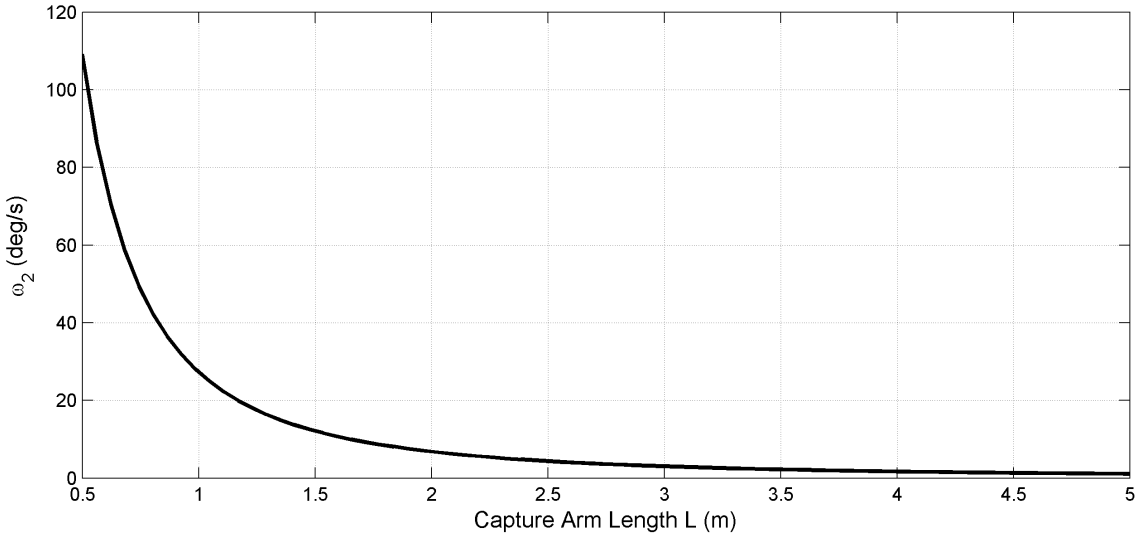

Figure 5.1: Initial angular rates for two-mass analysis

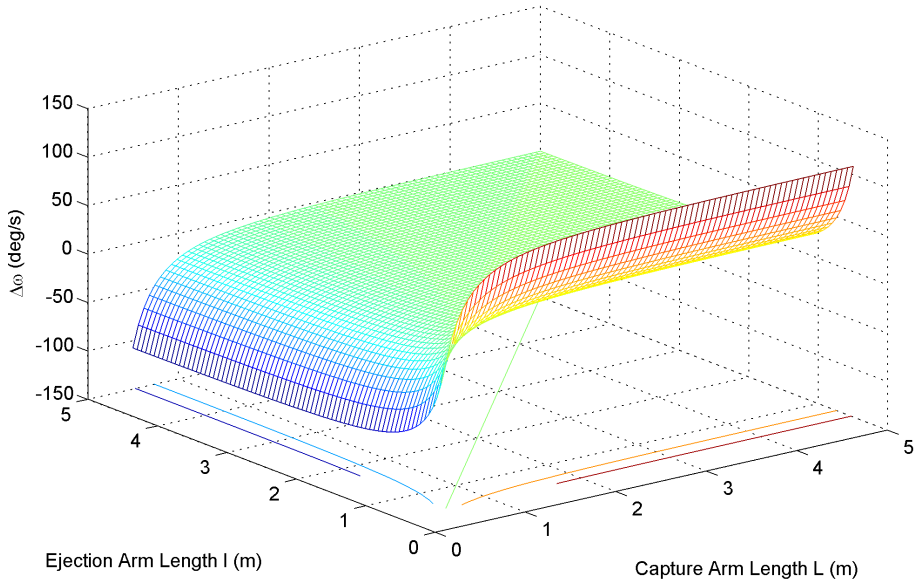

Figure 5.2: Change in angular rate for two-mass model

angular rate.

$$\omega_3 = \omega_2 \left(\frac{L}{l}\right)^2$$

Figure 5.2 shows how the angular rate changes as L and l are varied. These values

are used to find the change in tangential velocity of the debris.

$$\Delta v = \omega_3(l - L_{cm3}) - \omega_2(L - L_{cm2})$$

Figure 5.3 shows how tangential velocity changes during spin-up. This is an important parameter to consider, because it dictates the limits of the ejection velocity to deorbit debris, which is the objective of the spin-up process. The work required of the actuators to adjust the arms is derived in Section 4.2.2, and is rearranged as:

$$Work = \frac{1}{2}\left(\omega_3^2 l^2 - \omega_2^2 L^2\right)\left(\left(1 - \frac{m}{m+M}\right)^2\left(m + \frac{M}{2}\right) + \left(1 + \frac{m}{m+M}\right)^2 \frac{M}{2}\right)$$

Figure 5.4 shows the work associated with various arm lengths. Here, it is clear that the greatest changes in tangential velocity require the greatest work input, a seemingly intuitive consequence. However, this is not always the case, as will be seen for the five-mass model.

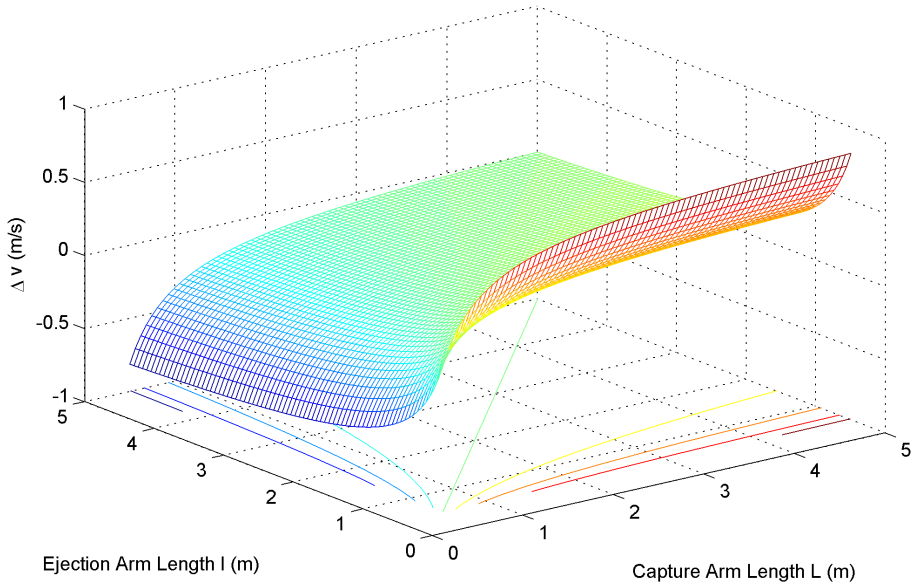

Figure 5.3: Change in tangential speed for two-mass model

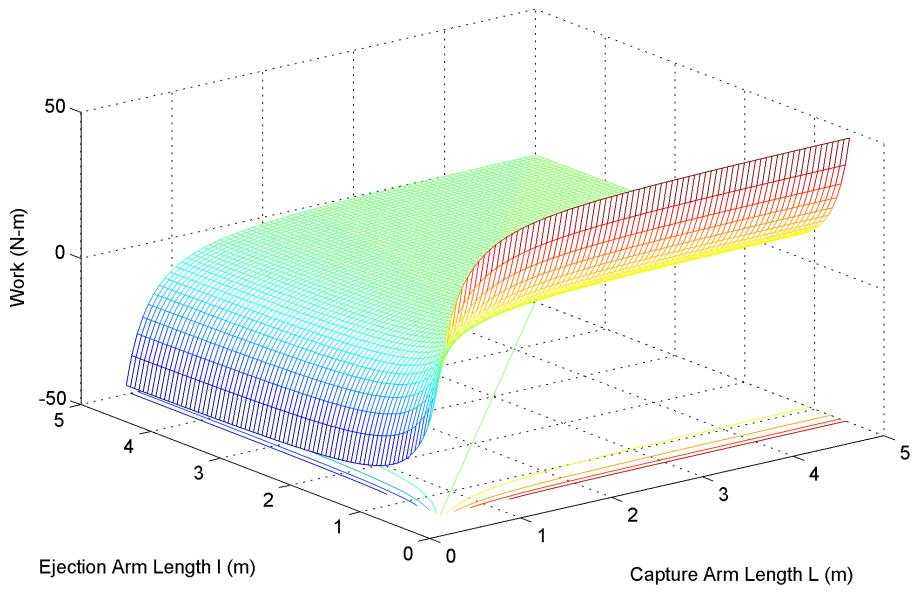

Figure 5.4: Work done to move arms for two-mass model

The similarities in Figures 5.2 and 5.4 results from their shared dependence on the ratio of the squared arm lengths, introduced by moment of inertia calculations. This is expected, and it demonstrates the classic trade-off between performance and cost. In most cases, the work is required to pull the arms in to eject debris; however, when the arms extend again, some of the energy is recovered. Therefore, the total work requirements for each ejection will not be as high as Figure 5.4 suggests. If the arms are returned to their standard length after debris is ejected, any difference in angular rate (compared to the same point in the previous removal cycle) is a result of that encounter. If this occurs, it may become problematic over time.

To investigate concerns that sequential interactions may have residual effects that accumulate undesirably, $10,000$ consecutive debris interactions are simulated. An $M = 100$ kg satellite with initial arm length of $L = 5$ m is required to eject debris at $\Delta v_4 = 100$ m/s. To span a set of realistic scenarios, the relative impact speed of the debris, impacting angle, and debris mass are randomly assigned between $\Delta v_1 =$ 0–100 m/s, $\theta = 0$–$\pi/16$ rad, and $m = 1$–5 kg, respectively. The rotation rate before

capture ω_1, as well as the ejection arm length l, and the total work to move and return the arms are observed for each interaction. At each stage, the angular rate before capture is found by:

$$\omega_1 = \frac{H_1}{ML^2}$$

The ejection arm length and angular velocity magnitude are then determined.

$$l = \frac{M(H_1 + mL\Delta v_1 \sin\theta)}{\Delta v(M+m)^2}$$

$$\omega_3 = \frac{H_1 + mL\Delta v_1 \sin\theta}{l^2(M+m)}$$

H_1 is the angular momentum of the craft before each capture. The total work follows the definition of Equation (4.21).

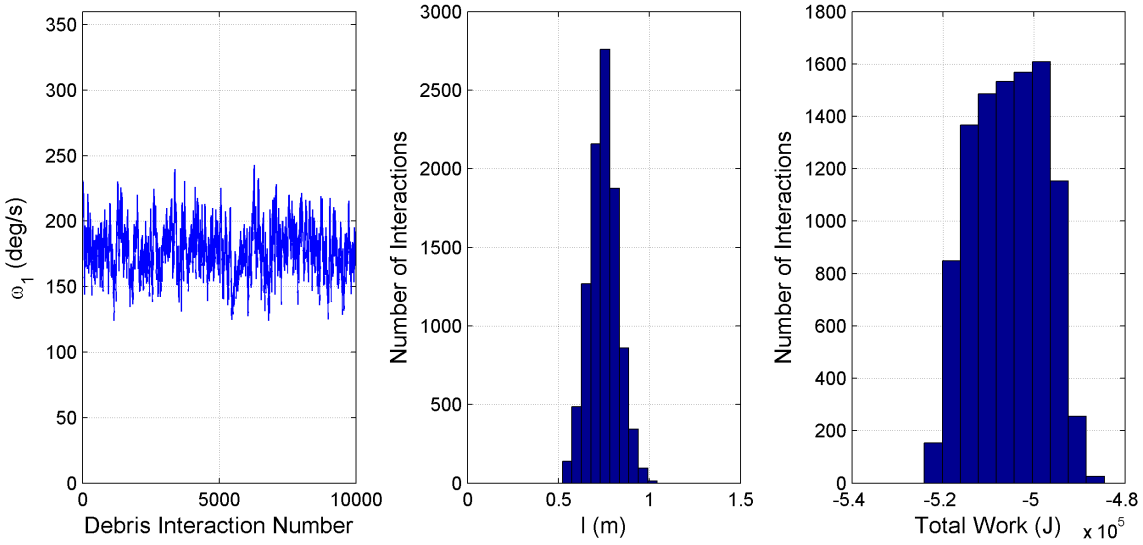

Figure 5.5: 10,000 consecutive debris interactions

Figure 5.5 shows the angular rate, ejection arm length, and work requirements for 10,000 interactions. ω_1 is plotted in order of occurrence to monitor any trends or long-term drifting. The chatter is an expected artifact of the discrete and random

nature of this mission. It is apparent that *no undesirable trends cause the angular rate to drift.* The histogram of ejection arm lengths shows the arms retract, in every case, to increase the angular velocity and achieve the prescribed ejection speed. The distribution is centered about .75 m and is Gaussian *in appearance.* The total work for an interaction averages roughly -500 kJ, meaning energy is being used and needs to be supplied by the satellite. Energy requirements of this magnitude are reasonable. A 1.5 m^2 solar array is able to recover from the average 500 kJ interaction in less than 4 minutes [38]. This estimate does not consider other power needs of the craft, but it suffices to show how inexpensive the process is.

This analysis does not simulate orbital responses (for full simulation, see Section 8); its intent is to gain a statistical perspective on key aspects of the satellite throughout the removal process. Identifying the existence or absence of undesired tendencies is an important step in early mission development. If, for example, angular rate loss concerns arose, integrating a fly-wheel could remedy this by judiciously allocating angular momentum as needed. As it stands, this analysis suggests that such precautions are not of immediate concern.

5.2 Five-Mass Analysis

To verify and compare the results of Section 5.1, spin-up of the five-mass model is also analyzed. With respect to the model outlined in Section 4.1, the assumption that the arms adjust in unison is added here. This makes for better comparison with the two-mass model and more defined results. As in Section 5.1, the change in debris tangential velocity, satellite angular rate, and the work done, are observed for spin-up over a swept range of capture and ejection arm lengths. The debris mass is $m = 5$kg, the two collectors have masses $M_C = 20$ kg, the two arms have masses $M_A = 5$ kg, the hub has mass $M_h = 50$ kg, and the moment of inertia of the hub is

$J_h = 30$ kg·m^2. The total mass of the satellite is therefore $M = 100$ kg. The satellite is given an initial angular momentum $H_2 = 50$ J·s. Angular momentum is used to determine the initial angular velocity ω_2, shown in Figure 5.6 for the range of initial arm lengths.

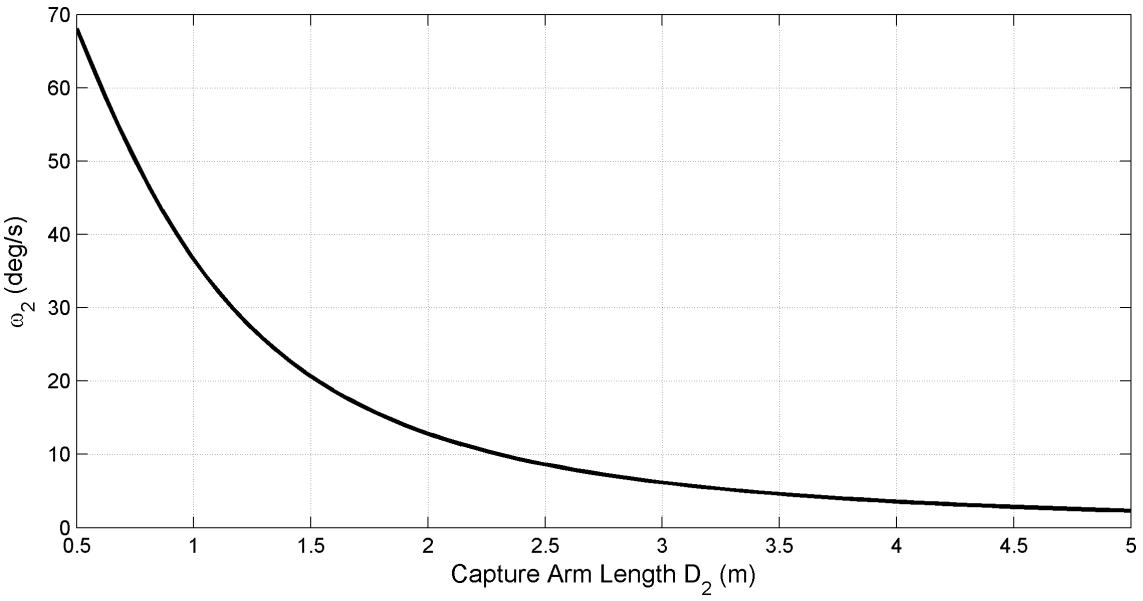

Figure 5.6: Initial angular rates for five-mass analysis

Calculating the results of spin-up for the five-mass model follows the development of Section 4.1. The assumption of symmetrical arm adjustments means that $D_2 = L_2$ at capture, and $D_3 = L_3$ at ejection. Equation (4.8) is applied to determine the work required to adjust the arms. As with the two-mass case, Figures 5.7 and 5.8 show a strong correlation between change in angular rate and work done. This indicates that the two-mass model suffices to quantitatively analyses such characteristics.

A more surprising result is the variation in tangential velocity shown in Figure 5.9. Change in tangential velocity magnitude is determined by:

$$\Delta v = \omega_3(D_3 - L_{cm3}) - \omega_2(D_2 - L_{cm2})$$

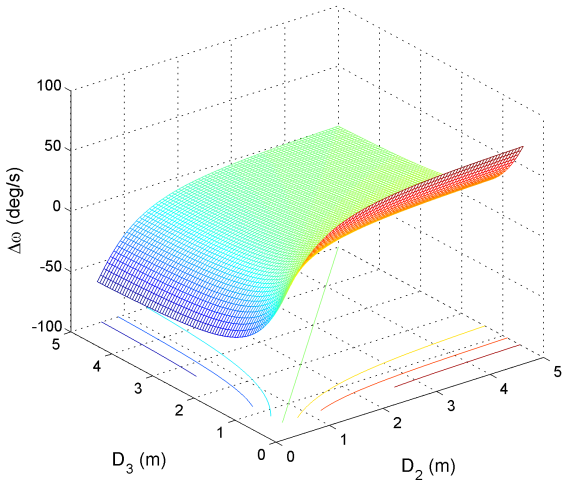

Figure 5.7: Change in angular rate

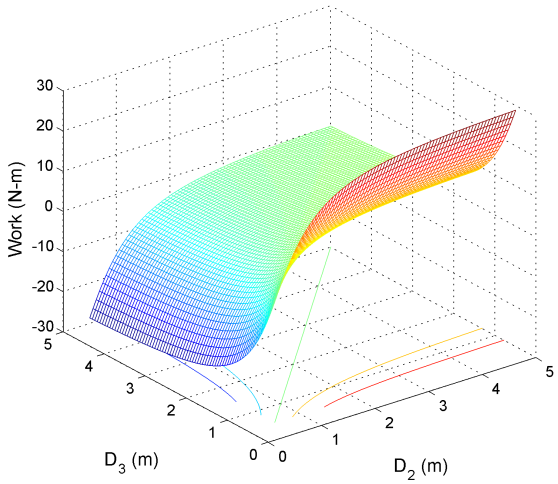

Figure 5.8: Work done for spin-up

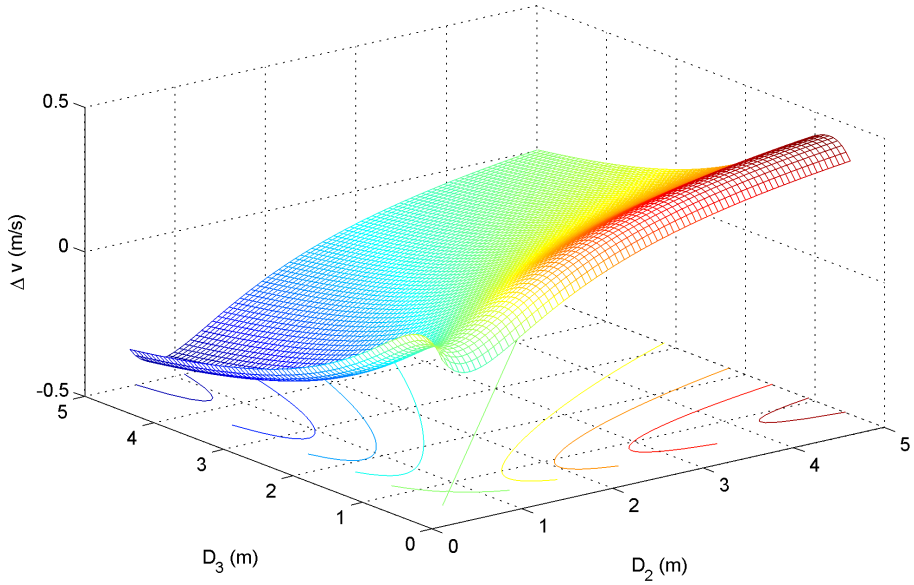

Figure 5.9: Change in tangential speed for five-mass model

Modeling the arms as slender rods, and the hub as an extended object, with a mass and moment of inertia, adds complexity to the intuition of this process. These results show that the maximum difference in tangential velocity (the relative ejection speed of debris) is not necessarily achieved by putting in the most work. Regions exist where smaller variations in arm length actually yield larger tangential velocity variations.

The shape of this surface grows increasingly complex as the arms are modeled to move independently, and as components are assigned more accurate inertia properties. A more complex relationship signifies a broader range of maneuvers to achieve a desired task–this makes room for optimization to begin satisfying secondary agendas. Continuing this study is important, as modeling and hardware develop, to fully understand the capabilities of *Sling-Sat*, and maximize efficiency.

6. CAPTURE CONTROL

To establish feasibility of conjunction between collectors at the end of a spinning satellite and incoming debris, capture controllers are demonstrated. This coordination poses an interesting nonlinear problem, solved here by fuel optimal controllers designed for application in the final moments before capture.

As a primary objective, controllers must capture debris. This is enforced by a final state constraint specifying that the collector and debris positions must be the same. Additionally, to mitigate the severity of impact, constraints are imposed on the tangential velocity of the collector to better match the impacting debris velocity at the time of capture. Only a small portion of the orbits are considered, so initial trajectories are assumed to be straight lines.

A high fidelity model of this problem is currently premature and exceeds its purpose: to obtain initial results for evaluating feasibility. Accordingly, assumptions are made to simplify the problem without affecting the qualitative accuracy of the results. Several variations of this problem have been considered and solved using appropriate techniques. Here, the focus is on only two scenarios which are solved with a common technique, so as not to get bogged down with the details of nonlinear control methodology.

6.1 Fixed Trajectory Capture

The goal here is to capture debris and reduce impact velocity without controlling *Sling-Sat*'s trajectory. Governing this description are the assumptions that all motion is planar, both arms move in unison, and the trajectories are uninfluenced by gravity.

By nature, the final time T and final states $\mathbf{x}(T)$ of this problem are free.[1] The model assumes no control of the satellite's position, only arm length. This necessitates that the satellite and debris already be on trajectories that will pass within arm's length, a condition met through path optimization. Since the trajectories are fixed, a *tangential* zero-impact solution may not exist in all cases. Zero-impact then requires a radial velocity component from arm adjustment rate, but this is costly and not ideal [23]. Therefore, the optimization compromises by minimizing the relative impact velocity without interfering with the capture constraint.

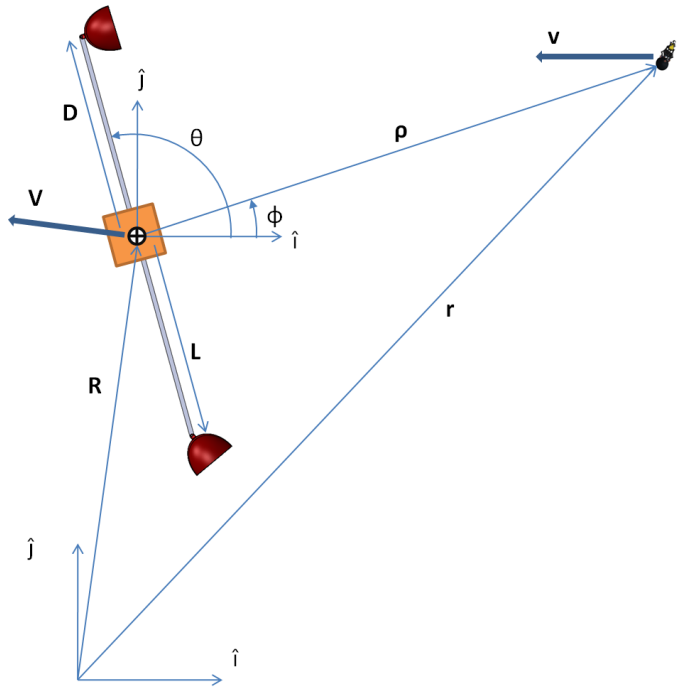

Figure 6.1: Debris capture schematic

[1]Final time is free within a small window–a few seconds–and does not conflict with macroscopic capture time prescribed by path optimization in Section 8.

In accordance with Figure 6.1, the equations of motion are:

$$\mathbf{x} = \begin{Bmatrix} D \\ \theta \\ \dot{D} \\ \dot{\theta} \end{Bmatrix}, \qquad \dot{\mathbf{x}} = \begin{Bmatrix} \dot{D} \\ \dot{\theta} \\ -u_D \\ \dfrac{-2\dot{\theta}\dot{D}}{J_h[2D(M_C + M_A/3)]^{-1} + D} \end{Bmatrix} \tag{6.1}$$

where, the control input is simply the negative of the arm acceleration, J_h is the moment of inertia of the satellite hub, M_C is the collector mass, and M_A is the arm mass. Euler's equation gives the angular acceleration from the time derivative of angular momentum. The control input u_D accounts for the efforts of both arms.

In-line with the efficiency objectives of the broader mission, the cost function is simply:

$$J = \frac{1}{2}\int_{t_0}^{T} u_D^2 \, dt$$

In reality, the fuel consumed is not proportional to the acceleration of the arm. Locks and braking mechanisms will be built into the hardware to counteract centrifugal effects. Centrifugal effects also put work back into the system when extending the arms. As a result, this control model yields conservative (higher) fuel requirements.

The positions and velocities of the debris and *Sling-Sat* are assumed to be uncontrolled and linear, meaning they are absorbed in the final state constraints and propagated linearly in time by Equation (6.2). This reduces the number of states

and associated equations of motion from eight to the four seen Equation (6.1).

$$\begin{cases} \dot{\mathbf{R}}_0 &= \dot{X}_0\hat{\mathbf{i}} + \dot{Y}_0\hat{\mathbf{j}} \\ \dot{\mathbf{r}}_0 &= \dot{x}_0\hat{\mathbf{i}} + \dot{y}_0\hat{\mathbf{j}} \\ \mathbf{R}(t) &= X\hat{\mathbf{i}} + Y\hat{\mathbf{j}} = (\dot{X}_0 t + X_0)\hat{\mathbf{i}} + (\dot{Y}_0 t + Y_0)\hat{\mathbf{j}} \\ \mathbf{r}(t) &= x\hat{\mathbf{i}} + y\hat{\mathbf{j}} = (\dot{x}_0 t + x_0)\hat{\mathbf{i}} + (\dot{y}_0 t + y_0)\hat{\mathbf{j}} \end{cases} \tag{6.2}$$

In this problem, the final state constraints $\boldsymbol{\Psi}$ are completely expressed in terms of the free final time T, free final states $\mathbf{x}(T)$, and known initial conditions.

$$\boldsymbol{\Psi}(\mathbf{x}(T), T) = \mathbf{0} = \begin{Bmatrix} \mathbf{D}(T) - \boldsymbol{\rho}(T) \\ \dot{\mathbf{D}}(T) - \dot{\boldsymbol{\rho}}(T) \end{Bmatrix} = \begin{Bmatrix} D\cos\theta - \Delta\dot{x}_0 T - \Delta x_0 \\ D\sin\theta - \Delta\dot{y}_0 T - \Delta y_0 \\ \dot{D}\cos\theta - \dot{\theta}D\sin\theta - \Delta\dot{x}_0 \\ \dot{D}\sin\theta + \dot{\theta}D\cos\theta - \Delta\dot{y}_0 \end{Bmatrix} \begin{matrix} \\ \\ \text{capture} \\ \\ \text{impact} \end{matrix}$$

Here, $\boldsymbol{\rho} = \mathbf{r} - \mathbf{R}$ and $\dot{\boldsymbol{\rho}} = \dot{\mathbf{r}} - \dot{\mathbf{R}}$. Decomposing $\dot{\boldsymbol{\rho}}$ gives:

$$\dot{\boldsymbol{\rho}} = \dot{\mathbf{r}} - \dot{\mathbf{R}} = (\dot{x} - \dot{X})\hat{\mathbf{i}} + (\dot{y} - \dot{Y})\hat{\mathbf{j}} = \Delta\dot{x}_0\hat{\mathbf{i}} + \Delta\dot{y}_0\hat{\mathbf{j}}$$

where, $\Delta\dot{x}_0$ and $\Delta\dot{y}_0$ are relative velocity components and are constant in time. Integrating this over time gives:

$$\boldsymbol{\rho} = (x - X)\hat{\mathbf{i}} + (y - Y)\hat{\mathbf{j}} = \Delta x\hat{\mathbf{i}} + \Delta y\hat{\mathbf{j}} = (\Delta\dot{x}_0 t + \Delta x_0)\hat{\mathbf{i}} + (\Delta\dot{y}_0 t + \Delta y_0)\hat{\mathbf{j}}$$

6.2 Fixed Trajectory Shooting Method

To solve this optimal control problem, the shooting method is applied [18]. This employs use of the Hamiltonian H to combine the constraints and performance index.

$$H = \frac{1}{2}u_D^2 + \lambda_D \dot{D} + \lambda_\theta \dot{\theta} - \lambda_{\dot{D}} u_D - \lambda_{\dot{\theta}} \frac{2\dot{\theta}\dot{D}}{J_h \left[2D(M_C + M_A/3)\right]^{-1} + D}$$

Taking the partial derivatives of the Hamiltonian with respect to the states gives the differential costate equations $\dot{\lambda} = -H_{\mathbf{x}}$.

$$\begin{cases} \dot{\lambda}_D &= -H_D = -\lambda_{\dot{\theta}} 2\dot{\theta}\dot{D} \dfrac{1 - J_h \left[2D^2(M_C + M_A/3)\right]^{-1}}{\left\{J_h[2D(M_C + M_A/3)]^{-1} + D\right\}^2} \\ \dot{\lambda}_{\dot{\theta}} &= -H_{\dot{\theta}} = -C_\theta + \lambda_{\dot{\theta}} \dfrac{2\dot{D}}{J_h[2D(M_C + M_A/3)]^{-1} + D} \end{cases}$$

Control is resolved from the stationary condition

$$H_{u_D} = 0 = u_D - \lambda_{\dot{D}} \qquad \rightarrow \qquad u_D = \lambda_{\dot{D}}$$

The free final time boundary condition $(\phi_T + \psi_T^{\mathrm{T}} v + H)|_T = 0$ gives:

$$0 = -\Delta\dot{x}_0 v_D - \Delta\dot{y}_0 v_\theta - \frac{1}{2}\lambda_{\dot{D}}^2 + \lambda_D \dot{D} + C_\theta \dot{\theta} - \lambda_{\dot{\theta}} \frac{2\dot{\theta}\dot{D}}{J_h[2D(M_C + M_A/3)]^{-1} + D}\Bigg|_T$$

and the free final state condition $\left(\phi_{\mathbf{x}} + \psi_{\mathbf{x}}^{\mathrm{T}} v - \lambda\right)^{\mathrm{T}}\big|_T = 0$ gives:

$$0 = v_D \cos\theta + v_\theta \sin\theta - \dot{\theta} v_{\dot{D}} \sin\theta + \dot{\theta} v_{\dot{\theta}} \cos\theta - \lambda_D \Big|_T$$

$$0 = -D v_D \sin\theta + D v_\theta \cos\theta - \left(\dot{\theta} D \cos\theta + \dot{D} \sin\theta\right) v_{\dot{D}} + \left(\dot{D} \cos\theta - \dot{\theta} D \sin\theta\right) v_{\dot{\theta}} - C_\theta \Big|_T$$

$$0 = v_{\dot{D}} \cos\theta + v_{\dot{\theta}} \sin\theta - \lambda_{\dot{D}}|_T$$

$$0 = -D v_{\dot{D}} \sin\theta + D v_{\dot{\theta}} \cos\theta - \lambda_{\dot{\theta}}|_T$$

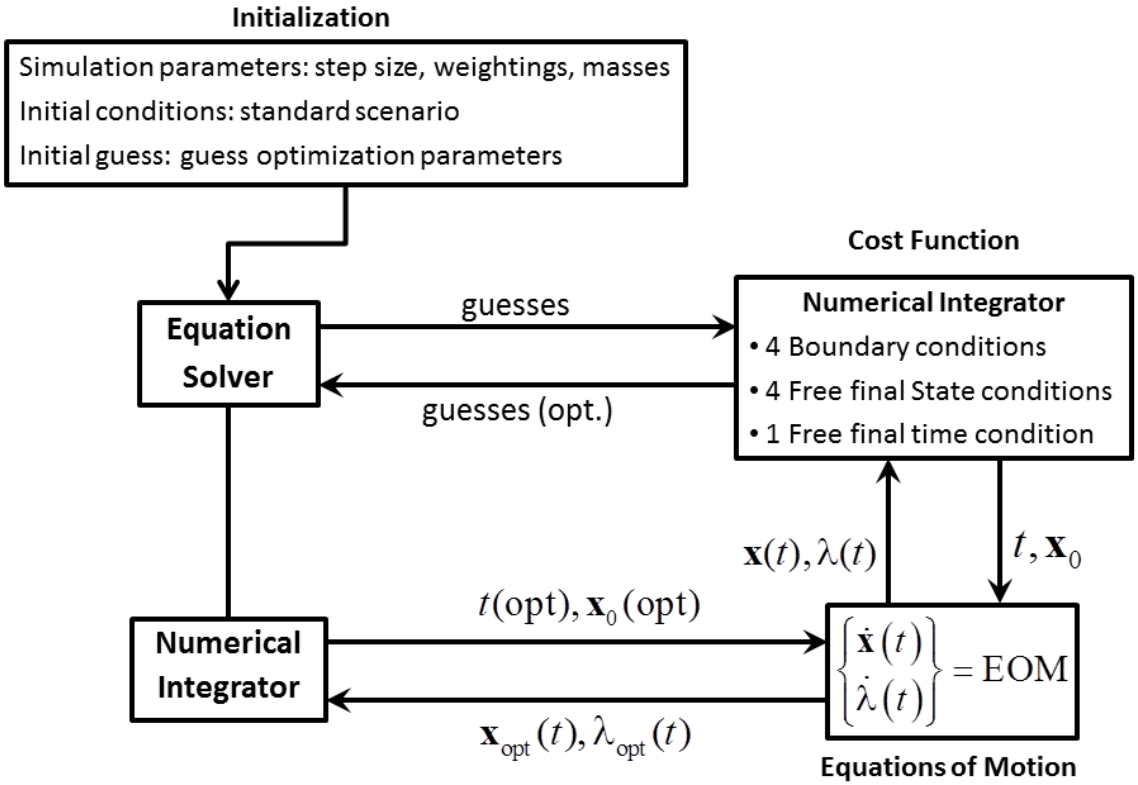

Figure 6.2: Shooting method implementation

With these nine constraint equations (four final state constraints and five boundary conditions), the shooting method is used to solve for the nine unknowns:

$$\lambda_D(0),\ C_\theta,\ \lambda_{\dot{D}}(0),\ \lambda_{\dot{\theta}}(0),\ T,\ v_D(T),\ v_\theta(T),\ v_{\dot{D}}(T),\ v_{\dot{\theta}}(T) \tag{6.3}$$

MATLAB's `fsolve()` function is used to execute the shooting method. The initial conditions, parameters, and guesses are passed into the function where `ode45()` integrates the state and costate equations (inside `fsolve()`) according to these guesses for the nine unknowns. The results from integration are used to evaluate the nine constraint equations `fsolve()` is attempting to satisfy by improving initial guesses and re-evaluating the equations. Figure 6.2 shows the general flow of the applied shooting method.

Weightings W_1 and W_2 are imposed to regulate the capture and impact constraints, respectively. As mentioned earlier, the relation between tangential velocity and arm length is generally prohibitive for zero-impact. Optimization focused on satisfying an insatiable constraint detracts from more imperative objectives. Accordingly, the capture constraint is heavily weighted to ensure priority. Some weighting is still needed on the zero-impact constraint to appreciably influence the response. The following weighting, tolerances, and initial guesses are applied for simulation.

$$\left\{\begin{array}{rcl} N & = & 200 \\ W_1 & = & 1,000 \\ W_2 & = & 100 \\ \text{Max Evaluations} & = & 5,000 \\ \text{Tolerance} & = & 10^{-5} \\ \text{Max Iterations} & = & 10,000 \end{array}\right. \qquad \text{guess} = \left\{\begin{array}{rcl} \lambda_D(0) & = & 230 \\ \lambda_\theta(0) & = & -16.1 \\ \lambda_{\dot{D}}(0) & = & 15.0 \\ \lambda_{\dot{\theta}}(0) & = & 97.3 \\ T & = & 2.99 \\ v_D(T) & = & -6.54 \\ v_\theta(T) & = & 114 \\ v_{\dot{D}}(T) & = & -3.60 \\ v_{\dot{\theta}}(T) & = & 138 \end{array}\right\}$$

Figures 6.3 and 6.4 show the state, control, costate, and constraint history for this solution. The controller's objective is to force the capture constraint to zero, and minimize the impact velocity. This is clearly satisfied by the response. Though no direct circumscriptions are in place, the arm length and arm length rate history show reasonable magnitudes. This is also true of the angular rate. If needed, limitation can be enforced on these values with relative ease. Future controllers may find it necassary to ensure the physical properties of the hardware are not tested.

Numerical values of cost and control effort are conservative (inflated) compared

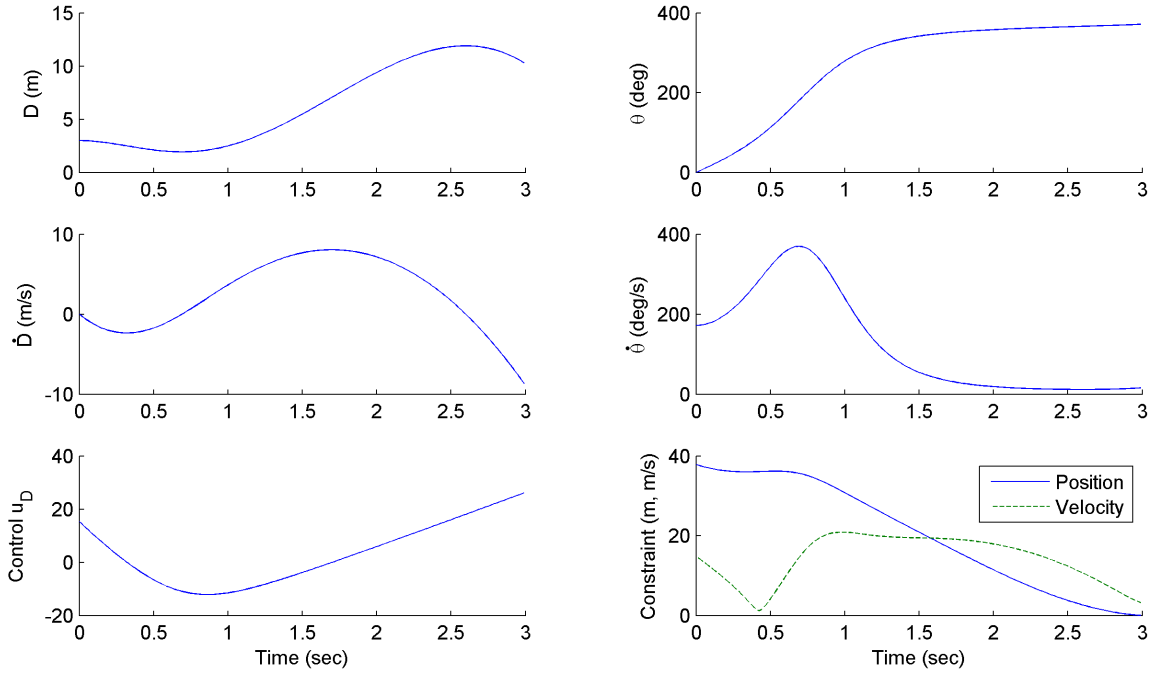

Figure 6.3: State, control, and constraint response

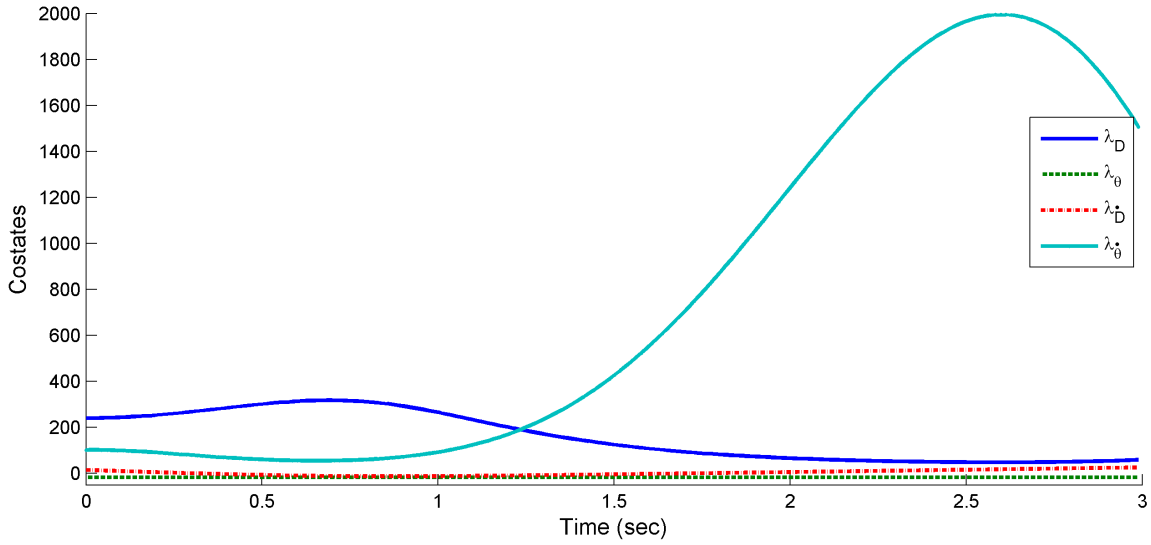

Figure 6.4: Costate response

to a final flown mission. Hardware and dynamics can enact much of the effort that is counted as control here. For example, arm extension happens naturally by centrifugal forces, and the rate may be regulated through controlled friction.

6.3 Controlled Trajectory Capture

In Section 6.1, the trajectories are assumed to pass within an arm's length, and control is restricted to manage arm length only. Doing so isolates the most important function of *Sling-Sat*, capture. This section considers a fuller model by adding planar trajectory control to accomplish more demanding objectives. Some form of trajectory control will be used in a flown mission, so it warrants consideration. It also provides a comparison between control effort versus benefit for the two forms of actuation.

With additional control over satellite trajectory, the cost function has three terms. These terms are independent, allowing the cost function to be decomposed into a scalar equation.

$$J = \frac{1}{2}\int_{t_0}^{T} \left\{\mathbf{u}^T R \mathbf{u}\right\} dt = \frac{1}{2}\int_{t_0}^{T} \left\{R_D u_D^2 + R_X u_X^2 + R_Y u_Y^2\right\} dt$$

u_X and u_Y are control inputs for the satellite's local horizontal and local vertical, or X and Y directions, respectively. To be consistent, all control inputs are accelerations. Required forces are easily determined as needed. R is a weighting matrix that specifies how aggressively to minimize each control input.

Controlling *Sling-Sat*'s trajectory requires its position and velocity to be properly treated as states. A simple force balance yields these equations of motion, giving a total of eight differential equations in the system.

$$\mathbf{x} = \begin{Bmatrix} D \\ \theta \\ \dot{D} \\ \dot{\theta} \\ X \\ Y \\ \dot{X} \\ \dot{Y} \end{Bmatrix}, \qquad \dot{\mathbf{x}} = \begin{Bmatrix} \dot{D} \\ \dot{\theta} \\ -u_D \\ \dfrac{-2\dot{\theta}\dot{D}}{J_h[2D(M_C + M_A/3)]^{-1} + D} \\ \dot{X} \\ \dot{Y} \\ u_X \\ u_Y \end{Bmatrix} \tag{6.4}$$

As before, debris states are determined from initial conditions and the current time, without integrating differential equations.

$$x = \dot{x}_0 t + x_0$$
$$y = \dot{y}_0 t + y_0$$

The final state constraints are:

$$\boldsymbol{\Psi}(\mathbf{x}(T), T) = \mathbf{0} = \begin{Bmatrix} \mathbf{D}(T) - \boldsymbol{\rho}(T) \\ \dot{\mathbf{D}}(T) - \dot{\boldsymbol{\rho}}(T) \end{Bmatrix} = \begin{Bmatrix} X + D\cos\theta - \dot{x}_0 T - x_0 \\ Y + D\sin\theta - \dot{Y}_0 T - y_0 \\ \dot{X} + \dot{D}\cos\theta - \dot{\theta} D\sin\theta - \dot{x}_0 \\ \dot{Y} + \dot{D}\sin\theta + \dot{\theta} D\cos\theta - \dot{y}_0 \end{Bmatrix} \begin{matrix} \\ \\ \text{capture} \\ \\ \text{impact} \end{matrix}$$

6.4 Controlled Trajectory Shooting Method

Even with the additional position states, the shooting method sufficiently accommodates this problem. The Hamiltonian is:

$$H = \frac{1}{2}\left(R_D u_D^2 + R_X u_Y^2 + R_Y u_Y^2\right) + \lambda_D \dot{D} + \lambda_\theta \dot{\theta} - \lambda_{\dot{D}} u_D$$
$$-\lambda_{\dot{\theta}} \frac{2\dot{\theta}\dot{D}}{J_h\left[2D(M_C + M_A/3)\right]^{-1} + D} + \lambda_X \dot{X} + \lambda_Y \dot{Y} + \lambda_{\dot{X}} u_X + \lambda_{\dot{Y}} u_Y$$

The differential costate equations are found by applying $\dot{\lambda} = -H_{\mathbf{x}}$.

$$\dot{\lambda}_D = -H_D = -\lambda_{\dot{\theta}} 2\dot{\theta}\dot{D} \frac{1 - J_h\left[2D^2(M_C + M_A/3)\right]^{-1}}{\left(J_h\left[2D(M_C + M_A/3)\right]^{-1} + D\right)^2}$$

$$\dot{\lambda}_\theta = -H_\theta = 0 \qquad \rightarrow \qquad \lambda_\theta = constant = C_\theta$$

$$\dot{\lambda}_{\dot{D}} = -H_{\dot{D}} = -\lambda_D + \lambda_{\dot{\theta}} \frac{2\dot{\theta}}{J_h\left[2D(M_C + M_A/3)\right]^{-1} + D}$$

$$\dot{\lambda}_{\dot{\theta}} = -H_{\dot{\theta}} = -C_\theta + \lambda_{\dot{\theta}} \frac{2\dot{D}}{J_h\left[2D(M_C + M_A/3)\right]^{-1} + D}$$

$$\dot{\lambda}_X = -H_X = 0 \qquad \rightarrow \qquad \lambda_X = constant = C_X$$

$$\dot{\lambda}_Y = -H_Y = 0 \qquad \rightarrow \qquad \lambda_Y = constant = C_Y$$

$$\dot{\lambda}_{\dot{X}} = -H_{\dot{X}} = -\lambda_X = -C_X \qquad \rightarrow \qquad \lambda_{\dot{X}} = C_X t + \lambda_{\dot{X}}(0)$$

$$\dot{\lambda}_{\dot{Y}} = -H_{\dot{Y}} = -\lambda_Y = -C_Y \qquad \rightarrow \qquad \lambda_{\dot{Y}} = C_Y t + \lambda_{\dot{Y}}(0)$$

Setting the partial derivatives of the Hamiltonian with respect to the control components equal to zero imposes the stationary condition.

$$H_{u_D} = 0 = R_D u_D - \lambda_{\dot{D}} \qquad \rightarrow \qquad u_D = \frac{\lambda_{\dot{D}}}{R_D}$$

$$H_{u_X} = 0 = R_X u_X + \lambda_{\dot{X}} \qquad \rightarrow \qquad u_X = \frac{\lambda_{\dot{X}}}{R_X}$$

$$H_{u_Y} = 0 = R_Y u_Y + \lambda_{\dot{Y}} \qquad \rightarrow \qquad u_Y = \frac{\lambda_{\dot{Y}}}{R_Y}$$

The boundary condition for free final time $(\phi_T + \psi_T^{\mathrm{T}} v + H)|_T = 0$ gives:

$$-\dot{x}_0 v_D - \dot{y}_0 v_\theta + H(T)|_T = 0$$

Finally, the free final state condition $\left(\phi_{\mathbf{x}} + \psi_{\mathbf{x}}^{\mathrm{T}} v - \lambda\right)^{\mathrm{T}}\Big|_T = 0$ gives:

$$0 = v_D \cos\theta + v_\theta \sin\theta - \dot{\theta} v_{\dot{D}} \sin\theta + \dot{\theta} v_{\dot{\theta}} \cos\theta - \lambda_D\Big|_T$$

$$0 = -D v_D \sin\theta + D v_\theta \cos\theta - \left(\dot{\theta} D \cos\theta + \dot{D} \sin\theta\right) v_{\dot{D}} + \left(\dot{D} \cos\theta - \dot{\theta} D \sin\theta\right) v_{\dot{\theta}} - C_\theta\Big|_T$$

$$0 = v_{\dot{D}} \cos\theta + v_{\dot{\theta}} \sin\theta - \lambda_{\dot{D}}|_T$$

$$0 = -D v_{\dot{D}} \sin\theta + D v_{\dot{\theta}} \cos\theta - \lambda_{\dot{\theta}}|_T$$

$$0 = v_D - \lambda_X|_T \qquad \rightarrow \qquad v_D(T) = C_X$$

$$0 = v_\theta - \lambda_Y|_T \qquad \rightarrow \qquad v_\theta(T) = C_Y$$

$$0 = v_{\dot{D}} - \lambda_{\dot{X}}|_T \qquad \rightarrow \qquad v_{\dot{D}}(T) = \lambda_{\dot{X}} = -C_X T + \lambda_{\dot{X}}(0)$$

$$0 = v_{\dot{\theta}} - \lambda_{\dot{Y}}|_T \qquad \rightarrow \qquad v_{\dot{\theta}}(T) = \lambda_{\dot{Y}} = -C_Y T + \lambda_{\dot{Y}}(0)$$

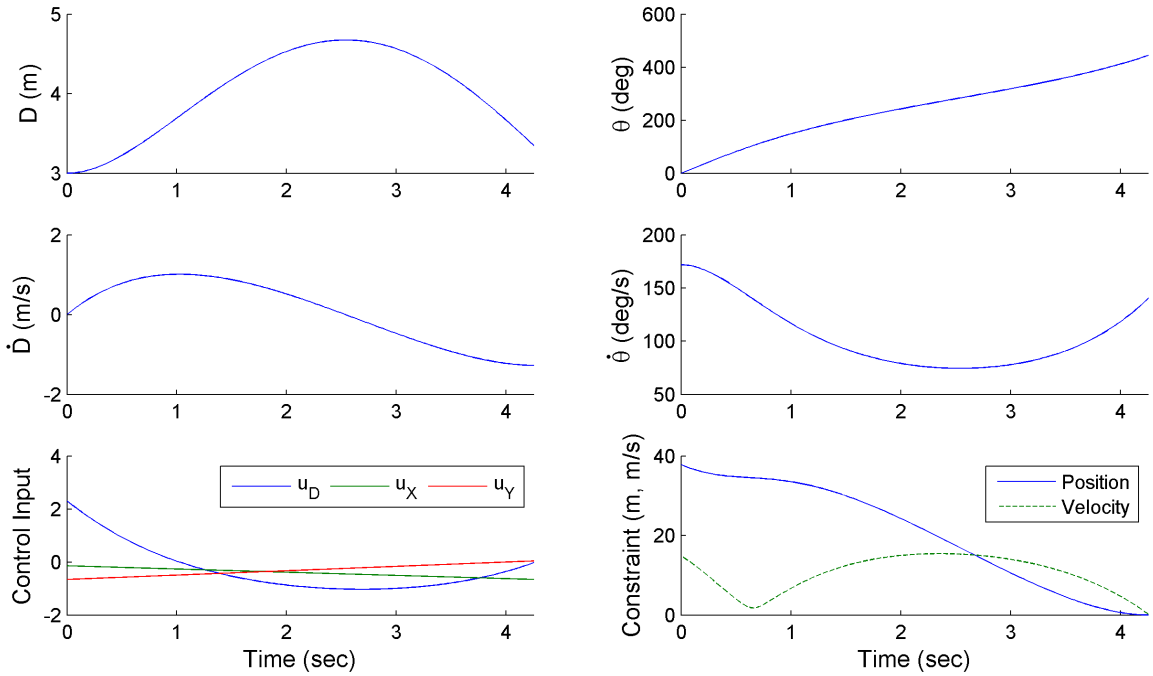

Figure 6.5: State, control, and constraint response with trajectory control

These equations can be combined to solve for all but nine unknowns: the final

time, and eight costates at the initial time.

$$\lambda_D(0),\ C_\theta,\ \lambda_{\dot{D}}(0),\ \lambda_{\dot{\theta}}(0),\ T,\ C_X,\ C_Y,\ \lambda_{\dot{X}}(0),\ \lambda_{\dot{Y}}(0)$$

The shooting method solves for these unknowns using the nine constraint equations (four final state constraints and five boundary conditions) and the following conditions:

$$\left\{\begin{array}{rcl} N & = & 200 \\ W_1 & = & 1 \\ W_2 & = & 2 \\ \text{Max Evaluations} & = & 5,000 \\ \text{Tolerance} & = & 10^{-5} \\ \text{Max Iterations} & = & 10,000 \end{array}\right. \qquad \text{guess} = \left\{\begin{array}{rcl} \lambda_D(0) & = & -.652 \\ \lambda_\theta(0) & = & 1.25 \\ \lambda_{\dot{D}}(0) & = & -2.30 \\ \lambda_{\dot{\theta}}(0) & = & 1.44 \\ T & = & 4.26 \\ \lambda_X(0) & = & -.121 \\ \lambda_Y(0) & = & .165 \\ \lambda_{\dot{X}}(0) & = & .143 \\ \lambda_{\dot{Y}}(0) & = & .658 \end{array}\right\}$$

Figures 6.5 and 6.6 show the state, control, costate, and constraint history for the trajectory controlled solution. The purpose of this controller is to demonstrate how effectively the impacting velocity can be minimized while sustaining priority for capture constraint. The constraint history in Figure 6.5 clearly shows a solution with almost no impact to the collector. Figure 6.7 shows the paths, as well as the configuration of *Sling-Sat* as it executes a nearly tangential capture. Residual non-tangential impact velocity components are compensated for by $\dot{D}$, radial velocity. This demonstrates how the addition of even minor trajectory control is used to unlock the purposed functionality of the hardware design.

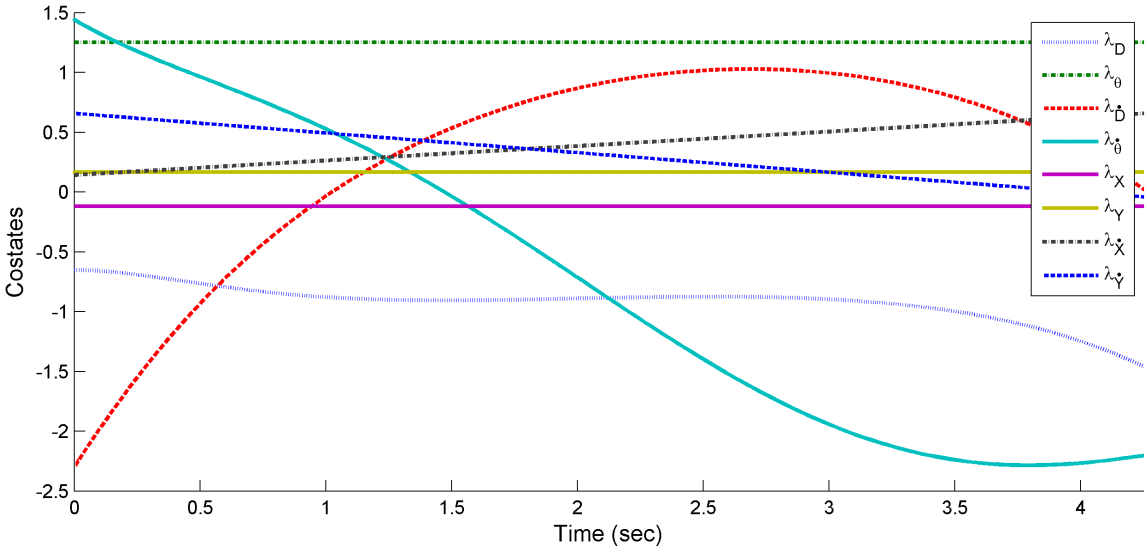

Figure 6.6: Costate response with trajectory control

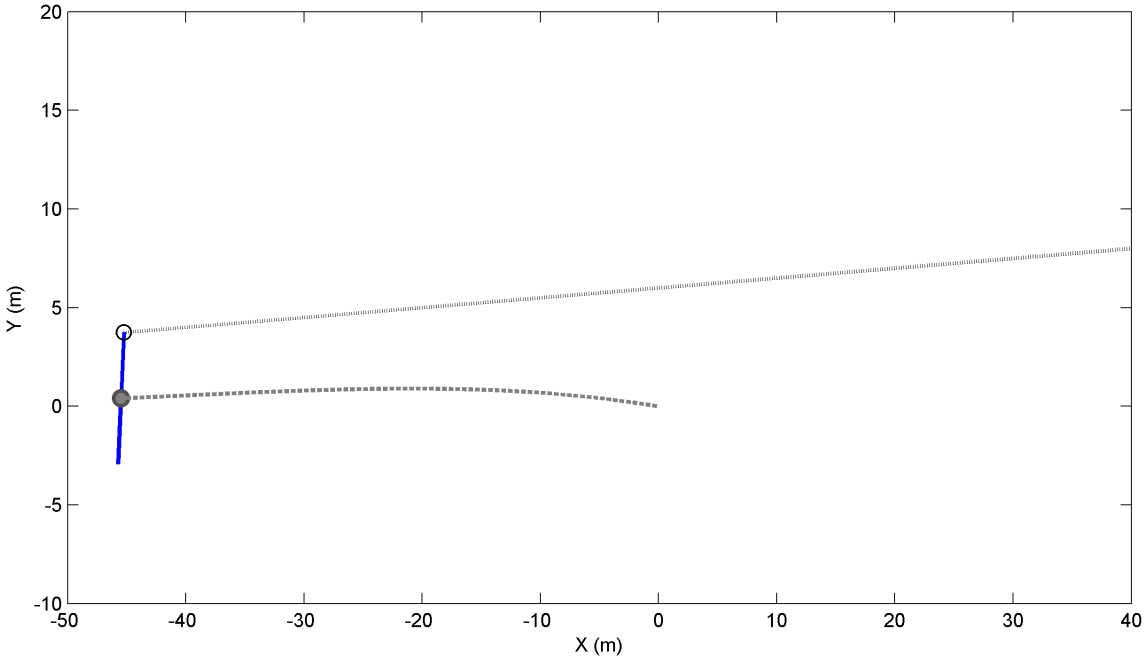

Figure 6.7: Path response with trajectory control

In both scenarios the arm control input is a generalized acceleration; this forces the problem to minimize arm acceleration. In the more general case, where control

is applied as a force, the arm's equation of motion is:

$$\ddot{D} = \dot{\theta}^2 D - \frac{u_D}{2M_C + M_A}$$

Using this model, both controllers work to minimize the input force holding the arms in. As a result, the arms extend to unrealistic lengths. This problem is corrected with the generalized acceleration definition, justified previously by hardware mechanization. Making this distinction is instructive for understanding how modifications to the system influence these optimal control methods. The results of this section are preliminary, and meant to establish feasibility of controlling *Sling-Sat*. More detailed control work awaits progress in hardware design.

7. ORBITAL ANALYSIS

A universal obstacle for active space debris removal is that object masses are unknown. The challenge is heightened for *4S* because it depends on exploiting momentum exchanges, which are intimately tied to mass. A fundamental understanding of velocity–the remaining variable in momentum–assuages uncertainty when predicting these events. This section analyzes orbital velocity responses to capture and ejection. Ejection events are the primary focus, but the principles translate to capturing debris as well.

To begin, excogitate the axiological question: Which requires greater ΔV to deorbit, a higher or lower altitude orbit? Basic celestial mechanics say that higher orbits have lower speeds, and therefore require less ΔV to reduce to a fixed speed (e.g., $V = 0$). This is evident in the vis viva equation,

$$V = \sqrt{\mu \left(\frac{2}{R} - \frac{1}{a} \right)} \tag{7.1}$$

where, V is the velocity at position R in an orbit with semi-major axis a. As a increases, the orbit gets "larger," and V decreases. However, the target speed to reenter is not a fixed value for all orbits. This is demonstrated with a straightforward example.

For concurrence, observe only circular orbits with radius R_{cr}. The semi-major axis of a circular orbit a_{cr} is equal to its radius, $a_{cr} = R_{cr}$. Applying this to Equation (7.1) gives the circular velocity.

$$V_{cr} = \sqrt{\frac{\mu}{R_{cr}}} \tag{7.2}$$

The most efficient way to deorbit is a transfer orbit with a radius of perigee that exactly matches the radius to the upper atmosphere R_{atm}. Here, $R_{atm} = 6,7281$ km is taken to be the radius of the Earth, plus 350 km of atmosphere. When deorbiting from a circular orbit in this way, the point of departure is the apogee of the transfer orbit $R_a = R_{cr}$, and the semi-major axis is the average of the perigee and apogee $a_{tr} = \dfrac{R_{atm} + R_{cr}}{2}$. Applying Equation (7.1) gives the required velocity at apogee of the transfer orbit.

$$V_a = \sqrt{2\mu \left(\frac{1}{R_{cr}} - \frac{1}{R_{cr} + R_{atm}} \right)} \tag{7.3}$$

The difference $\Delta V = V_{cr} - V_a$ is the required impulse to deorbit.

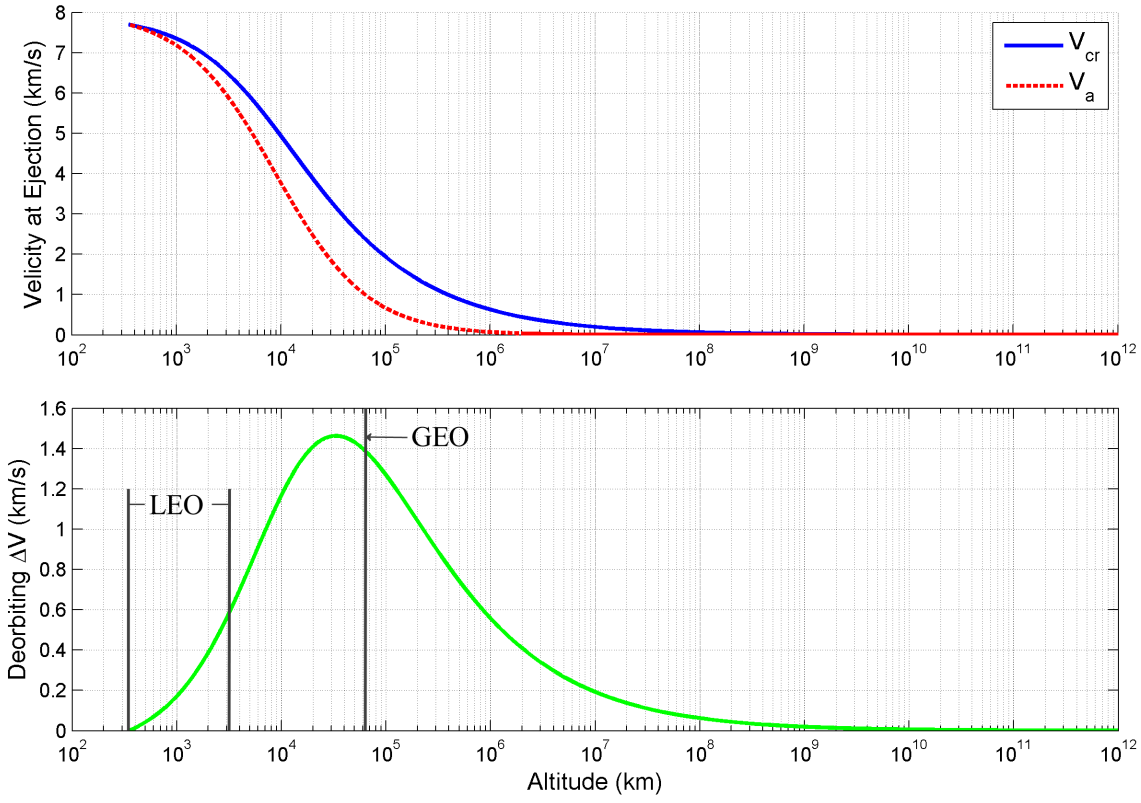

Figure 7.1: Long-range deorbit

Observing Equations (7.2) and (7.3) for a large range of circular orbit altitudes, Figure 7.1 illustrates how deorbiting impulse increases up to $\Delta V = 1.463$ km/s at

an altitude of 33.2 Mm. Above this altitude, the ejection impulse asymptotically decrease to zero, and becomes sensitive to error. At GEO, orbit velocities are very low, and the ejection impulse is near maximum. This relationship is influential when considering operation altitude. The higher orbital speeds and lower ejection velocity demands of LEO are ideal conditions for *4S*. Coincidentally, LEO is also home to the largest and most threatening debris populations. In addition, GEO poses three specific challenges for operating a *4S* mission: 1) ejected debris that does not deorbit will return to the GEO belt with magnified collision risk, 2) perigee reduction demands are very high and, 3) the tightly banded field is prohibitive for path optimization.

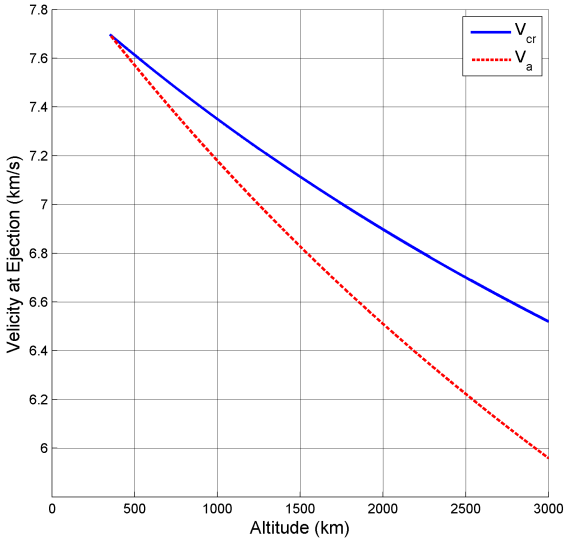

Figure 7.2: Speeds at ejection

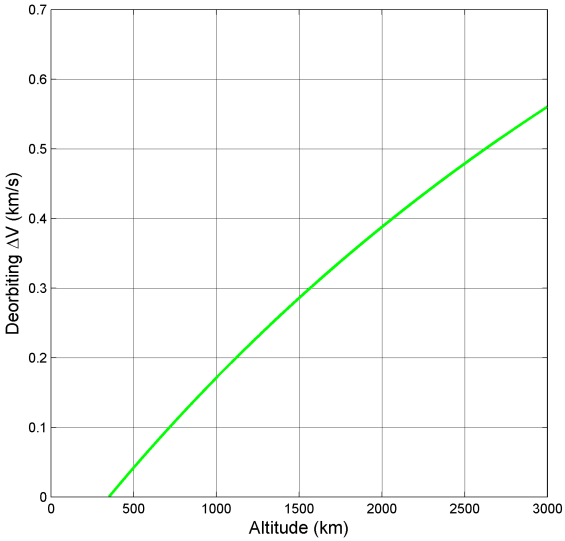

Figure 7.3: ΔV required to deorbit

Figures 7.2 and 7.3 span LEO altitudes pertinent to the space debris problem. Narrowing the scope permits linear scaling, and a more insightful perspective on how circular orbit velocity decreases with altitude, as does the required deorbiting velocity V_a. Figure 7.3 shows ΔV increasing with altitude, despite the constituent velocities decreasing. Knowledge of this is helpful for tuning path optimization. If

impact velocities are too high, or ejections are too demanding, altitude can be shifted accordingly.

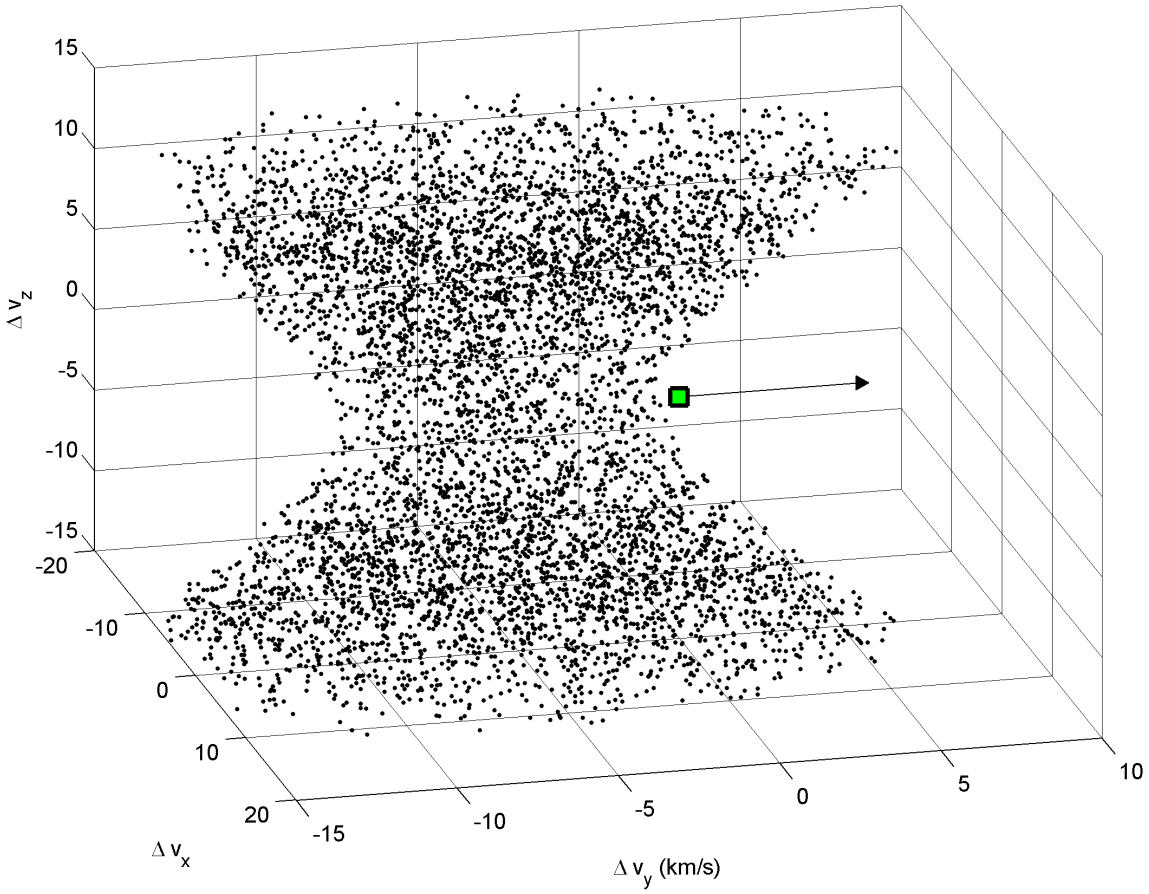

Figure 7.4: Impacting velocities for LEO example

To develop an intuition of deorbiting requirements in three dimensions, a Monte Carlo simulation is used to consider a large number of ejection scenarios. Starting from a satellite in a representative orbit, defined in the Earth-Centered Inertial (ECI) frame by $\mathbf{R} = \{0;\ 0;\ 11,100\}^{\mathrm{T}}$ km and $\mathbf{V} = \{5.62;\ 0;\ 0\}^{\mathrm{T}}$ km/s, debris is given a random relative ejection velocity $\Delta\mathbf{v}$ with respect to the satellite. With an inertial ejected velocity of $\mathbf{v} = \mathbf{V} + \Delta\mathbf{v}$, the debris' resulting perigee is determined according to $r_p = a\,(1 - e) \leq R_{atm}$, where R_{atm} and r_p are the respective atmosphere and perigee radii, and the condition $r_p \leq R_{atm}$ is the criteria to deorbit. This gives a point

cloud to visualize the shape of successful ejection velocities. Note that deorbiting debris does not necessarily mean a direct Earth-impact, if the perigee is lowered enough, atmospheric drag reduces the debris lifetime [2]. The semi-major axis a and eccentricity e are evaluated from energy and eccentricity vector expressions, $a = \dfrac{\mu\, R}{2\mu - R\, v^2}$ and $e = \left| \dfrac{\mathbf{v} \times (\mathbf{R} \times \mathbf{v})}{\mu} - \hat{\mathbf{R}} \right|$, thus obtaining the condition to deorbit.

$$R_{atm} \geq r_p = \frac{\mu\, R}{2\mu - R\, v^2} \left[1 - \left| \frac{\mathbf{v} \times (\mathbf{R} \times \mathbf{v})}{\mu} - \hat{\mathbf{R}} \right| \right]$$

Given 25,000 randomly chosen ejection impulses, Figure 7.4 shows the cloud marking the end points of deorbiting impulses. In other words, each relative impulse vector starts at the origin and terminates at its respective point in the cloud. The impulse randomization is uniform and spans the plotted range. Its intent is simply to populate the cloud, not analyze distributions. The arrow points along the satellite's inertial velocity, and the square at the origin marks the satellite's velocity relative to itself (i.e., zero).

Though specific scenarios vary, this cloud gives the characteristic shape of ejection requirements for most relevant orbits. Shape and orientation of the point cloud depends on shape and orientation of the satellite's orbit, as well as the position within it. Higher orbits have an elongated cloud. The minimum impulse required to deorbit debris is the point closest to the origin, which is an impulse of 0.41 km/s, in this scenario. The outer surface of the hourglass shape (which extends predictably beyond the limits plotted) represents the boundary velocities that are exactly deorbiting, $r_p = R_{atm}$. It also contains the minimum impulse case, which is the goal for efficiently ejecting debris. The equation of this surface is clearly of interest; however, the cross products used in determining the radius of perigee prevent a closed form solution from readily being backed out. To circumvent this, the two-dimensional case is analyzed,

where ejected debris remains in the satellite's orbital plane. This is a relevant subset of trajectories, as they are the most efficient paths to re-enter.

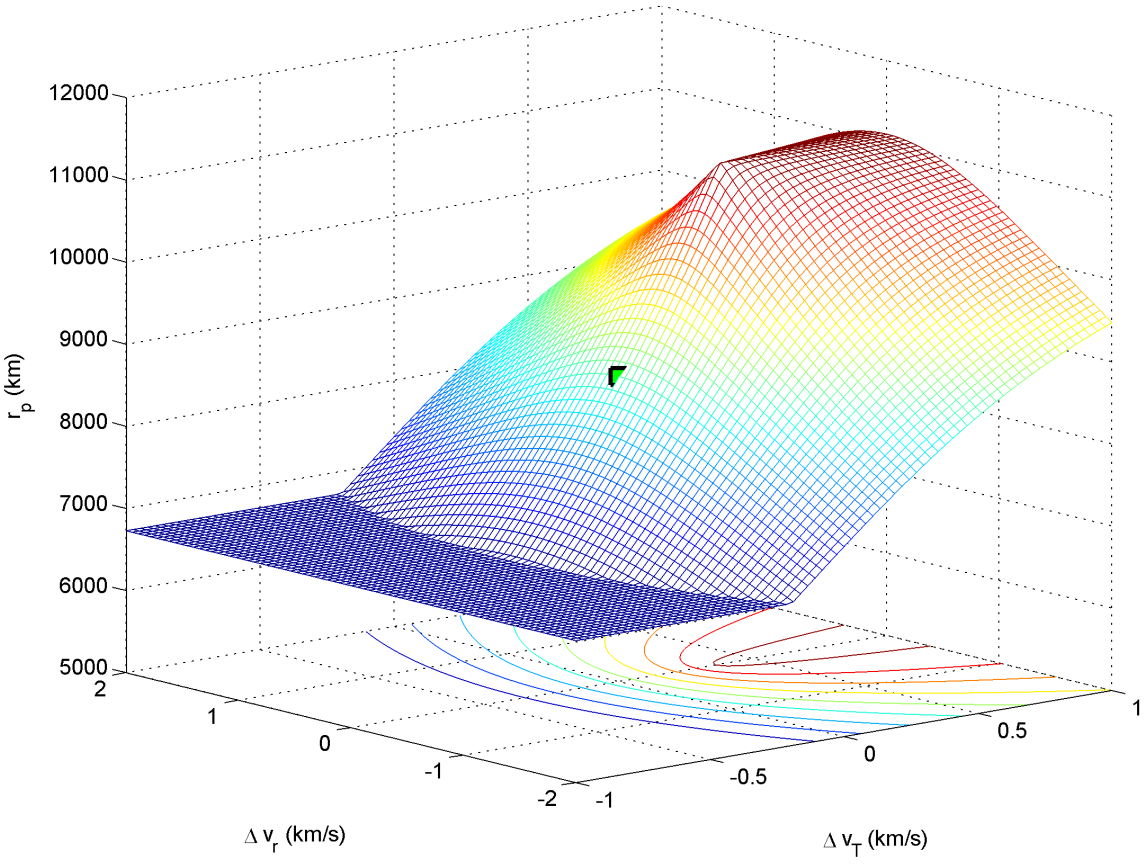

Figure 7.5: Planar ejection perigee mesh

Decomposed into radial and tangential velocity components, the mesh in Figure 7.5 depicts the associated radii of perigee for in-plane ejection impulses. The surface changes depending on the state of the satellite at ejection, but this decomposition shows the qualitative trend for a large set of initial orbits. The square marks the original perigee, $R_p = 8,713$ km. The constraint $r_p \geq R_{atm}$ is enforced, evidenced by the "deorbiting plane" at $r_p = 6,728.1$ km. Projected contours of this mesh are included to further characterize the surface. The contour corresponding to the leading edge of the deorbiting plane is the locus of all minimum deorbiting impulses

over a range of ejection angles.

Ejecting debris also modifies the satellite's orbit. It is insightful to discern how critical orbital elements of both the satellite and debris are altered by these events. This is analyzed for a specified initial orbit ($a_0 = 10,000$km and $e_0 = .3$) of the combined debris/satellite system, and an energy difference $\Delta\mathcal{E} = 2.5$ J to describe the ejection. Plastic collisions do not conserve kinetic energy; therefore, the debris and satellite impulses are respectively determined according to:

$$\Delta v = \sqrt{\frac{2M\Delta\mathcal{E}}{m(M+m)}}, \quad \text{and} \quad \Delta V = \sqrt{\frac{2m\Delta\mathcal{E}}{M(M+m)}}$$

where, $M = 200$ kg and $m = 3.1$ kg correspond to the satellite and debris masses, respectively. The apogee, perigee, semi-major axis, and eccentricity are calculated for both objects as the eccentric anomaly E and ejection angle α are fully swept.

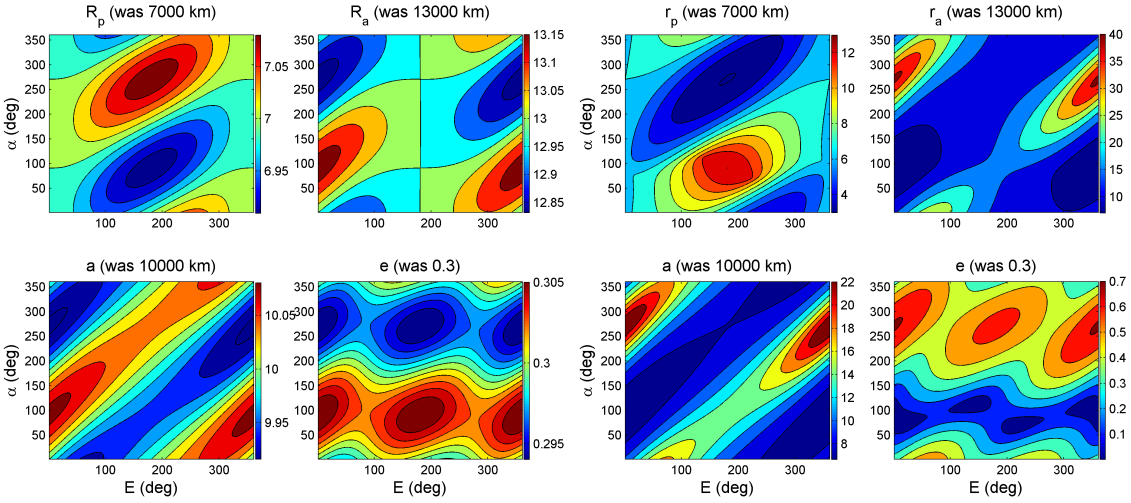

Figure 7.6: Satellite response to ejection

Figure 7.7: Debris response to ejection

Figures 7.6 and 7.7 map the resulting parameter variations for the satellite and debris, respectively. Areas where the parameters increase are red, and areas where they decrease are blue. This analysis shows a heavy dependence of resulting orbits on

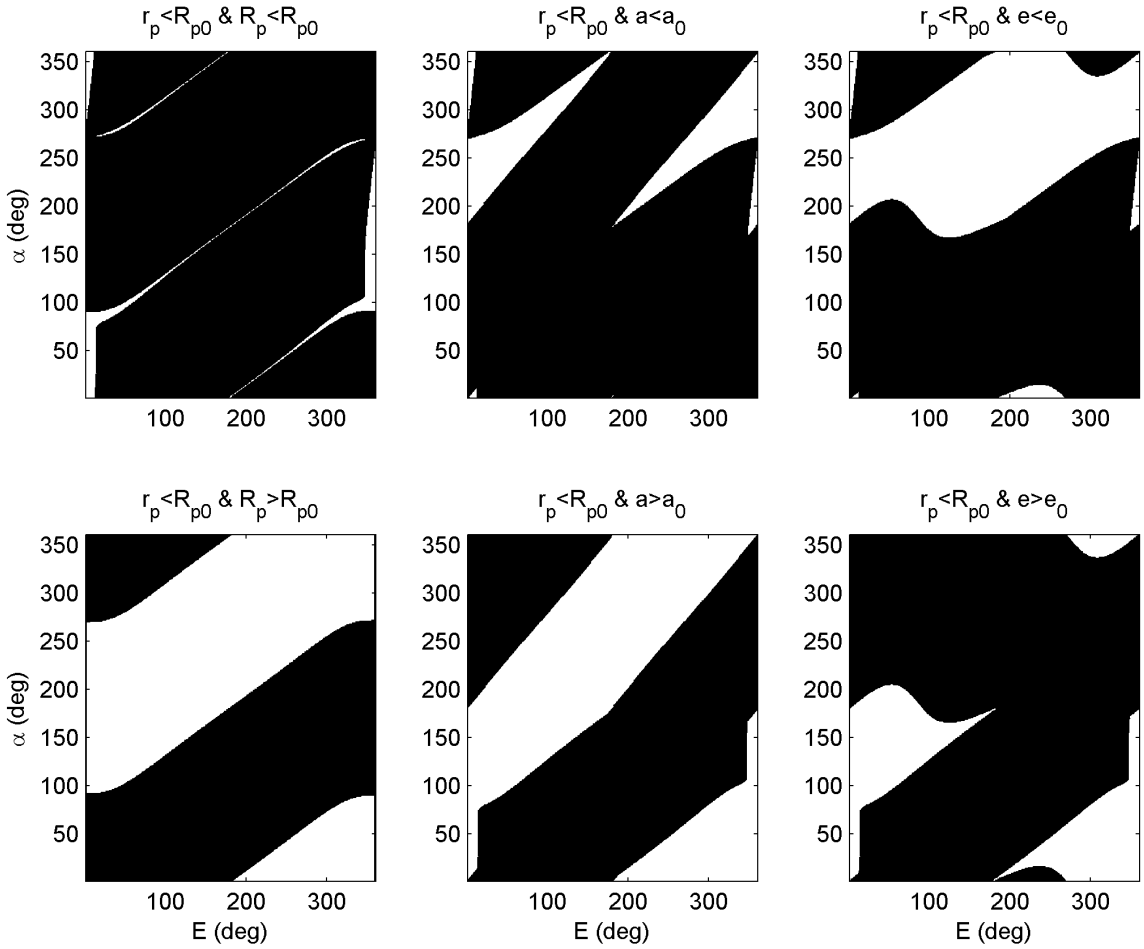

Figure 7.8: Saturated orbit response comparison

the ejection angle and location within an orbit. Comparing the two orbits confirms a loose inverse correlation in parameter variations, but it is not stringent. This suggests scenarios exist where an ejection (or capture) will have counter intuitive resulting orbits. The task now is finding useful ways to exploit this.

An initial concern regarding *4S* is that repeatedly ejecting debris "downward" may cause *Sling-Sat*'s orbit to grow beyond its targeted debris cloud. Figure 7.8 investigates this by showing the response of the satellite for cases where debris perigee is reduced. For clarity, the plots are saturated such that white regions satisfy both conditions being observed. The 0 subscript denotes the values before ejection. Fil-

tering the data in this way highlights the exceptions to intuition. Most significantly, that there are regions where the perigee of *both* objects can be reduced. Furthermore, at every location in the orbit E, there exists an ejection angle α that will reduce both perigees. This is a provocative result, because it shows potential for orbital maintenance to be worked into the mission, without impeding the removal objective.

8. PATH SEQUENCE OPTIMIZATION*

Consider the gravity assist technique. In this opportunistic method, well-timed maneuvers allow a spacecraft to steal momentum from other bodies to extend its scope. Similarly, *4S* is an opportunistic method that harvests debris momentum through precise choreography. However, the choreography is much more abstract for *4S*. The nearly infinite impulse, timing, and event order combinations makes discovering beneficial paths a formidable challenge. This section serves to establish and demonstrate the feasibility of finding such paths through application of an evolutionary search optimization algorithm [21]. To accomplish this, a mission simulation is built, and the results are discussed.

8.1 Scenario

Though the physical principles of *4S* can be scaled to accommodate objects of varying size in any earth orbit, this simulation focuses on "medium–small" debris in LEO, removing objects as large as a micro-satellite. Only debris fields from the 2007 anti-satellite missile test and 2009 Cosmos/Iridium collision are considered, making this a cleanup mission to prevent feedback collisions. The masses of these cataloged objects are unknown, this is incorporated in the simulation by strategically redefining them at key junctures.

Sling-Sat is appropriately modeled as a spinning satellite with collectors at the ends of adjustable arms. Rotation rate is controlled by adjusting the arm lengths. The relative ejection velocity is simply the tangential velocity of the contained debris. Ejected debris is sent into a lower perigee orbit, or to directly re-enter the Earth's

*Portions reprinted with permission from "Optimization of Debris Removal Path for TAMU Sweeper" by Jonathan Missel and Daniele Mortari, 2012. Advances in Astronautical Sciences, volume 143, pages 935–945, Copywrite 2012, Advances in Astronautical Sciences.

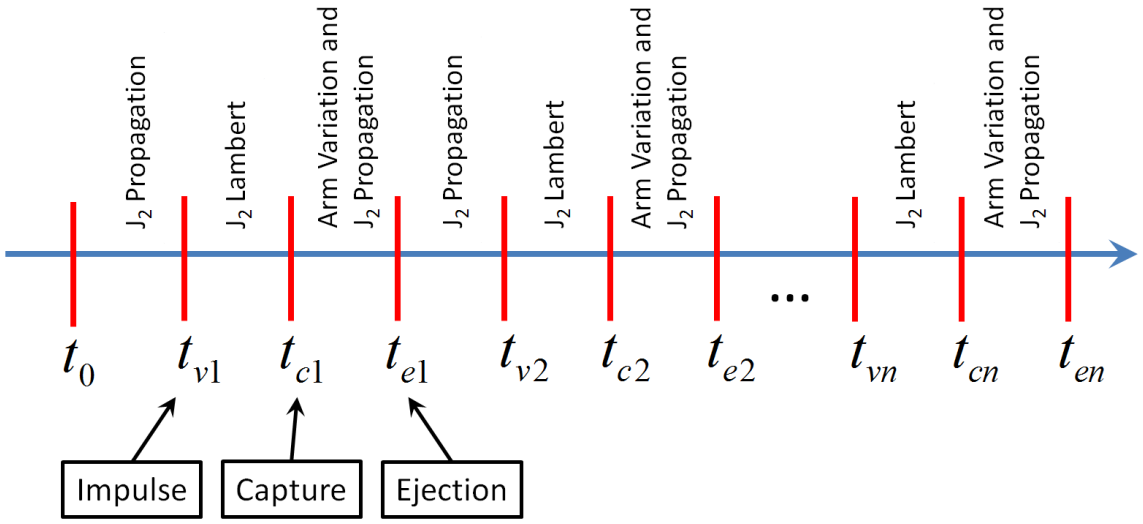

Figure 8.1: Time sequence

atmosphere.

Each debris interaction has three orbital maneuvers associated with it. In order, these are a fuel consuming impulse, a free impulse from capture, and a free impulse from ejection. Figure 8.1 shows the order of events and interim propagations as they repeat. The optimization scheme works to minimize the fuel consuming impulses while maximizing effective debris perigee reductions for deorbit.

8.2 Simulation

This section outlines the simulation procedure, various elements of which are expanded upon in later sections. Following the main simulation structure shown in Figure 8.2, debris are first read into a catalog, propagated to a common initial time,[1] and then filtered such that only a select group of "close" objects remain (see Section 8.4.1). Then constants and variables are defined. These include physical properties of *Sling-Sat*, randomly generated debris masses, optimization options, initial guesses, and mission length (defined by the number of debris interactions). Next, a mission

[1] J_2 perturbations are considered for all propagations in this simulation.

loop is executed for each debris interaction. Within this loop, a Genetic Algorithm (GA) is applied for a seeded or random initial guess (see Section 8.3). The GA refines these genes and outputs the set yielding the lowest value of the fitness function. These results are applied to the simulated mission (see Section 8.4.4) using redefined debris masses to mirror the reality that they are unknown. The resulting behaviors of this simulation are stored and updated accordingly. Based on the current orbit of *Sling-Sat*, a new filtered catalog is generated. Deorbited debris is removed from the catalog to avoid future consideration. The loop is then repeated for the next interaction in the mission. If the mission is over, the results are output and plotted.

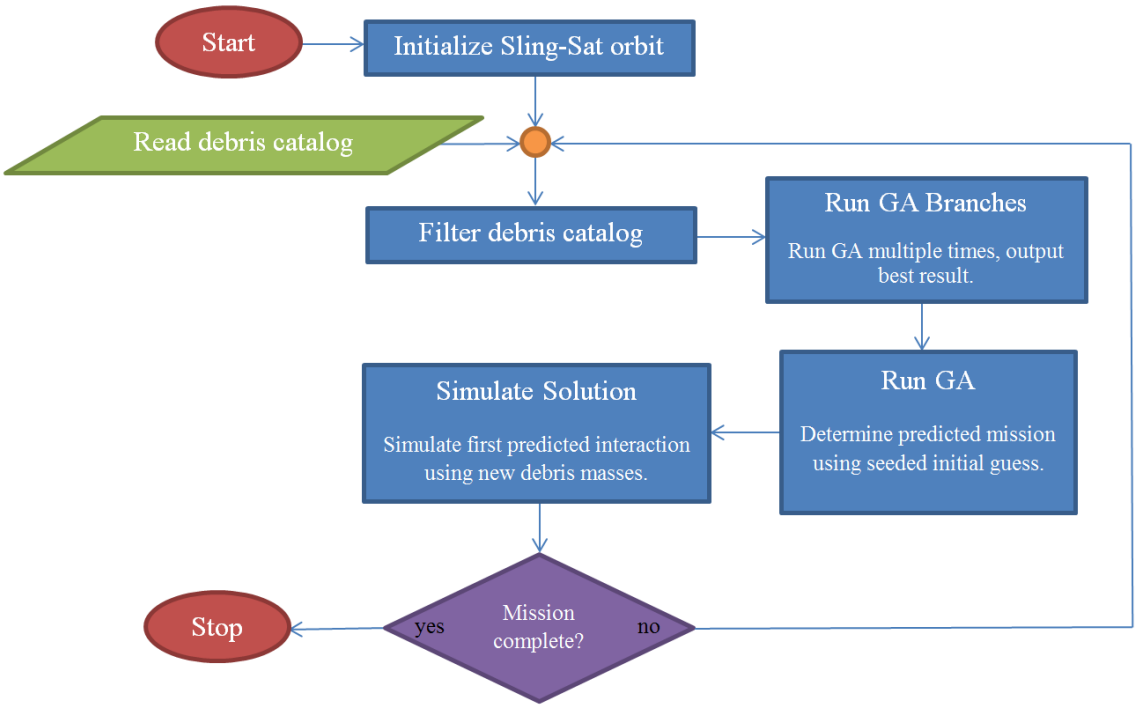

Figure 8.2: General simulation flow

Within this process are several options which tune the search–two are significant enough to modify the structure of the procedure: using a predicted mission, and using (what will be referred to as) the branch method. The branch method is simple. By nature, multiple runs of a GA may arrive at different conclusions for what to call the

optimal solution. Sometimes it gets stuck at a poor solution due to local minima. Just one instance of this compromises an entire mission. To hoodwink this, the GA can be applied several times for each interaction. These solutions are branches, and the best is chosen to seed a final GA application. This prevents rogue solutions from corrupting the mission.

To explain and justify a predicted mission, perpend the following: In the game chess, a player's current move is most wisely chosen after thinking ahead by two or three moves.[2] The optimization process uses the same approach to improve its results. When applying the GA, a small predicted mission of n interactions is evaluated. Only the first predicted interaction is applied to the simulated mission; this is done using different debris masses than those assumed in the GA. The predicted mission is re-evaluated after each interaction with debris of uncertain mass. Predictions beyond the first interaction, which are not directly applied to the mission, are used to seed favorable initial guesses for the next prediction. This approach sets up for the next move by thinking of the broader mission. The second predicted interaction becomes the initial guess for the first interaction in the next step, and so on.

Figure 8.3 shows an illustrative schematic of how this works for a mission with two interactions, and $n = 2$ predicted interactions. Note that this figure only tracks the discrete velocity impulses versus time, while variations from orbital propagation are ignored for simplicity. The first prediction starts at the beginning of the mission. Error between the predicted and applied mission is introduced at the first capture t_{c1} due to unknown debris mass. The ejection at t_{e1} also has uncertainty. However, a new predicted mission is enlisted, and it is without error until the next capture at t_{c2}. Predictions are updated after every interaction, and unapplied predicted interactions

[2]Thinking beyond this is of little use. It requires an exhausting amount of mental energy, and distant predictions are inaccurate due to unpredictable elements of the game.

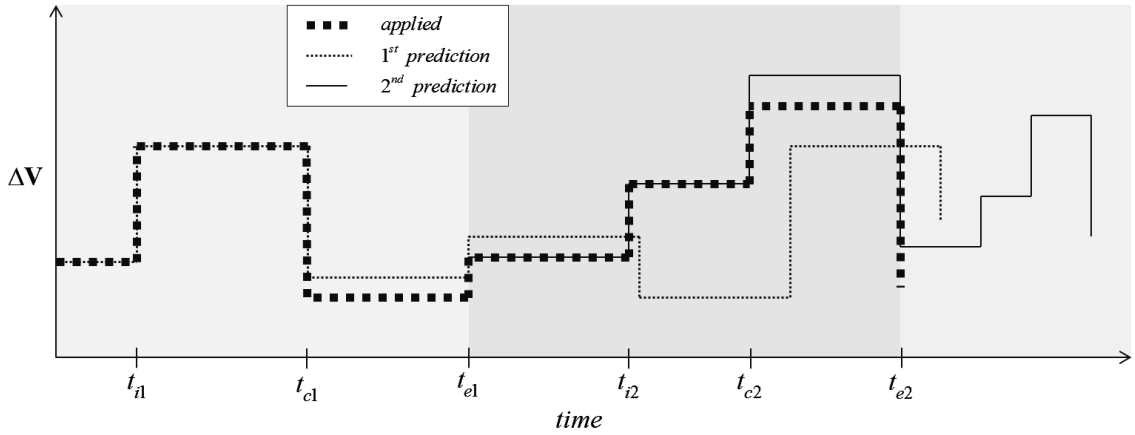

Figure 8.3: Sample $n = 2$ predicted mission

are used to seed subsequent predictions.

8.3 Genetic Algorithm and Fitness Function

In a Genetic Algorithm, each member of a population is given a set of genes that is applied to a fitness function. The fitness function is a simulation that outputs a single value quantifying the cost associated with that set of genes. When every member of the population has a cost assigned, the next generation of the population is formed based on the previous genes with crossover and mutations. Following a simplified version of the theory of evolution, the GA gives successful genes higher probability to be passed to the next generation. The goal is to find the set of genes yielding the lowest cost. MATLAB's `ga()` function, in their optimization toolbox, is used for this application.

To assign cost, the overall mission objectives are considered: save fuel and mitigate the debris problem. As mentioned in Section 8.2, a predicted mission, of assigned length n objects, is considered at this stage. Therefore, cost J is assigned according to Equation (8.1) based on the total fuel requirements of the predicted mission, $\Delta\mathbf{V}_{\text{tot}}$, and the change in perigee of the ejected debris, Δr_p.

$$J = \frac{\Delta \mathbf{V}_{\text{tot}}}{\sum_{k=1}^{n} \Delta r_{pk}} = \frac{\sum_{k=1}^{n} |\, \Delta \mathbf{V}_k \,|}{\sum_{k=1}^{n} \Delta r_{pk}} \tag{8.1}$$

Let $r_{p\,\min} \equiv 6,728$ km (350 km above Earth's surface) be the minimum allowable perigee before atmospheric drag is trusted to deorbit an object [2]. If the k-th ejected debris of the predicted mission has a perigee below this altitude, then the debris is considered removed. In this case, the distance from the perigee to the atmosphere of the original debris orbit $\Delta r_{pk} = r_{pk_{original}} - r_{p\,\min}$ is used for calculating cost. This modification prevents rewarding overly aggressive ejections, without restricting them (as the resulting free impulses may be desired).

The perigee and impulse values needed to calculate the fitness function cost are extracted from a simulated mission orchestrated by $6n$ genes. These $6n$ genes specify:

- n impulse, n capture, and n ejection times (t_{vk}, t_{ck}, t_{ek},)
- n debris selection indices (I_k) in the active debris catalog
- n ejection arm lengths (D_{ek})
- n relative debris ejection angles (α_k)

Using these $6n$ genes, the fitness function simulates a mission that interacts with n debris within a specified total maximum time $T_{\max}$. Following the timeline in Figure 8.1 and the flowchart in Figure 8.4, the simulation loops through the event sequences for each of the n predicted debris interaction. Note, the k subscript is excluded (with a few exceptions) from here on, with the understanding that the k-th interaction is being observed. From the current time, *Sling-Sat* is propagated to the gene-specified impulse time. The target debris is then selected. This selection is ultimately made

by a gene, but the active catalog is preprocessed (in addition to, and after, filtering) to give higher probability to promising objects. Probability is based on estimated costs-to-transfer, which are detailed in Section 8.4.2.

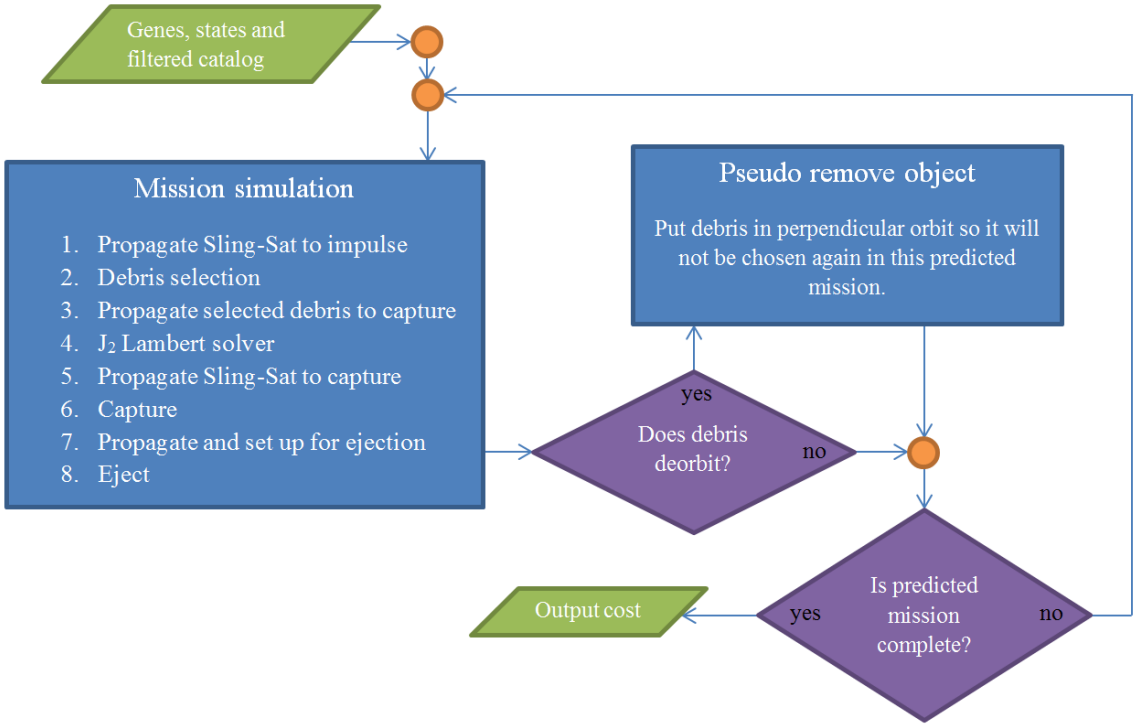

Figure 8.4: General fitness function flow

Selected debris is propagated to the gene-specified capture time. This presents a two-point boundary value problem to determine the impulse $\Delta\mathbf{V}_k$ needed for *Sling-Sat* to intersect the debris at the capture time. A J_2-compliant Lambert solver is used to derive this (see Sections 8.4.3). This is the only fuel-consuming impulse of the k-th debris interaction, making it the only impulse contributing to the cost in Equation (8.1). Given $\Delta\mathbf{V}_k$, *Sling-Sat* is propagated to the time and point of capture.

Capture is simulated with rigid body motion using conservation of angular and translational momenta. It is assumed that *Sling-Sat*'s angular velocity is orthogonal

to the debris' relative impacting velocity at capture. For the sake of definition, Figure 8.5 shows the collector mass M_C, arm length D_c, arm mass M_A, hub mass M_h, hub moment of inertia J_h, debris mass m_k, debris velocity $\mathbf{v}$, and *Sling-Sat* velocity $\mathbf{V}$. *Sling-Sat*'s arms are assumed to move in unison. Figure 8.6 shows the notation used to distinguish variables before and after capture and ejection. Subscript "c" represents states immediately prior to capture, "$c+$" is immediately after capture, "$e-$" is immediately prior to ejection, and "e" is immediately after ejection.

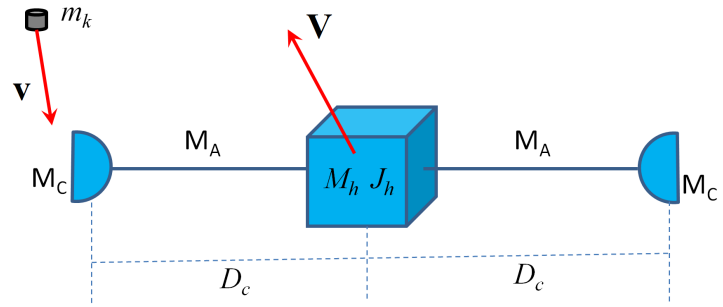

Figure 8.5: Model components

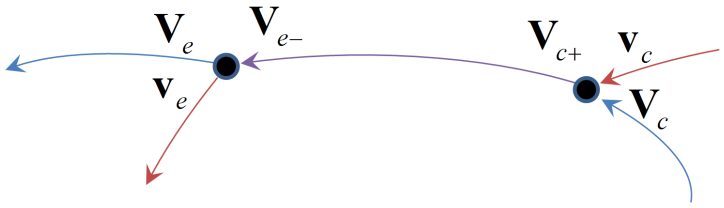

Figure 8.6: Event notation

The velocity after capture is derived from the translational momentum equation,

$$m_k \, \mathbf{v}_c + M \, \mathbf{V}_c = (M + m_k) \, \mathbf{V}_{c+}$$

where, $M = M_h + 2M_C + 2M_A$ is the total mass of *Sling-Sat*. The moment of inertia

(with arms at length D_c) is:

$$J_{Dc} = J_h + 2M_C D_c^2 + \int_{D_c-2L}^{D_c} M_A x\, dx + \int_{-D_c}^{2L-D_c} M_A x\, dx = J_h + 2D_c^2 \left(M_C + \frac{M_A}{3} \right)$$

At the beginning of the simulation and after each ejection, the arms are extended to a standard length of $D_c = 5$ m. The resulting angular velocity ω_{0k} is the angular velocity prior to capture $\omega_c = \omega_{0k}$. The planar angular momentum equation gives the angular velocity after capture ω_{c+},

$$J_{Dc}\, \omega_c + m_k D_c v_{rel} = (\, J_{Dc} + m_k D_c^2 \,)\, \omega_{c+}$$

where, $v_{rel} = |\mathbf{v}_c - \mathbf{V}_c|$ is the relative velocity of the debris with respect to the satellite and is assumed to be orthogonal to the arm at capture.

Note that in practice, the debris' relative velocity to the *collector* at capture will be minimal, *even zero* (which also requires nearly orthogonal capture). This is enforced by the capture controller developed in Section 6. Through actuation of the arm lengths, *Sling-Sat*'s reach and rotation are controlled to ensure the debris and collector intersect for capture. In addition, the controller has an optimization objective to intersect with zero relative impact velocity for the collector. Though critical to the final mission, high fidelity aspects, such as capture control, are not incorporated in this simulation. Their impact on the broader mission is minimal, and their level of detail detracts from the true objective of path sequence optimization.

After capture, the orbit of the combined system is propagated to the gene-specified ejection time. Preparations for ejection are made during this flight. Changing geometry to the gene-specified ejection arm length D_e alters *Sling-Sat*'s moment

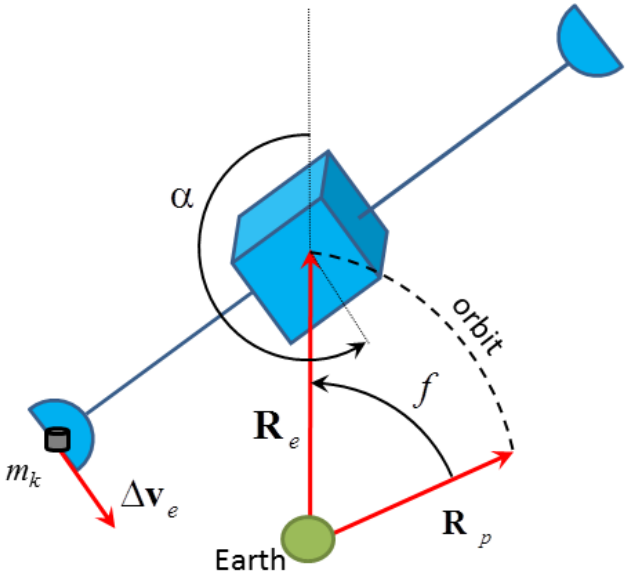

Figure 8.7: Ejection angle convention

of inertia.

$$J_{De} = J_h + 2D_e^2 \left(M_C + \frac{M_A}{3} \right)$$

Conservation of angular momentum then gives ω_{ek-}, *Sling-Sat*'s angular rate prior to ejection.

$$(J_{Dc} + m_k D_c^2) \omega_{c+} = (J_{De} + m_k D_e^2) \omega_{e-}$$

As with capture, ejection is modeled using basic conservation principles and careful sorting of reference frames. With the debris onboard, the distance from the center of the satellite to the combined center of mass is changed to $L_{cm} = \dfrac{m_k D_e}{M + m_k}$. Ejection velocity is determined by a combination of the ejection arm length and the ejection angle α, defined as the direction of the relative ejection velocity as measured from the local position vector with respect to the Earth. Following the convention of Figure 8.7, the relative tangential velocity of the ejected debris is expressed in the

body frame as:

$$\Delta \mathbf{v}_e^{body} = \omega_{e-}(D_e - L_{cm})\,\hat{\mathbf{i}}_\theta$$

This is rotated from the body frame into the Local Vertical Local Horizontal (LVLH) frame and then into the orbit frame through the ejection angle and the true anomaly f, collectively.

$$\Delta \mathbf{v}_e^{orbit} = \omega_{e-}(D_e - L_{cm}) \begin{Bmatrix} \cos(f+\alpha) \\ \sin(f+\alpha) \\ 0 \end{Bmatrix}$$

To express this velocity change in the Earth-Centered Inertial (ECI) frame for direct application, the transformation matrix T_{313} is constructed. It is a "3-1-3" Euler angles sequence using orbital element angles in the order of longitude of the ascending node Ω, inclination angle i, and argument of perigee ω.

$$\Delta \mathbf{v}_e^{\mathrm{ECI}} = T_{313}\,\Delta \mathbf{v}_e^{orbit} = R_3^{\mathrm{T}}(\Omega) R_1^{\mathrm{T}}(i) R_3^{\mathrm{T}}(\omega)\,\Delta \mathbf{v}_e^{orbit}$$

With all vectors expressed in the ECI frame, the inertial ejected debris velocity is found by adding this impulse to the combined velocity before ejection.

$$\mathbf{v}_e = \mathbf{V}_{e-} + \Delta \mathbf{v}_e^{\mathrm{ECI}}$$

This allows the new satellite velocity $\mathbf{V}_e$ to be computed from the conservation of translational momentum.

$$(M + m_k)\,\mathbf{V}_{e-} = M\,\mathbf{V}_e + m_k\,\mathbf{v}_e$$

Angular momentum conservation provides ω_e, *Sling-Sat*'s angular rate after ejection.

$$\omega_e = \left[1 - \frac{m_k^2 \, D_e^2}{J_{De}(M + m_k)}\right] \omega_{e-}$$

After ejecting the debris, the arms are returned to their standard length D_c, giving a new ω_0 for the next interaction.

$$\omega_{0\,k+1} = \frac{J_{De}}{J_{Dc}} \, \omega_e$$

The process is repeated for the next interaction in the predicted mission. If the predicted mission is complete, the fitness function cost is computed by Equation (8.1), and is output to the GA for evaluation. This is repeated for every set of genes representing a member of the population–and further repeated for every generation. This network of repeating and nested loops leads to lengthy run-times.

8.4 Modularization

With several predictive, corrective, iterative, and nested operations, this mission simulation is quite involved. To help break it down, frequent and major routines are modularized. This section houses descriptions of the most significant subroutines in the simulation.

8.4.1 Read and Filter Debris

The dimensionality and nature of this combinatory problem makes the solution search space massive. Scattered throughout it are extremely efficient solutions, but they are difficult to find. Properly filtering the debris catalog distills the search space to increase the chance of finding attractive solutions.

At several stages throughout the simulation, the active debris catalog–the body

of objects being considered for removal–is redefined and filtered to include only a small subset of objects that are least expensive to reach from *Sling-Sat*'s current orbit. This is done by first reading Two Line Element (TLE) files of the debris fields, provided by NORAD through `celestrak.com` (update on 11/28/2012), and then removing all but a handful (e.g., 15) of "close" objects. Figure 8.8 provides a description of TLEs and how information is stored in them.

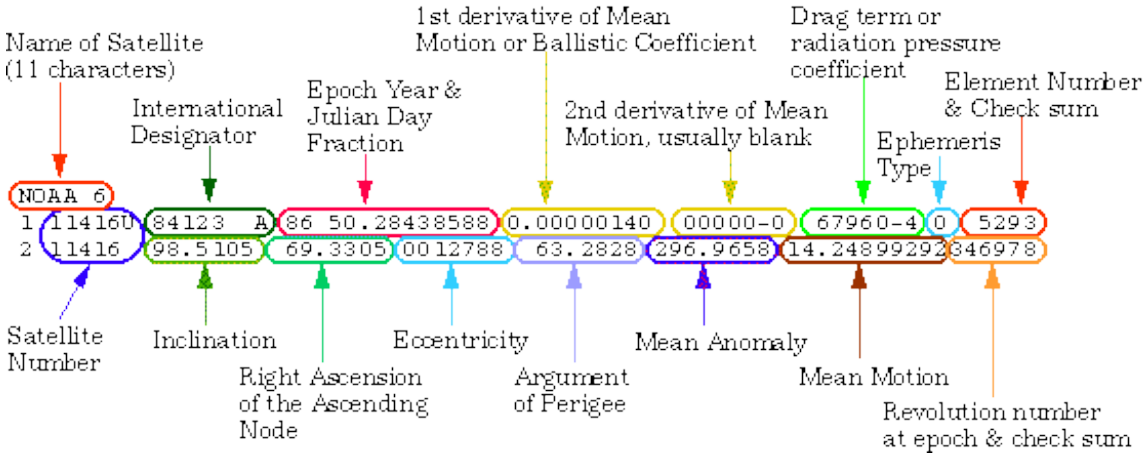

Figure 8.8: Two Line Element composition (Image: NASA)

Estimated costs of in-plane and out-of-plane maneuvers are used as filtering criteria. Note that the debris data was acquired several years after the fragmentation events, allowing time for the debris fields to disperse from tight bands to well distributed clouds. This accurately represents current and future missions. Debris from user-specified fields are read into a catalog where information like object identification and orbital elements are extracted and stored according to the TLE. Linear J_2 orbital propagation brings all objects to the current time of interest. To select the "closest" objects, orbital parameters of the debris and *Sling-Sat* are used to estimate orbit transfer costs. These costs define the subset of selected debris used for optimization, to ensure only debris that can be reached at low orbit transfer cost will remain. Figure 8.9 shows a typical active catalog filtered about *Sling-Sat*'s orbit.

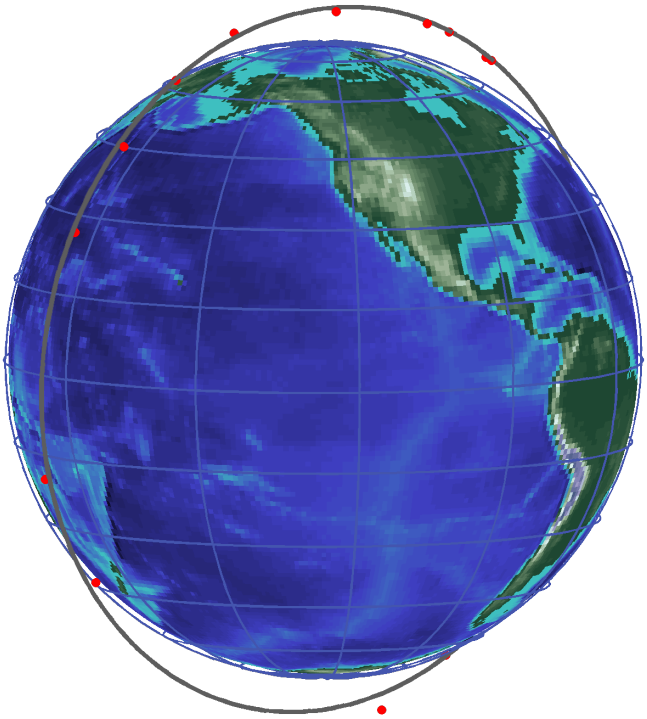

Figure 8.9: Active debris catalog after filtering

At the start of the main program, *Sling-Sat*'s initial orbital parameters are defined by "averaging" orbital angular momentum and mean radius of a targeted debris field. This ensures that *Sling-Sat* is given a practical and representative initial orbit, while not exploiting any clustered debris that may skew results of these short simulations. For a flown mission, clustered regions will likely be sought out to maximize effectiveness of initial orbits.

8.4.2 Debris Selection

During the simulated mission, only the filtered active catalog (see Section 8.4.1) is considered for target debris selection. Even so, solutions greatly benefit from further streamlining selection by assigning higher probability to debris with lower approximated cost to rendezvous ΔV_{est}. Estimated costs are based on two approximations. The first considers the circular equivalents of the debris and satellite orbits

using their angular momenta, $\mathbf{h} = h\,\hat{\mathbf{h}}$, and $\mathbf{H} = H\,\hat{\mathbf{H}}$, respectively. This facilitates a cost estimate of a plane change maneuver. The second approximation considers the in-plane orbit transfer cost as the first half of a Hohmann transfer. Only the first Hohmann impulse is observed because it better estimates the transfer cost for intercepting the debris, versus rendezvousing.

The angular momentum modulus gives the circular equivalent radius and velocity for *Sling-Sat* and all debris.

$$\begin{cases} \text{debris}: & r_{eq} = h^2/\mu & v_{eq} = \mu/h \\ \textit{Sling-Sat}: & R_{eq} = H^2/\mu & V_{eq} = \mu/H \end{cases}$$

Using these equivalent radii, the in-plane transfer cost is evaluated for each object.

$$\Delta V_H = \sqrt{\frac{\mu}{R_{eq}}} \left| \sqrt{\frac{2r_{eq}}{R_{eq} + r_{eq}}} - 1 \right|$$

The angular momentum unit vectors are used to find the angle between *Sling-Sat*'s and the debris' orbital planes, $\cos\vartheta = \hat{\mathbf{H}} \cdot \hat{\mathbf{h}}$. This intersection yields two points in the orbit for the satellite to change planes. The furthest has lower cost requirements, so it is used to calculate plane change cost.

$$\Delta V_p = \begin{cases} = 2V_{eq}\,\sin(\vartheta/2) & \text{if} \quad R_{eq} > r_{eq} \\ = 2v_{eq}\,\sin(\vartheta/2) & \text{if} \quad R_{eq} < r_{eq} \end{cases}$$

The total estimated cost is the sum of the approximate in-plane and plane change costs $\Delta V_{est} = \Delta V_H + \Delta V_p$. For each i-th debris in the catalog, the total estimated cost ΔV_{esti} is calculated and arranged in descending order. Let j be the length of the filtered catalog. Since selection probability must be greater for those debris charac-

terized by smaller ΔV_{est}, the following probability p_i, and its cumulative probability $\bar{p}_i$ are introduced:

$$p_i = \frac{1}{\Delta V_{esti} \sum_{m=1}^{j} \frac{1}{\Delta V_{estm}}} \qquad \text{and} \qquad \bar{p}_i = \sum_{m=1}^{i} p_m \tag{8.2}$$

Equation (8.2) guarantees the probability constraint $\sum_{i=1}^{j} p_i = 1$. The result is an ascending array of values $\bar{\mathbf{p}}$ between zero and one, with the more costly options packed tightly at the lower end, and the less costly options spread out at the higher end. The difference between the debris selection gene (a value between zero and one) and the elements of $\bar{\mathbf{p}}$ are evaluated, and the debris associated with the smallest difference is targeted for removal.

8.4.3 Perturbed Lambert Solver

The task of determining the required velocity for *Sling-Sat* to transfer from its position at impulse to its position at capture, in a known amount of time, is a two-point boundary value problem. For unperturbed Keplerian orbits, this is called Lambert's problem, and there are established iterative methods for solving it. To include the effects of J_2 perturbations, a new scheme is created [22]. Given the initial position, final position, and the time of flight, the unperturbed Lambert problem is first solved, and its solution is used as a starting point for a shooting method, driven by numerical Jacobian, that converges to the perturbed solution.

The unperturbed solution gives an initial velocity guess that the J_2 Lambert solver uses to propagate *Sling-Sat* from the known initial position to a final position. The error between this and the desired final position is used to update the initial velocity guess for the next iteration. The required initial velocity is found when

the propagated final position converges to the desired final position. Assigning this velocity to *Sling-Sat* ensures that it will intercept the debris' trajectory at the time of capture. This J_2 Lambert solver usually converges to the correct value (within machine error accuracy) in less than three iterations.

8.4.4 Applying the Solution

When the GA outputs its best set of genes, as measured by the cost of the predicted mission, the solution must be applied to the simulated mission. Procedure for simulating the applied solution is similar to that of the predicted mission in Section 8.3, but there are three main differences. Firstly, the debris masses are redefined to replicate the fact that they are unknown to a real mission. The uncertainty intro-

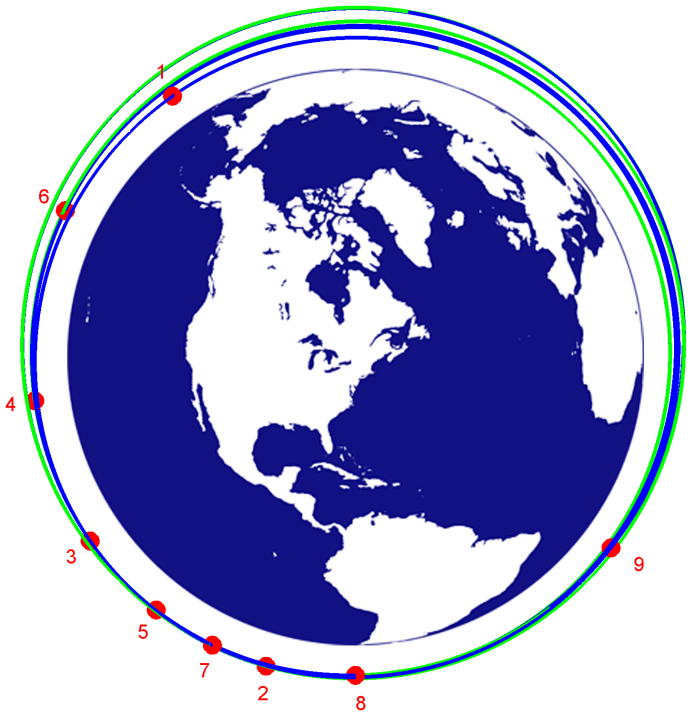

Figure 8.10: Three-interaction example solution

duced by interacting with unknown masses is a significant consideration that needs to be included. Secondly, of the n debris interactions specified by the predicted

mission, only the first is simulated. After that single interaction is applied, a new predicted mission is constructed based on the updated states. Figure 8.10 shows an example of what a three-interaction solution looks like when applied. Thirdly, rather than outputting a cost, the applied simulation outputs states, times, and all other variables necessary to analyze and track the behavior.

8.5 Results

Results are obtained for a ten-interaction mission to represent a portion of a full-length mission. Three branches and one main application of the GA are carried out for each interaction. All 40 instances of the GA have the same settings: 32,000 members of the population, 15 generations, a crossover of 0.6, and a mutation rate of 0.2. Since the branches and the main GA all have 15 generations, the accepted solution for each interaction undergoes 30 total generations of refinement, and is selected half way through as the best of three options. With these specifications, more than $1.9 \cdot 10^7$ predicted missions are simulated. Parallel computing across four consumer-level processors gives a runtime of roughly 16 hours. When applying this to a real system, all computations will have to be done on the ground by a dedicated high-performance computer.

M_h	m_k	M_C	J_h	M_A	D_c
50 kg	$\sim \mathcal{N}(1.5, 0.04)$ kg	20 kg	30 kg·m^2	5 kg	5 m

Table 8.1: Physical property assignments

Following the convention of Figure 8.5, Table 8.1 gives the physical specifications. Applying these to the GA yields different results every time; however, the following results are representative of the magnitudes and trends to be expected. Consistently, all ten encountered debris are successfully removed. Figure 8.11 shows *Sling-Sat*'s angular rate prior to capture, when the arms are extended to their standard length

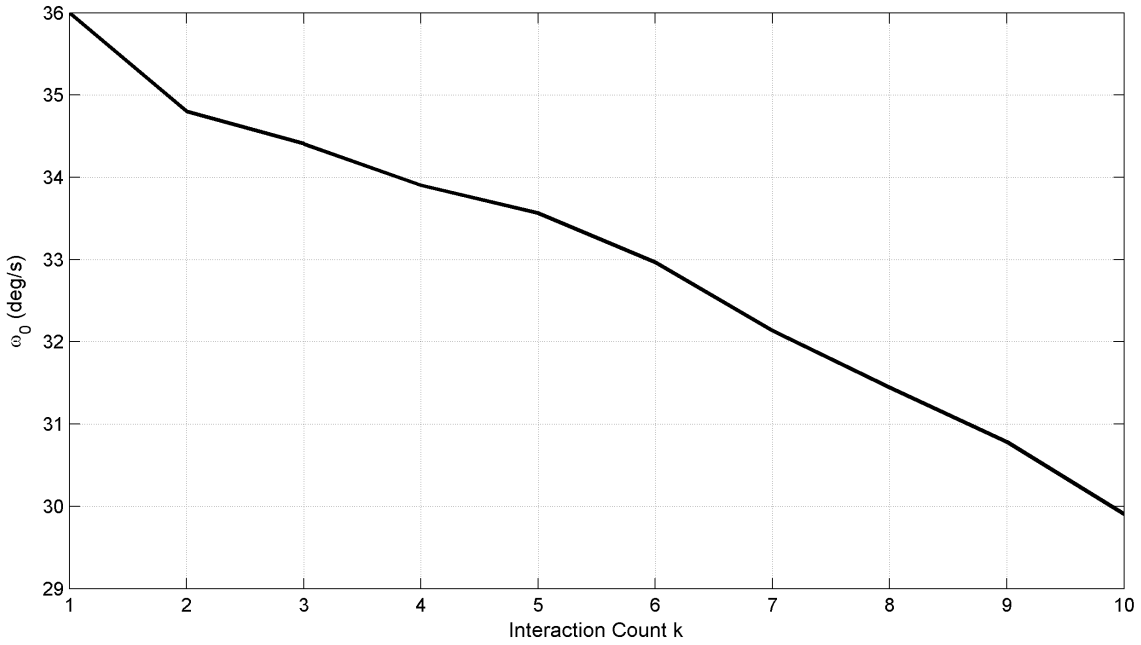

Figure 8.11: Angular rate before each capture

D_c. Enforcing this configuration provides a point of comparison between each interaction, which shows a slow, persistent loss of angular momentum. Though losses are minor ($\Delta\omega_0 < 1$ deg/s per interaction) and easily compensated for by hardware (e.g., solar powered flywheel), this is an important trend to monitor from early stages of development.

Ejection arm length is tracked in Figure 8.12 for each interaction. As the control variable for attaining prescribed ejection speeds (which vary), this value is fairly sporadic. If the minor angular momentum losses are left uncorrected, it is expected that the average ejection arm length will gradually decrease over time and limit the maximum ejection speeds; however, simulating partial missions of only ten consecutive interactions does not provide sufficient statistical data to confirm or refute this expected trend. The results of Section 5 do not forecast losses of this nature for long duration missions, once the system settles into a range of operation.

Figure 8.13 shows the fuel consuming impulse, the free impulse from capture,

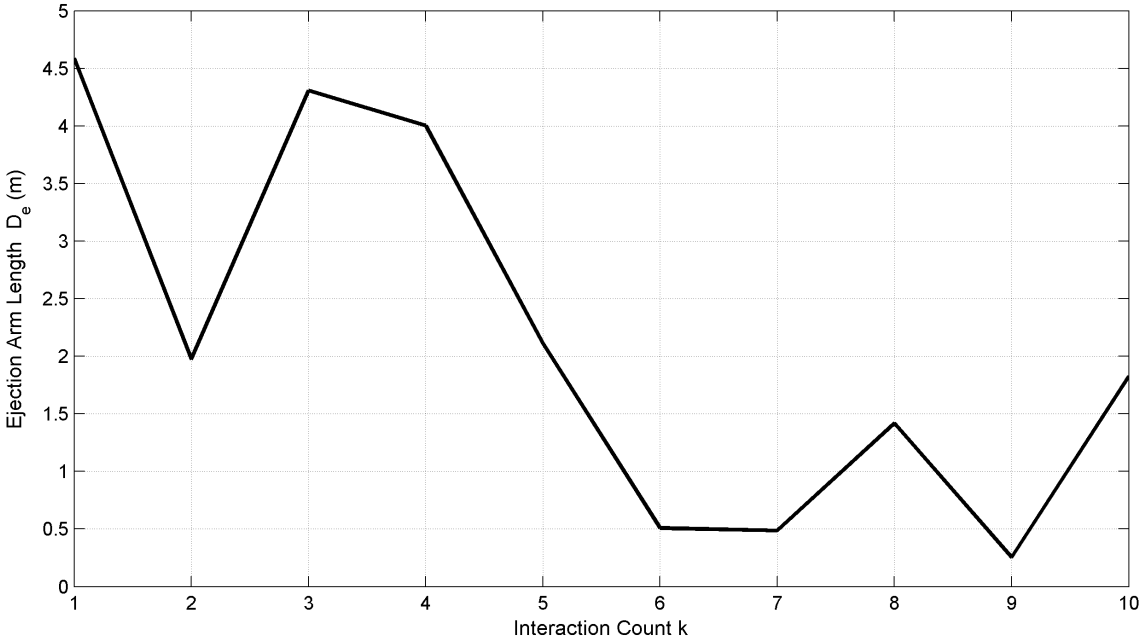

Figure 8.12: Ejection arm length for each interaction

and the free impulse from ejection for every interaction. In most cases, the impulse from capture is the lowest of the three. This characteristic is not enforced, though it is welcomed since debris mass is unknown at capture, and the associated impulse has the greatest uncertainty. The impulse from ejection is regularly the largest of the three. Again, this characteristic naturally emerges, and is welcomed. A feature of *Sling-Sat*'s rotating design is that debris mass can be determined shortly after capture. At the time of ejection, a real mission will have almost no uncertainty, providing high confidence in the largest impulse.

All ten debris encountered are removed using a required total impulse of $\Delta V =$ 0.33 km/s. The sum of all 20 free impulses from capture and ejection is $\Delta V_{free} = 0.89$ km/s. Therefore, *4S* is extracting 2.7 time more free impulse from the debris fields than it requires from fuel. 73% *of the mission is driven at no cost.* To put these numbers in perspective, ten objects are removed using the same required ΔV that a standard mission consumes during a single Hohmann transfer from an altitude of

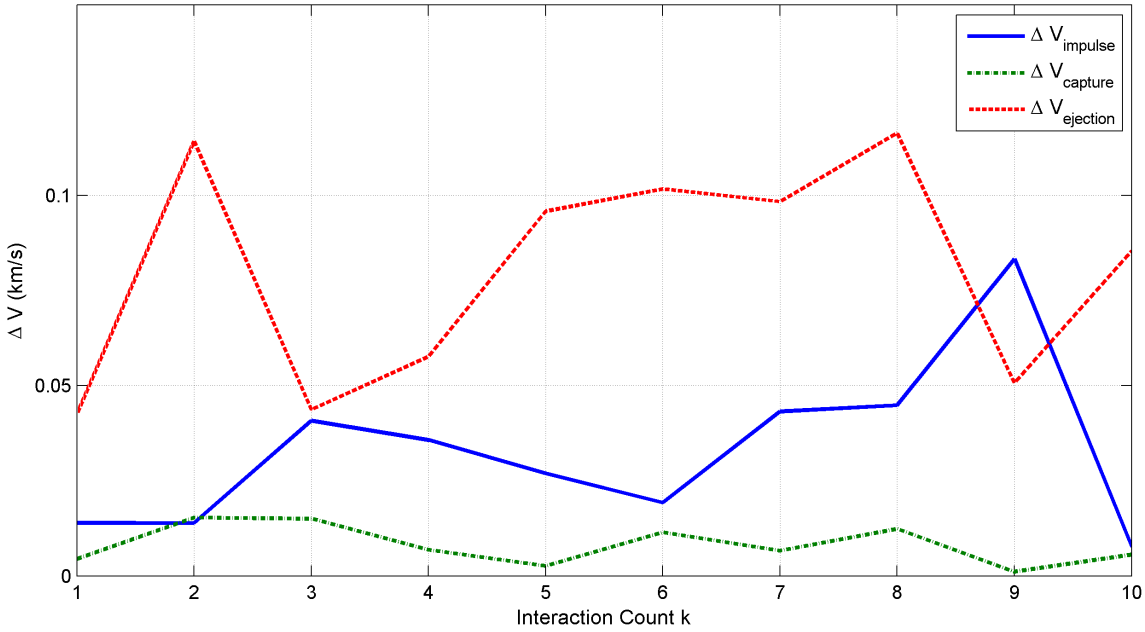

Figure 8.13: ΔV magnitudes for each interaction

400 km to 1,000 km.

As promising as these figures sound, they can certainly be improved upon. While developing this method, every refinement and modification consistently yielded improved results. For example, focusing the computational effort on just one debris interaction readily uncovers solutions where more than 91% of the total ΔV is free! In addition, the pace of this mission plan is very aggressive. The code ensures that all 30 maneuvers are executed in only 6.125 days. This is because the available computational power was unable to handle the larger search space of longer missions. More powerful optimization and processing can handle a much larger search window that undoubtedly contains improved solutions.

9. CONCLUSIONS

This work proposed an efficient mission for active space debris removal, *Space Sweeper*, that plastically captures and ejects debris to harvest momentum, and reduce fuel consumption. Feasibility was studied through analysis and simulation. A suggested hardware design for the accompanying satellite, *Sling-Sat*, was conceptualized, along with alternatives and variations. In short, *Sling-Sat* is a dual-spinning satellite designed to capture and eject debris at the ends of adjustable-length arms. Arm design and sensor needs were emphasized.

Fundamental conservation principles were used to derive sets of sequential equations that step through the phases of debris interaction: capture, spin-up, and ejection. A five-mass model and a simplified two-mass model were engendered for analysis and simulation throughout this work. Three methods were derived for estimating unknown debris mass after capture; these make use of *Sling-Sat*'s rotation, and are arguments for the design. The energy-optimal relationship between the independent arm lengths of the five-mass model was derived for achieving a prescribed ejection velocity with minimal effort.

The spin-up process was analyzed for the two-mass and five-mass models. Both confirmed the intuitive correlation between work input and change in angular rate, suggesting the simpler two-mass model qualitatively suffices for such analyses. The two-mass model showed this correlation extending to change in tangential velocity of the debris; however, the five-mass model demonstrated that increased work input does not necessarily result in larger changes in tangential velocity. When partially modeled as an extended object, coupling between arm length and angular rate showed the maximum change in tangential velocity is achieved before the lower limit of arm

length. The complexity of this relationship is expected to increase with higher-fidelity modeling, making room for optimization to begin addressing secondary goals, such as efficiency and material constraints. This study should be revisited as the proposed mission develops.

To investigate concerns of angular momentum loss in long-term missions, 10,000 random, consecutive debris interaction were simulated with no ill effect. Statistical estimates of the net energy required to actuate the arms showed a standard solar array can sufficiently replenish the energy stores in less than 4 minutes. This supports sustainability of extended missions.

Optimal controllers were successfully designed to enforce capture–establishing feasibility of regulating such interactions. Two versions were demonstrated, and, in addition to capture, both were tasked with maximizing efficiency and minimizing the impact velocity at the collector. The first controller assumed the trajectories were fixed and successfully exhibited capture with minimal impact by controlling arm lengths only. The second included trajectory control and demonstrated capture with zero impact velocity. This was not accomplished through traditional rendezvous; rather, minor trajectory control positioned the craft such that the tangential velocity of the collector negated the relative velocity of the impacting debris. Further progress in hardware design will allow high-fidelity models to test more sophisticated and precise control methodology.

A study was conducted to analyze orbital behaviors due to debris interaction. The ΔV required to re-enter the Earth's atmosphere was observed for circular orbits of varying altitude. This confirmed that ideal conditions for operating a *Space Sweeper* mission are in LEO, where orbital speeds are highest and the requirements to deorbit are lowest. This is favorable because LEO has the greatest need for space debris removal.

A point cloud was generated to show the three-dimensional distribution of deorbiting ejection velocities for a representative orbit. The surface of this cloud defines the minimum required impulse to deorbit debris through any given point in the atmosphere. Planar ejections were analyzed to characterize the relationship between perigee reduction and the components of ejection velocity. The curve of minimum deorbiting impulses was identified for a range of ejection angles. Variation in orbital parameters resulting from ejection were analyzed for both the satellite and debris. This proved orbital maintenance can be applied within the confines of the mission. Most importantly, it disproved the notion that decreasing debris perigee necessitates an increase in the satellite's perigee. In fact, scenarios exist where both perigees decrease.

Path optimization is potentially the most critical aspect of *4S*. A technique was developed to search for efficient debris removal paths compliant with the *Space Sweeper* mission architecture. A genetic algorithm was successfully applied to optimize debris mitigation and fuel economy. J_2 perturbed propagations and current cataloged debris field data were used for accuracy and reliable conclusions. Results showed that 73% of the total mission ΔV was free, and all targeted objects were removed. Extending these figures to a mission with an assumed available impulse of 4 km/s from fuel, one *Sling-Sat* would remove 121 objects in its lifetime. This is a significant impact considering the trackable debris cloud from Iridium-33 has about 451 members. Refueling stations or launching multiple missions would remedy the debris problem in just a few months.

The results of this optimization technique sufficiently assert *4S* as a low cost and effective option for active space debris removal. Even so, better results unquestionably exist. The presented method was limited to aggressive, short-duration missions and only analyzed a portion of all cataloged debris. Refinement of the optimization

technique, and more processing power, will accommodate larger searches containing more efficient solutions. It is probable that sequentially interacting with debris for its removal will allow large portions of the mission to consume no fuel at all.

REFERENCES

[1] John R. Amend, Eric Brown, Nicholas Rodenberg, Heinrich M. Jaeger, and Hod Lipson. A positive pressure universal gripper based on the jamming of granular material. *IEEE Transactions on Robotics*, 28(2):341–350, April 2012. doi: 10.1109/TRO.2011.2171093.

[2] HQ TRADOC Army Space Reference TextSpace Division. Space environment and orbital mechanics. Technical report, Space Division, HQ TRADOC, Fort Monroe, VA, 2009. Chapter 5.

[3] Ivan Bekey. Project Orion: orbital debris removal using ground-based sensors and lasers. In *Second European Conference on Space Debris*, page 699, 1997. ESA SP-393.

[4] Claudio Bombardelli and Jesus Peláez. Ion beam shepherd for contactless space debris removal. *Journal of Guidance, Control and Dynamics*, 34(3):916–920, May–June 2010. doi: arXiv:1102.1289v1.

[5] Jonathan W. Campbell. *Using Lasers in Space: Laser Orbital Debris Removal and Asteroid Deflection*, volume 20. Center for Strategy and Technology, Air War College, Air University Maxwell Air Force Base, Alabama, 2000.

[6] Erika Carlson, Steve Casali, Don Chambers, Garner Geissler, Andrew Lalich, Manfred Leipold, Richard Mach, John Parry, and Fole Weems. Final design of a space debris removal system. Technical report, NASA/CR-189976, 1990.

[7] Macomber B. Moody C. Probe A. Cavalieri, K. A. and J. L. Junkins. Laboratory experiments supporting autonomous space debris mitigation. In *AAS Guidance,*

Navigation, and Control Conference, Breckenridge, CO, February 2013. paper number: AAS 13-011.

[8] Committee for the Assessment of NASA's Orbital Debris Programs. Limiting future collision risk to spacecraft: an assessment of NASA's meteoroid and orbital debris programs. Technical report, National Research Council, Washington, D.C, 2011.

[9] Leonard David. Boom! NASA to demolish spacecraft in the name of science. www.space.com/18349-debrisat-spacecraft-destroy-space-junk.html, November 2012. Accessed:2.10.2013.

[10] ESA/ADMIN/IPOL. Space debris mitigation for agency projects. ESA Director General's Office, April 2008. Paris, France.

[11] Ed Grayzeck and E. Bell. NASA national space science data center master catalog. Houston, TX, 2012. www.nssdc.gsfc.nasa.gov/nmc/spacecraf tSearch.do Accussed: 1.2.2013.

[12] Brandon Holladay. Validation of the ballistic limit equation for monolithic aluminum shielding at geostationary orbital debris impact velocity. California Polytechnic State University, San Luis Obispo, October 2012. Thesis.

[13] Susan Ireland. Dodging bullets: the threat of space debis to U.S. national security. U.S. Army, June 2010. Masters of Science Thesis.

[14] T.S. Kelso. Analysis of the Iridium 33-Cosmos 2251 Collision. In *Advances of the Astronautical Sciences*, volume 135, pages 1099–1112, 2009. paper number: AAS 09-368.

[15] D.J. Kessler. Collisional cascading: the limits of population growth in low earth orbit. *Advances in Space Research*, 11(12):63–66, 1991. doi:10.1016/0273-1177(91)90543-S.

[16] Heiner Klinkrad. Monitoring space: efforts made by European countries. ESA, ESOC, July 2012. Darmstadt, Germany.

[17] David Kushner. Cluttered space. *Popular Science*, 2(8):3, and 60–64, August 2010.

[18] Frank L. Lewis and Vassilis L. Syrmos. *Optimal Control*. Wiley-Interscience, 2nd edition, 1995.

[19] Daniel Michaels. A cosmic question: How to get rid of all that orbiting space junk? *Wall Street Journal*, March 11 2009. ESA SP-393.

[20] Jonathan Missel and Daniele Mortari. Sling Satellite for debris removal with Aggie Sweeper. In *Advances in the Astronautical Sciences*, volume 140, pages 70–74, 2011. paper number: AAS 11-256.

[21] Jonathan Missel and Daniele Mortari. Optimization of debris removal path for TAMU Sweeper. In *Advances in the Astronautical Sciences*, volume 143, pages 935–945, 2012. paper number: AAS 12-167.

[22] Jonathan Missel and Daniele Mortari. Path optimization for Space Sweeper with Sling-Sat. *Advances in Space Research*, 2013. submitted.

[23] Jonathan Missel and Daniele Mortari. Removing space debris through sequential captures and ejections. *AIAA Journal of Guidance, Control and Dynamics*, 2013. in print, doi: 10.2514/1.58768.

[24] Union of Concerned Scientists. UCS satellite databasel. www.ucsusa.org/assets/documents/nwgs/UCS_Satellite_Database_12-1-12.txt, December 2012. Cambridge, MA. Accessed: 2.2.2013.

[25] NASA Orbital Debris Program Office. An update of the FY-1C, Iridium 33, and Cosmos 2251 fragments. *Orbital Debris Quarterly*, 17(1):4–5, 2013.

[26] NASA Orbital Debris Program Office. Orbital debris mitigation. www.orbitaldebris.jsc.nasa.gov/mitigate/mitigation.html, 2013. Houston, TX. Accessed: 2.2.2013.

[27] J. H.; Roh D. G.; Chung H. S.; Kim K. D.; Cappallo Roger Oh, S. J.; Yeom. A study on the development of playback control software for mark5b vsi system. *Journal of Astronomy and Space Sciences*, 27(2):107–116, 2010. doi: 10.5140/JASS.2010.27.2.107.

[28] Jerome Pearson. Low-cost launch system and orbital fuel depot. *Acta Astronautica*, 19(4):315–320, 1989. doi: 0094-5765/89.

[29] Jerome Pearson. Active debris removal: EDDE, the electrodynamic debris eliminator. In *International Astronautical Congress*, volume 61, pages 1–9, Prague, CZ, December 2010. paper number: IAC-10-A6.4.9.

[30] Jerome Pearson, J. Carroll, E. Levin, and J. Oldson. Active debris removal: EDDE, the ElectroDynamic Debris Eliminator. In *61st International Astronautical Congress*, Prague, Czech Republic, September 2010. paper number: IAC-10-A6.4.9.

[31] Jerome Pearson and Tetsuo Yasaka. Tether-assisted disposal of inoperative satellites. In *International Symposium on Space Technology and Science*, Tokyo, Japan, 1990.

[32] G. Hirzinger S. Abiko. On-line parameter adaptation for a momentum control in the post-grasping of a tumbling target with model uncertainty. In *IEEE/RSJ Int. Conf. on Intelligent Robots and Systems*, pages 847–852, San Diego, CA, November 2007. doi: 10.1109/IROS.2007.4399190.

[33] Jones H.M. Perkins C.W. Shapiro, I.I. Orbital properties of the West Ford dipole belt. *Proceedings of the IEEE*, 52(5):469–518, 1964. doi: 10.1109 /PROC.1964.2992.

[34] I. Sharf T. C. Nguyen-Huynh. Adaptive reactionless motion for space manipulator when capturing an unknown tumbling target. In *IEEE Int. Conf. on Robotics and Automation*, pages 4202–4207, Shanghai, China, May 2011. paper number: 978-1-61284-385-8/11.

[35] Thomas Benjamin Walsh. Effects of rotational motion on the ballistic coefficient of space debris. Master of Science Thesis, Auburn University; Auburn, Alabama, August 2012.

[36] Fred L. Whipple. Meteorites and space travel. *Astronomical Journal*, 52:131, 1947. doi: 10.1086/106009.

[37] T. Hanaha Y. Kitazawa A. Kawabe Y. Ariyioshi, S.i Kashima. Effectiveness of passive orbital debris removal for future environment. In *Institute of Space and Astronautical Science*, pages 3–6, Okinawa, Japan, 2011. paper number:2011-r-38.

[38] Harold A. Zahl and Hans K. Ziegler. Power sources for satellites and space vehicles. *Annals of the International Geophysical Year*, 4(1):32–38, 1960. doi: 10.1016/0038-092X(60)90047-5.